CENTRO DE INVESTIGACIONES
EN OPTICA, A.C.

"WHITE LIGHT GENERATION THROUGH EXCIPLEX AND DOWN-CONVERSION MECHANISMS FOR ORGANIC SOLID-STATE LIGHTING"

Thesis submitted in fulfillment of the requirements for the Ph.D. degree in science (Optics)

Wilson-Esneider Bernal-Pinilla

Advisor: Dr. J. Oracio C Barbosa García

Co-advisor: Dr. Enrique Pérez Gutiérrez

León · Guanajuato · México

December 2020

To Diana Marcela Montoya

my strength and my breath

...my life partner

"pequeñas acciones en conjunto pueden acarrear grandes beneficios"

Magdalena Rius de Riepen

ACKNOWLEDGMENTS

I am very grateful to advisors Dr. J. Oracio Barbosa García and Dr. Enrique Pérez Gutiérrez for their guided academically and promptly throughout this stage and thus can carry out the work on time. Also, appreciate that they have shared some tools from their professional experience for scientists' formation.

I am grateful to the thesis committee made up of Dr. Judith Percino Zacarias, Dr. Braulio Molina, Dr. José Luis Maldonado, and Dr. Alfredo Benitez Lara for their valuable contributions during the execution and presentation of the thesis. Their timely comments allowed us to evaluate objectives, propose new ideas, and face the challenges during this work.

Thanks to the group of optical properties of matter (GPOM), both researchers, technicians, and students for their constant support, advice, and help. Especially to Dr. Antonio Meneses and Dr. Mario Rodríguez, who offered their academic advice on some of the objectives developed.

Thanks to the group of polymers and organic electronics of the Benemérita Universidad Autónoma de Puebla, headed by Dra. Percino and Dr. Pérez, for allowing me to do a doctoral stay and develop new ideas and projects. Thanks to Dr. Molina's research group at UNAM, which supplied us with part of the materials with which the proposed studies were carried on.

Thanks to the CIO, I had the opportunity to train in the research field and grow professionally and personally. Thank all the scientific and human personnel that are part of this institution. Thanks to CONACyT for 789043/616460 scholarship during these four years.

I am very grateful to M.Sc. Diana Marcela Montoya, who was my support and company in this life cycle. Thanks to classmates and friends from different nationalities that I had the opportunity to know, which were fundamental not only in academic help but also for my emotional side was balanced.

Thanks to my family, Bernal and Montoya families, for their emotional help. Especially to my parents, Doris Pinilla and Jaime Bernal, to my siblings, Johanna Bernal and Jaime H. Bernal, to my mother-in-law and sister-in-law Maria Montoya and Vanesa Moncada Montoya.

Finally, I want to sincerely thank Dr. Anandhan Karnambaram (RIP) for his valuable collaboration and friendship during my doctoral stay in the city of Puebla.

Abstract

This work reports the experimental study of two mechanisms, exciplex and down-conversion, to obtained white light with organic and hybrid materials for solid-state lighting (SSL). Exciplexes are complex states generated by intermolecular interaction between two molecules, usually an electron donor and an acceptor material; they were studied in the OLED structure: ITO/HTL/EML/ETL/Ca-Ag. Commercial materials and a new carbazole derivative were employed as the emissive layer (EML), and for the first-time, exciplex emissions from two interfaces were achieved. The thickness of the hole transport layer (HTL) was a determinant parameter for the exciplex states formation at HTL/EML interface. Meanwhile, the appropriate barrier energy between LUMO levels of the EML and ETL was crucial in allowing the bimolecular states to emerge at the EML/ETL interface. Therefore, due to emissions from the EML (S_1-S_0 transitions) and the two interfaces, a broad electroluminescence spectrum corresponding to white light with excellent CIE (0.31, 0.33) and CRI >85 was accomplished. The devices exhibited acceptable luminance (< 9000 cdm-2) and turn-on voltage (5 V). On the other hand, the studied down-conversion mechanism involved the full or partial absorption of the light emitted from an inorganic LED by the organic material. Thicknesses of the organic films were optimized to obtain a proper absorption of the converter material, which allowed the adequate combination between the electroluminescence (EL) and photoluminescence (PL) intensities from LED and the organic converters, respectively. Thus, the mechanism was tested in partial and full conversion configuration known as luminesce converter (LUCO). Using benzothiadiazole derivatives as organic converter, LUCO devices exhibited white light with excellent CIE (0.32, 0.33), outstanding CRI (>90) and good conversion efficiency of 73%. With these results, it was demonstrated that organic materials could be a real alternative in the field of SSL.

TABLE OF CONTENTS

LIST OF FIGURES

LIST OF TABLES

1. INTRODUCTION.

1.1. Brief Background of Artificial Lighting and the State of the Art.

Artificial lighting plays an indispensable role to daily life of any human being. Electrical light sources are responsible for an energy consumption around 16 to 20 % of the worldwide electricity production. Classic lighting technologies like incandescent, fluorescent and halogens are now mature. Their luminous efficiency and power conversion together with their quality of the emitted light have been reached almost to their limit (see in Fig. 1.1 for power conversion of different lighting sources).[1–4] As a result, the world of light sources has experienced a major revolution: after 150 years of operation, incandescent lamps are banned from the market, while Solid-State Lighting (SSL) systems which are based on inorganic and organic semiconductors, are the most commonly used today.[5–7]

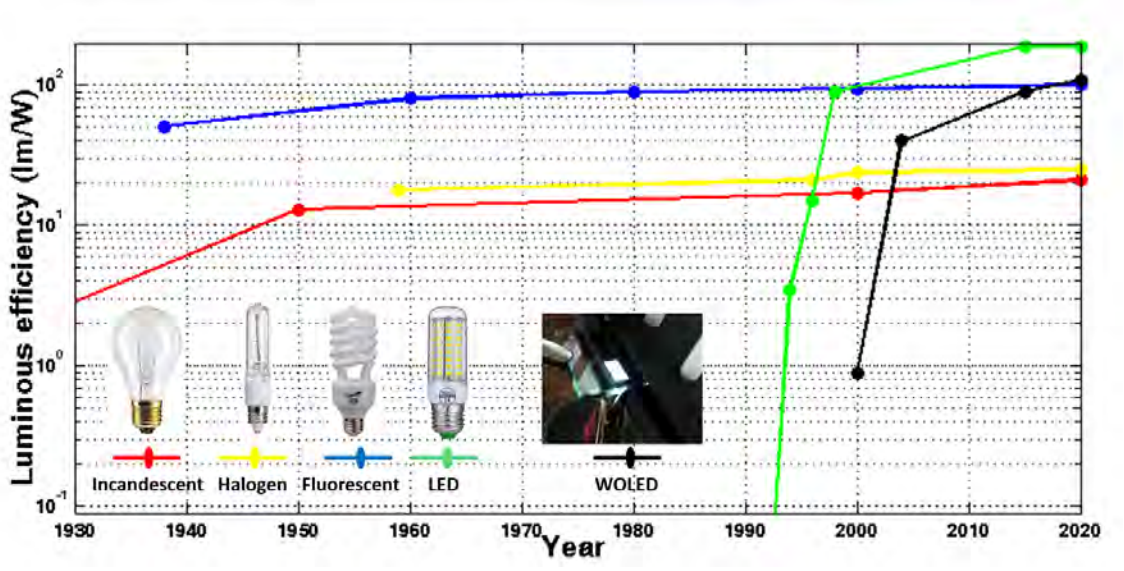

Figure 1.1. Growth of efficiency in lighting technologies since incandescent to SSL lamp (LED and OLED).

SSL devices generate visible light through the electroluminescence phenomenon when an electric current is applied. The luminescence properties depend on the structure of the device, the chemical composition and the properties of the semiconductor material.[2] In the case of inorganic semiconductor diodes that are based, for instance, in InGa or GaAs, they are used widely and the technology is known as light emitting diode (LED).[8] For the case of light emitting diodes based on organic semiconductor, a wide variety of organic materials that includes small molecules and polymers have been reported, this technology is named organic LED (OLED).[9] For lighting application, white light from SSL implies the combination of different wavelengths in almost all visible spectrum, besides, the electroluminescence (EL) must have acceptable illumination parameter, color rendering index (CRI) >80, stable correlated color temperatures (CCTs) and good CIE coordinates (from its French name, "Commission internationale de l'éclairage"). Notwithstanding that an ideal white light is considered to have CIE coordinates as close as possible to (0.33, 0.33). Giovanella et al.,[10] have reported that nowadays LED and OLED technologies show better parameter for luminous efficiency, lifetime and color rendering index than conventional lighting sources. However, in terms of the manufacture price, incandescent and fluorescent lamps are still cheaper than SSL. For example, OLEDs are two orders of magnitude more expensive to produce than incandescent lamp.[11]

By now, white LEDs (WLED) have achieved over 260 lm/W in the laboratory whereas commercial LEDs have >50 lm/W. Apart from high efficiency, WLEDs show some advantages when compared with other light sources as described by De Almeida and co-workers.[2] They point out that LEDs stand for their low power consumption and low operating voltage, long lifetime, mercury-free, no UV or IR radiation, among other properties. Despite Inorganic LED is a mature technology; it presents some disadvantages that need to be solved. Research groups and some government agencies have been

reporting that LED sources lack of standardization, risk of glare as a result of small lamp size and temperature dependence (ambient temperature greatly influences the LEDs' performance), for example.[2,12–14]

On the other hand, OLEDs devices exhibit attractive properties as emission in a wide range of colors, easy fabrication, flexibility, among others. However, the luminous efficacy of commercial organic devices for lighting applications still is low, being about 50 lm/W.[15] The research effort on OLEDs is focused on increasing the value of this parameter but at laboratory level it has been reported values over 100 lm/W[16,17] as well as enlarging the emitting surface and extending the device lifetime. Typically, the luminance of OLEDs decreases down to 50% (LT 50 lifetime parameter) of its initial value after 15,000 h, which is 90% less than the inorganic LEDs. The degradation of these devices is a serious issue that affects the luminance of OLEDs and is basically caused by three mechanisms, electrode degradation, organic degradation and the intrinsic decrement of the electroluminescence efficiency of the emissive area.[7,18] In fact, LEDs, with a continuous growth of their luminous efficiencies, establish themselves as breakthrough solutions while organic LEDs (OLEDs) recently found their first application field on TV screens and cell phones (see Fig 1.2), but as a white lighting system still is necessary to achieve better performance than LEDs do; for this reason, the OLED devices for lighting are being widely studied and investigated around the world.[19]

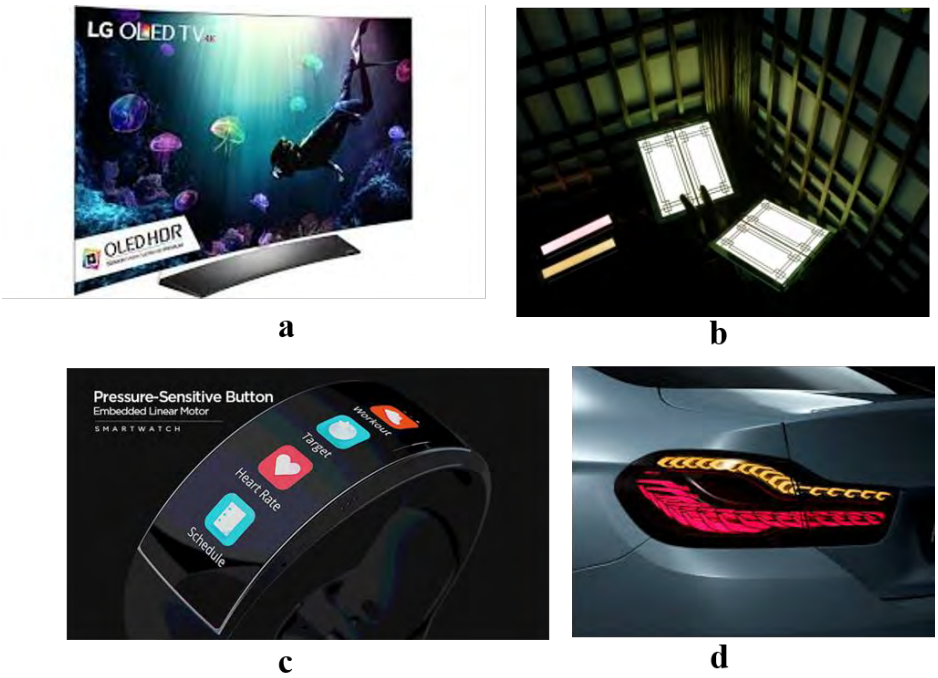

Figure 1.2. Examples of OLED applications; a) OLED TV[20]*;b) lighting panels*[21]*; c) smartwatch*[22]*; d) tail lights for cars.*[23]

1.2. White Light From Inorganic LED.

LEDs are based on inorganic semiconductor materials, in 1907 Captain Henry Joseph Round observed the electroluminescence phenomenon when a current flowed through a crystal of silicon carbide.[24] Later, the Russian radio technician Oleg V. Lossev made the first attempt to explain the electroluminescence in p-n junctions with a scientific approach, describing the current versus voltage characteristic of the new device in 1923.[25] In 1960s, Robert Hall, Nick Holonyak, Marshall Nathan, and Robert Rediker reported simultaneously the laser emission of gallium arsenide crystals.[26] Since then, LEDs have been commercially available in red, amber, and green colors. Most of the applications of LEDs have mainly been signaling, seven-segment displays, and remote control.[7,27]

Figure 1.3 shows the mechanism of operation of the LED. To create the LED diode, two regions are joined: **n**-side and **p**-side. At the **p-n** junction of the regions a potential barrier is formed known as a depletion zone whose function is to prevent the passage of electrons from the **n** to the **p** region. When a voltage is applied, electrons begin to flow. Each time an excess electron with a negative charge present in the **n** region acquires energy to be able to overcome the resistance offered by the potential barrier, crosses it and combines with a hole in the **p** region. At the same instant that this combination occurs, the excess energy that the electron acquired to be able to cross the potential barrier is transformed into electromagnetic energy, which is released in the form of photons.

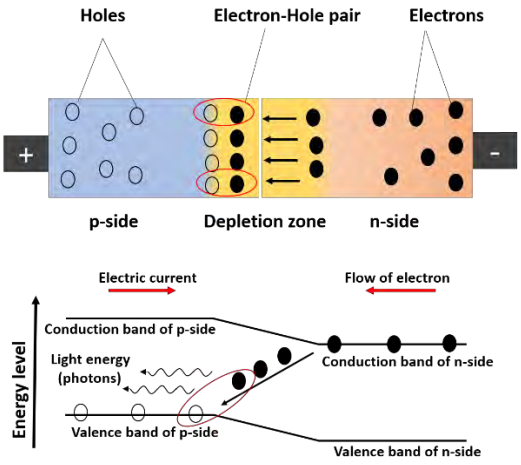

Figure 1.3. Basic architecture of inorganic LED.[28]

Figure 1.4 shows the conventional mechanisms to achieve white light using LEDs; the first one is known as R-G-B that requires the emissions of three LEDs (red, green, and blue) whose wavelengths combine to form white light (see Fig. 1.4a).[29–31] The other two mechanism are called down-conversion (see Fig 1.4b and 1.4c) based on the combination of emission from a LED and a phosphor[7,32, 33]; thus, for the white LED, phosphors are

essential. The most successful approach for white light has been the so called *partial conversion* which is the combination of blue light (from LED), green light (from phosphor), and red light (from phosphor).[32] The other approach, known as *full conversion,* is based on the use of an ultraviolet (UV) or a violet LED and a phosphor that absorbs completely the UV or violet light and converts it to a broadband white light[28,32] as can be observed in Figure 1.4c. Additionally, in the literature new ways to achieved white light have been proposed using for example quantum dots, metal-based, and perovskites.[34–36]

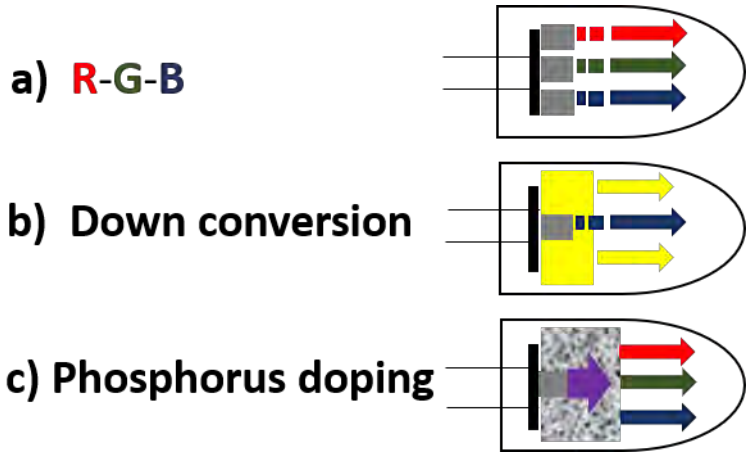

Figure 1.4 White LED mechanisms, a) mixture of three LEDs (Red, Green, and Blue), b) Down conversion, c) Phosphorus doping.[28–30]

In relation with the phosphorus materials, Shimizu et al.[37,38] in 1996 developed the first phosphor to partial conversion white LED, cerium-doped yttrium-aluminum garnet phosphor (YAG:Ce). This phosphor is able to absorb blue light and to emit red and green light.[28,39,40] In the same year, the first phosphor to full conversion white LED was patented by Baretz and Tischler [41] of the ATMI Company. From these two works, numerous papers on phosphors for full and partial conversion were developed; including reports and patents.[28,32,42].

Currently, 95% of LEDs in the market are focused to generate white light by using blue LEDs of GaN or InGaN with the broad yellow emission of the $Y_3A_{l5}O_{12}:Ce_3+$ (YAG:Ce) phosphor. The system YAG:Ce/blue LED gives a low color-rendering index (CRI < 80) and high correlated color temperature (CCT > 5000 K), whereby requires the addition of expensive and moisture-sensitive red phosphors (fluoride or nitride). These phosphors involve rare-earth that are extensively used in other high-technology devices like: mobile phones, flat panel displays, and sectors such as military, energy renewable, among others.[43,44] Consequently, the research on white LEDs is mainly focused on the development of rare-earth-free phosphors.[45,46]

By 2025, the worldwide will demand 200.000 tons per year of rare-earth elements (REEs) while the current annual supply is estimated to be only 113.000 tons. The attempt to increase the REEs supply at a rate sufficiently high to meet the increase in demand faces economic, political and environmental limitations that also will affect the LED production. This led to a 600% price increase. Moreover, the cost of a white LED lamp is strongly linked to the price of REEs as the latter represents 12% of the total.[47–49] For Nyalosaso et al.,[43] the explosion of demand combined with a monopolistic supply source represents a real risk for the development of LED technology in the years to come. Balachandra and his group,[50] who did a deep description of extraction and application of the REEs, mention that only the extraction of individual rare earths is a complex process, that leads in turn, a number of other complicated and expensive processes. According to Nair and his research group,[51] phosphors require an exceptionally clean chemical laboratory to synthesize very pure substances.

For the above reasons, white LEDs free of rare earths are desired. In that way, materials such as quantum dots and nanoparticles have been explored and acceptable results have been reported.[52,53] However, the use of organic dyes has gained new interest because they

have characteristics and optical properties that can be perfectly used in down conversion white LEDs.

1.3. White Light From Organic Materials.

Organic materials are mainly based on carbon atoms, their semiconducting properties arise from the delocalized π-electrons that can move along the conjugated chain. Due to their electronic configuration ($1s^2$, $2s^2$, $2p^2$), carbon atoms can form hybrid orbitals (sp^3, sp^2, *and* sp) where each atom has four valence electrons. Thus, a molecular orbital may be approximated by a linear combination of atomic orbitals. According to the valence bond theory, in conjugated materials, carbon atoms present sp^2 hybridization due to the merging of the *2s* orbital with two *2p* orbitals ($2p_x$, $2p_y$) which determine the geometry of the molecule. The overlap of $2p_z$ orbitals, which are not hybridized, form the π (bonding) and π* (antibonding). The extent of this overlap defines the conjugation length of the chain and determines the Highest Occupied Molecular Orbital - Lowest Unoccupied Molecular Orbital (HOMO-LUMO); the energy difference between HOMO-LUMO defines the bandgap of the conjugated material.[54]

Electroluminescence in organic materials was reported in early 1950s.[55] The first OLED was reported by Tang and Van Slyke in 1987.[56] The device was obtained by vacuum evaporation of organic small-molecule materials with a metallic cathode on a conductive substrate. The first OLED based on polymers was created in 1990 by Burroughs and co-workers with a single layer device of polyphenylenevinilene made by using a spin coating process.[57] Presently, OLEDs based on small molecules and polymers are feasible with similar performances for both materials.[58, 59]

OLEDs are devices of thin films fabricated from organic semiconducting materials with luminescent properties and working under the electroluminescence phenomenon. The

working scheme of OLEDs is shown in Figure 1.5. Electrons and holes are injected from the cathode and anode to the electron transport layer (ETL) and hole transport layer (HTL), respectively. Next, both charges cross the ETL and HTL to the emitting layer EML to form the electron-hole pair named exciton, which decays radiatively as photons.

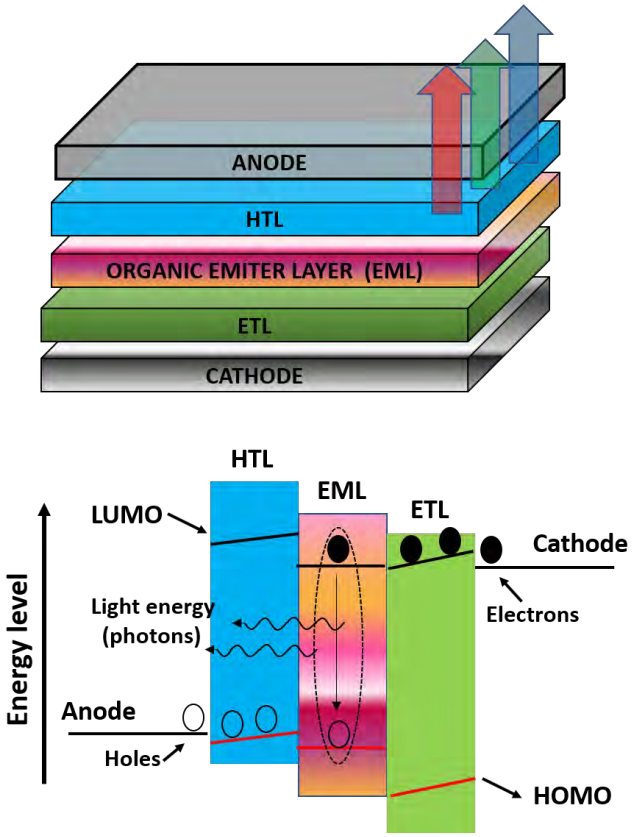

Figure 1.5. Basic architecture of Organic LED.[60]

In principle, a single emitter can only cover some spectral fraction of the visible light.[61] Thus, the emitted light would be produced by the mixture of complementary primary colors. Another possibility is trough intermolecular interaction that allows complementary emissions from excimer, exciplex or electroplex states. In either case, the matched materials and device engineering are necessary for obtaining a balanced and efficient white light.[62] The tandem configuration can also be considered, for this case independent OLEDs are stacked as shown in Figure 1.6a. Here, optical optimization is

challenging because the emitters must all be in an adequate position within the device structure for efficient out coupling. The main disadvantage is their difficult manufacturing process due to the high number of layers with the adequate energy level at each interface. If any of the interfaces has not the appropriate energy barrier, the device would not work properly.[63,64–66] Other two architectures for white light are the bi-layer structure with a blue and orange emitter,[67] see Fig 1.6b, and single layer doped with various dyes.[68] The former structure can be fabricated easier than the tandem, however, it could be difficult to fabricate if the HOMO-LUMO levels between the materials are not adequate; therefore, additional buffer layers would be required to balance the energy barrier.[69] The other architecture has been considered as one of the most convenient and simple approaches for white light OLED devices. For this case, multiple emitters (blue/orange, or red/green/blue) are incorporated into a single layer as shown in Figure 1.6c; this structure can offer a very simple fabrication process compared to other approaches. However, the concentrations of dopant emitters in this structure need to be precisely regulated since a very small change in the dopant concentration would lead to a pronounced variation in the energy transfer among the emitting molecules and the color balance would be unsuitable.[70,71]

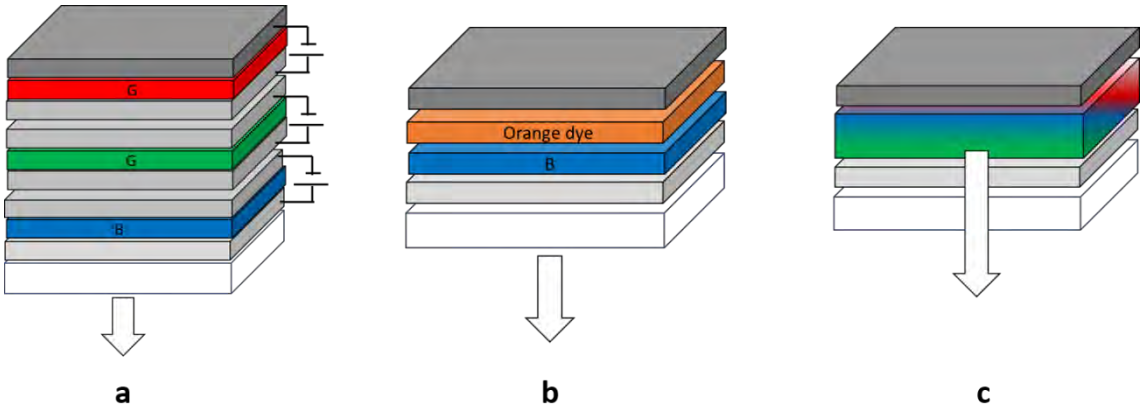

Figure 1.6. more conventional white OLED configurations. a) tandem, b) bi-layer structure with a blue and orange emitter, c) single -EML, doped with various dyes.

Other mechanisms less successful for WOLED devices such as blue OLEDs with external or internal down-conversion layers [72,73], the individual device units emitting red, green, and blue in a pixelated approach,[74] multilayer emission,[65,75] the single dopant-based devices using the monomer/excimer emission.[76–79] Nevertheless, WOLED devices offer a number of advantages such as fast response time, lambertian emission (wide viewing angle), low operating voltage, emission colors across the entire visible spectrum and the possibility of being fabricated over flexible substrates.[2,19,76,80, 81]

1.4. Alternatives Mechanisms to White LED and OLED.

As noticed above, although LEDs and OLEDs exhibit extraordinary properties that make SSL the most used in the lighting field today. It presents some disadvantages that new proposals and mechanisms could solve and aim to be the new generation of SSL, two of which will be developed in this thesis. In the case of OLED devices, contrary to multi-layer structures, mechanisms for easy fabrication, acceptable performance, and good white color are desirable, and one of these promising mechanisms is through

intermolecular interaction that allows emerging complementary emissions from excimer, exciplex or electroplex states.[82] Exciplex is a complex state generated by intermolecular interaction between two molecules, usually an electron donor (D) and acceptor (A) materials. In this complex, the electron-hole pair is formed with an electron in the LUMO level of one molecule and a hole in the HOMO level of another molecule. This complex generates new transitions which are of lower frequencies than the intrinsic transition (π - π^*). These additional transitions generate the widening of the electroluminescence spectrum and therefore white color coordinates would be obtained. One of the challenges to the formation of exciplex is to find materials whose HOMO and LUMO levels be suitable to allow this kind of intermolecular interactions.

On the other hand, another approach where organic fluorescent materials can be used to obtain white emission, is by using them as replacement of phosphors based on REE's in inorganic white LEDs. This would be the case of hybrid SSL, where LED excites organic dyes, and the LED emission together with dye emission will produce white light. These devices are known as hybrid luminescence converter (LUCO).

Outline of this thesis: After this introduction, is addressed the Experimental Method (Chapter 2). This chapter describes the materials, characterization, and equipment used to generate white light from two different mechanisms studied.

The first studied mechanism is "Exciplex States" in Chapter 3, divided into two sections. Section 3.1 describes the photophysical processes involving exciplex mechanisms and white light generation in OLEDs using this mechanism.

In Sections 3.2 are reported experiments and results using the emission of white light from one and two interfaces and using commercial and new materials as emissive layers.

The rule of the energy barrier value at the EML/ETL interface for white light emission is shown in sec 3.2.1. For this study, a commercial copolymer was used as the emissive layer and three electron transport layers with distinct HOMO-LUMO values. Hence with each ETL, a different energy barrier is formed at the EML / ETL interface. Sec. 3.2.2 describes the use of the optoelectronic properties of the CZDD compound, which allow intermolecular interactions with the HTL and the ETL, leading to a double emission at the corresponding interfaces. The luminance parameters of the fabricated devices as color and efficiency are reported and discussed.

The second mechanism is LUCO-Inorganic/Organic devices, Chapter 4. This chapter shows the generation of white light with hybrid devices by using the mechanism of Down-Conversion. This chapter is divided into two sections. Section 4.1 describes the down-conversion mechanism for the fabrication of hybrid devices. Section 4.2 describes the experimental study of the adequate organic converter's thicknesses to achieve white emission in LUCO devices. The partial down-conversion case and full down-conversion case are reported, respectively, in secs 4.2.1 and 4.2.2. For the former case, white light generation from the combination of a commercial blue LED plus the commercial copolymer ADS233YE is shown; additionally, the comparison of partial LUCO results with commercials white LED is presented. In the case of a full down-conversion, the generation of white light from different mixtures of organic compounds is discussed. For this study, were used two small organic molecules and two commercial copolymers as converters. Details such as the correct ratios between converters and color characterization were mainly described.

In Chapter 5, a brief comparison and discussion between WOLEDs and LUCOs are presented, pointing out advantages and disadvantages. In the following Chapter, general conclusions, perspectives, and future work are presented.

In Chapter 7, other contributions, a brief report of additional works as the manufacture of tunable OLEDs based on halochromism and thermochromism using an imidazole derivative, and the manufacture for matrix and encapsulation for OLED are presented, followed by the reference Section. In Appendix A, some definitions and concepts are given to help the reader in the subject, while in Appendix B, figures corresponding to the micrographics study are presented.

2. EXPERIMENTAL METHOD.

In this chapter, the experimental development for the exciplex and down-conversion studies are present.

2.1 Experimental Method for Exciplex Study.

Materials. The chemical structures of the organic materials used in the Exciplex study are shown in Figure 2.1. As emissive layer were employed; the commercial copolymer Poli[(9,9-dioctilfluorenil-2,7-dil)-co-(1,4-benzo-{2,1'-3}-tiadiazol)] (ADS232GE**)** obtained from American Dyes Sources and the small molecule 1,4-Bis(9H-carbazol-9-yl)phenyl)ethynyl)benzene (CZDD), which is a new carbazole derivative synthetized by Braulio Molina group from Universidad Nacional Autónoma de México (UNAM). Details of the synthesis as well as some physicochemical characterization of CZDD compound can be found in ref.[83] Compounds used as EMLs were Poly[(9,9-bis(3'-(N,N-dimethylamino)propyl)-2,7-fluorene)-alt-2,7-(9,9–dioctylfluorene)] (PFN), 2,2',2"-(1,3,5-Benzinetriyl)-tris(1-phenyl-1-H-benzimidazole (TPBi) and 4,7-diphenyl-1,10-phenanthroline (BPhen) obtained from Ossila while poly(3,4-ethylenedioxythiophene) polystyrene sulfonate (PEDOT:PSS; Clevios PVP AI4083) was the material used as HTL. ITO/glass substrates with 5–15 Ω/square were purchased from Delta Technologies employed as anode while Ca and Ag act as cathode and were acquired from Sigma Aldrich.

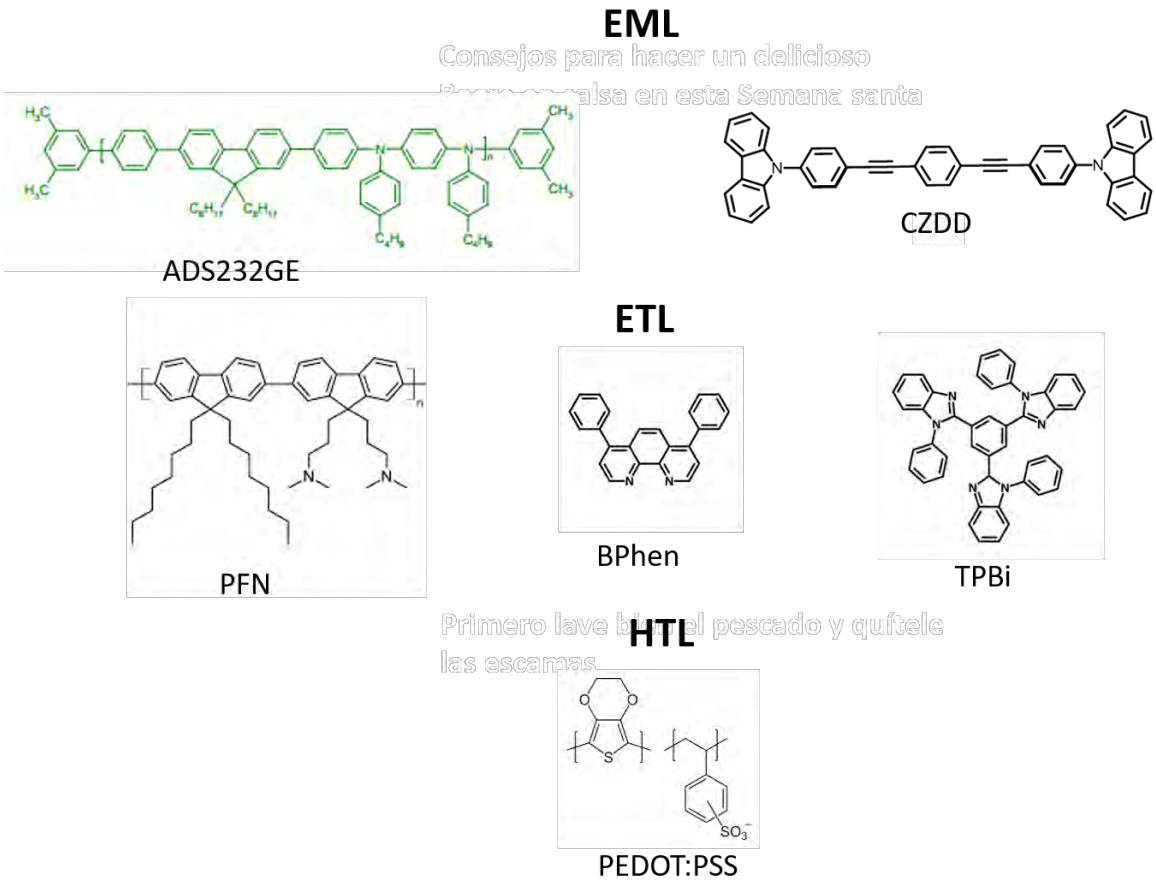

Figure 2.1.Chemical structure of the organic materials used in the WOLED devices.

OLED structures. Seven different OLED structures were tested to achieve exciplex and white emission. In the next table are summarized the different OLED structures employed.

Table 2.1. OLED structures of the different devices fabricated.

Name	Structure	HTL	EML	ETL
OLED-1	ITO/PEDOT:PSS/ADS232GE/Ca-Ag	PEDOT:PSS	ADS232GE	None
OLED-2	ITO/PEDOT:PSS/ADS232GE/PFN/Ca-Ag	PEDOT:PSS	ADS232GE	PFN
OLED-3	ITO/PEDOT:PSS/ADS232GE/TPBi/Ca-Ag	PEDOT:PSS	ADS232GE	TPBi
OLED-4	ITO/PEDOT:PSS/ADS232GE/BPhen/Ca-Ag	PEDOT:PSS	ADS232GE	BPhen
OLED-5	ITO/PEDOT:PSS/CZDD/Ca-Ag	PEDOT:PSS	CZDD	None
OLED-6	ITO/PEDOT:PSS/CZDD/BPhen/Ca-Ag	PEDOT:PSS	CZDD	BPhen

OLED-7	ITO/PVK/PEDOT:PSS/ADS232GE/Ca-Ag	PEDOT:PSS/PVK	CZDD	BPhen

Device fabrication and characterization. ITO substrates were cleaned with ethanol and then put through a 24-hour drying process. they were then subjected to another cleaning process and plasma treatment for 15 minutes. For OLED-1-4, PEDOT:PSS and ADS232GE were deposited using the spin coating method, with thicknesses of 40 and 80 nm, respectively. PFN was dissolve in a mixture of methanol-acetic acid (1:0.01), and also deposited by the spin coating method, the thickness of this film was 15 nm. BPhen, TPBi, Ca, and Ag were deposited by thermal evaporation method with a rate of 0.5 Å/s. For OLED-5-7, PEDOT:PSS thicknesses were 60 nm, 45 nm, and 30 nm. Then, substrates were transferred to an evaporation chamber and 100 nm of the CZDD compound was evaporated at 0.25 Å/s, the chamber pressure was 2×10^{-6} torr.

The thicknesses and micrographics of the organic layers were measured through Atomic Force Microscopy (AFM) Nanosurf EasyScan. The emissive area of samples was of 9 mm^2. OLEDs devices were characterized by J-V-L curves, a source-meter Keithley 2450 was used. The EL, luminance and CIE coordinates were measured with an Ocean optics USB4000 spectrophotometer, calibrated with the HL-3P-CAL lamp. Current efficiency and luminous efficacy were estimated from the values of luminance, voltage and current.

2.2. Experimental Method for Down-Conversion Study.

Materials. chemical structures of organic converters are shown in Figure 2.3. Poli[(9,9-dioctilfluorenil-2,7-dil)-co-(1,4-benzo-{2,1'-3}-tiadiazol)] (ADS233YE) was obtained from American Dyes Sources. The HOMO and LUMO levels of this material are 5.8 and 3.1 eV, respectively, measured by cycle voltammetry. The dyes were 4,7-

diphenylbenzo[*c*][1,3,5]thiadiazole (ACN1) green dye reported by Tsutomu et al.,[132] and 4,4'-benzo[*c*][1,3,5]thiadiazole-4,7-diylbis(tiophene-5,2-diyl))bis(*N,N*-diphenylaniline) (JP5) whose synthesis was reported by Kusakaky group.[133] Both dyes were synthetized in our laboratory by palladium cross coupling reactions from benzothiadiazol derivatives and fluorene moieties.[134] The material ADS232GE used in exciplex study also was employed in this down-conversion study. For partial conversion case, the blue LED employed was an InGaN LED (SMD 5730-BLUE-SAMSUNG-465 nm series). AlGaInP LED (465 nm) and InGa/GaN, were used to explore others LUCO configurations. While to full conversion case, a commercial InGaN UV-LED (385 nm) was used.

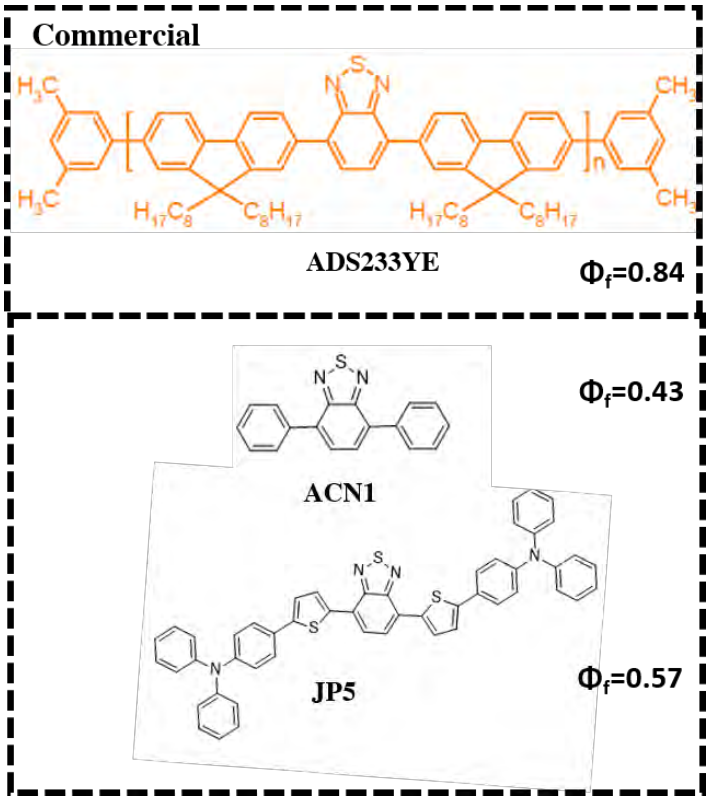

Figure 2.2. Chemical structure of Poli[(9,9-dioctilfluorenil-2,7-dil)-co-(1,4-benzo-{2,1'-3}-tiadiazol)] (ADS233YE) used as organic converter.

Fabrication and characterization of films. Films of these material were formed by spin-coating onto glass substrates. The concentration of ADS232YE was varied from 5 to 80 mg/ml in toluene solvent and the film thickness from 0.1 to 1.0 μm. ACN1 and JP5 were dissolved in chlorobenzene. Absorbance spectra were measured using a PelkinElmer UV-NIR Spectrophotometer, the quantum yield and PL by Edimburg Instruments Fluorometer (FS5 model). Thicknesses and micrographics were measured through Atomic Force Microscopy (AFM) Nanosurf EasyScan.

Fabrication and characterization of LUCO Devices. LUCO devices were fabricated as is illustrated in Figure 2.4a (partial conversion) and 2.4b (full conversion) where a commercial LED is used as the excitation source and a film of the converter is put on LED. For partial LUCOs were tested films at different concentrations and thicknesses. For full LUCO devices, the thickness and concentration parameters were optimized based on the study of the partial LUCO devices. Thus, the employed concentration was 35 mg/ml with thicknesses around ~0.5 μm at spin coating rate of 1500 rpm. ADS232GE and ADS233YE were dissolved in toluene while ACN1 and JP5 in chlorobenzene. All mixtures of the materials were dissolved in toluene solvent. EL and luminance with an Ocean Optics USB4000 spectrophotometer, calibrated with the HL-3P-CAL lamp and the energy efficiency by an Extech light meter. CRI, CCT and CIE coordinates were calculated from the luminance spectra.

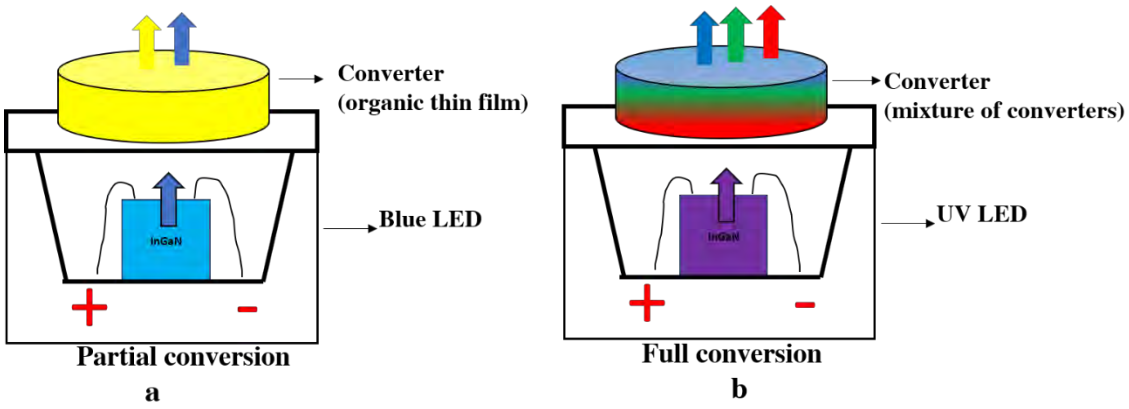

Figure 2.3. Schematic diagram of LUCO devices, a) Partial conversion; b) Full conversion.

The different structures and characteristics of the LUCO devices fabricates for partial and full down-conversion cases are summarized in Table 2.2.

Table 2.2. LUCO structures, LED, wavelengths of the LED λ and Thickness of the converter of THE devices fabricated in this chapter are summarizes in Table.

Case	Device	LED/λ(nm)	Converter	Thickness of converter (µm)
Partial down-conversion	LUCO	InGaN/465	ADS232YE	0.04 to 1
	LUCO A	InGaN/465	ADS232YE	0.59
	LUCO B	InGaN/465	ADS232YE	0.31
	LUCO C	InGaN/465	ADS232YE	0.94
	LUCO D	InGaN/460	ADS232YE	0.45
	LUCO E	InGaN-GaN/480	ADS232YE	0.45
	LUCO F	InGaN/465	ADS232YE	0.45
	FULL LUCO 1	InGaN UV- LED/380	ADS232GE:JP5	
	FULL LUCO 2	InGaN UV- LED/380	ADS232GE:ACN1:JP5	0.5 to 0.6

Full down-	FULL LUCO 3	InGaN UV- LED/380	ACN1:ADS233YE
conversion	FULL LUCO 4	InGaN UV- LED/380	ACN1:ADS233YE:JP5

3. EXCIPLEX STATES AND THE EMISSION OF WHITE LIGHT.

Exciplex is a bimolecular excited state complex and termed from the terms *exci* (excited state) and *plex* (complex). Exciplex states have been investigated since the 70's by different research groups. First studies with inorganic materials demonstrated that some noble gases such Ar, Xe or Kr with some halides like F, Br or Cl could form new electronic transitions. When these new transitions were considered within the laser technology, the exciplex/excimer laser showed up in the market.[84,85] More recently, for organic materials similar excited states were reported when a D and/or an A molecules interact with the emissive layer and new emissions occur besides the exciton emission; mainly, this mechanism has been exploited in WOLED devices.[86–88] Zhao et al.,[89] were one of the first group to report WOLEDs based on exciplex mechanism; they achieved white electroluminescence by mixing blue exciton emission with broad yellow-red exciplex emission. In other example, Jhulki and co-workers[90] reported exciplex formation by a twisted bianthryl core and TPBi, the devices exhibited CIE coordinates (0.28, 0.33) with acceptable luminance of 15,600 cd/m^2, however, the luminous efficiency reported was as low as 1.78 lm/W.

Excitons are generated by the bulk of the emissive layer meanwhile the emission of exciplex states takes place either within the bulk or at the interfaces of that layer.[91,92] For the former case, the D and A molecules are blended to form a film while for the latter case, termed interfacial exciplex, the D and the A molecules in the device are defined by two independent films which form an interface; here at least one of the two materials, either the D or the A, defines the emissive layer.[93,94 95] For example Angioni and his group reported a single emitting layer WOLED based on interfacial exciplex emission.[96] They synthesized a new benzothiadiazole derivative compound that was used as emitting material. It was found that this compound generated exciplex states at the interface with

the N,N′-bis(3-methylphenyl)-N,N′-diphenylbenzidine (TPD), used as HTL. In their work, the maximum achieved brightness was 5219 cd/m^2 with CIE coordinates (0.38, 0.45).

Exciplexes can be formed under light and/or electrical excitation, and therefore be observed in photoluminescence (PL)) and/or EL.[97] With this mechanism white OLED have been reported but challenges as good color and acceptable parameters still need to be faced.

3.1. Photophysical Description of Exciplex States in Organic Materials.

The photophysical analysis of the exciplex states has been described on the basis of quantum mechanics. When the photoluminescence (PL) or electroluminescent (EL) emitter consists of two-molecule, excited states can be formed since a located hole of the donor (D^+) approaches a located electron of the acceptor (A^-), and the exciplex states are defined as $|\mathrm{AD}\rangle^*$. This ket is defined by

$$|\mathrm{AD}\rangle^* = c_1|\mathrm{AD}\rangle^*_{LOC} + c_2|\mathrm{AD}\rangle^*_{CT} \qquad (1)$$

Therefore, $|\mathrm{AD}\rangle^*$ is the quantum mechanical mixing of the locally (LOC) excited states configuration $|\mathrm{AD}\rangle^*_{loc}$ and charge-transfer (CT) exciplex configuration $|\mathrm{AD}\rangle^*_{CT}$, which in turn express themselves by eigenfunctions of the Hamiltonian pair [61,98]

$$|\mathrm{AD}\rangle^*_{LOC} = a_1|A^*D\rangle + a_2|AD^*\rangle \qquad (2)$$

$$|\mathrm{AD}\rangle^*_{CT} = b_1|A^+D^-\rangle + b_2|A^-D^+\rangle \qquad (3)$$

Coefficients c_1 and c_2 in (1) determine the contributions of the LOC and CT configurations to the exciplex state, whereas in (2) coefficients a_1 and a_2 are the amplitudes of the two-component state of the local excited LOC configuration emerging as a result of the excitonic resonance between states $|A^*D\rangle$ and $|AD^*\rangle$ with the excitation

localized on the donor and the acceptor, respectively. Furthermore, coefficients b_1 and b_2 in (3) determine the amplitudes of two CT states $|A^+D^-\rangle$, and $|A^-D^+\rangle$.

The relation among amplitudes of various components of Eq. (1) and the exciplex energy E_{exc} depends on the difference between the ionization potential and electron affinity of the molecular components. In order for exciplex formation to occur, one of the molecules should have a small ionization potential (*IP*) so that it can donate an electron to the second molecule, which should have a high electron affinity (*EA*). The emission wavelength of the exciplex state is determined by the energy difference between the electronic affinity (EA_A) of the acceptor molecule and the ionization potential (IP_D) of the donor molecule (see Fig. 3.1).[99,100] It is possible to tune the emission wavelength by choosing compounds with appropriate energy levels.[95]

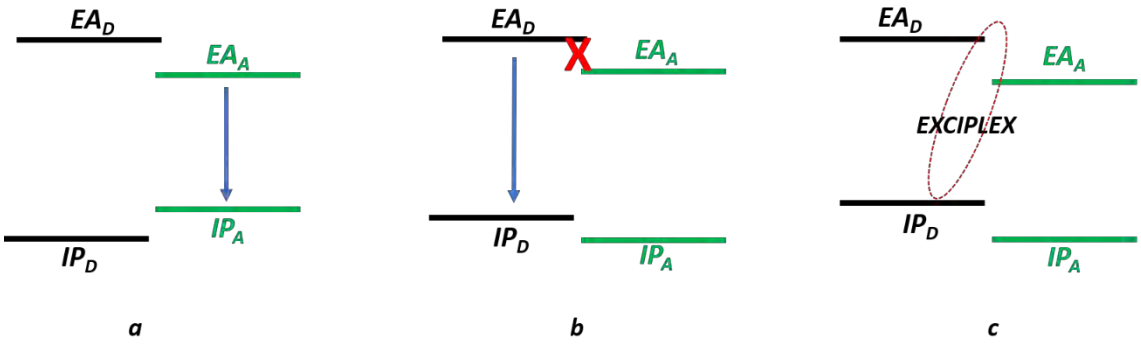

Figure 3.1.Typical relation of ionization potentials (IP) and electron affinities (EA) of organic materials. a) none of the materials is a donor or acceptor, charge transfer is not possible and the energy transfer can occur; b) donor and acceptor have very similar electron affinities, what makes electron transfer efficient but the exciton can be form at the donor or at the acceptor; c) the donor and acceptor with properly adjusted energy levels enough to the formation of an exciplex.

The peak of energy emission of the exciplex states is given by [95,101]

$$E_{exc} = hv_{exc}^{max} = IP_D - AE_A - E_C \qquad (4)$$

Where E_C is the coulombic attraction energy between the donor and acceptor thin films and defined by:

$$E_C = \frac{e^2}{4\pi\epsilon_0\epsilon_r} \qquad (5)$$

where e is the elementary charge and ϵ_0 and ϵ_r are the vacuum and relative dielectric constants, respectively.[97] Other mechanisms like electrochemical measurements for calculating exciplex energy were reported by Piotr et al.,[94] however, this involves to have the donor and acceptor materials in a solution that, in turn, requires approximations and calculations considering the materials in a gaseous state. These approximations are accepted for bulk exciplex.

Kalinosky[61] found that the shape of the emission spectrum depends on the composition of the mixed exciplex; large wavelengths transitions correspond to a substantial contribution of the CT excimer ($a \approx b$), and shorter wavelengths transitions correspond to a larger contribution of the LOC exciplex. From quantum mechanical calculations, it infers that no pure LOC and CT excimers can exist.

A typical interfacial exciplex OLED configuration is shown in Figure 3.2a. It consists of an anode, donator and acceptor films and an electrode. In the energy diagram of Figure 3.2b, it is shown how the mechanism of the generation of exciplex states is (here is not shown the intrinsic transition of the emissive layer that can be from the D or A). Electrons and holes are injected from the respective electrodes and the energy barrier, formed by the energy levels $LUMO_A$-$LUMO_D$ and $HOMO_A$-$HOMO_D$ between the acceptor (A) and the donor (D) molecules, play an important rule for the exciplex transitions to take place.

Note that due to the optoelectronic properties, the D and A molecules are also often used as transport hole layer (HTL) and as electron transport layer (ETL), respectively, this is for some OLED structures.

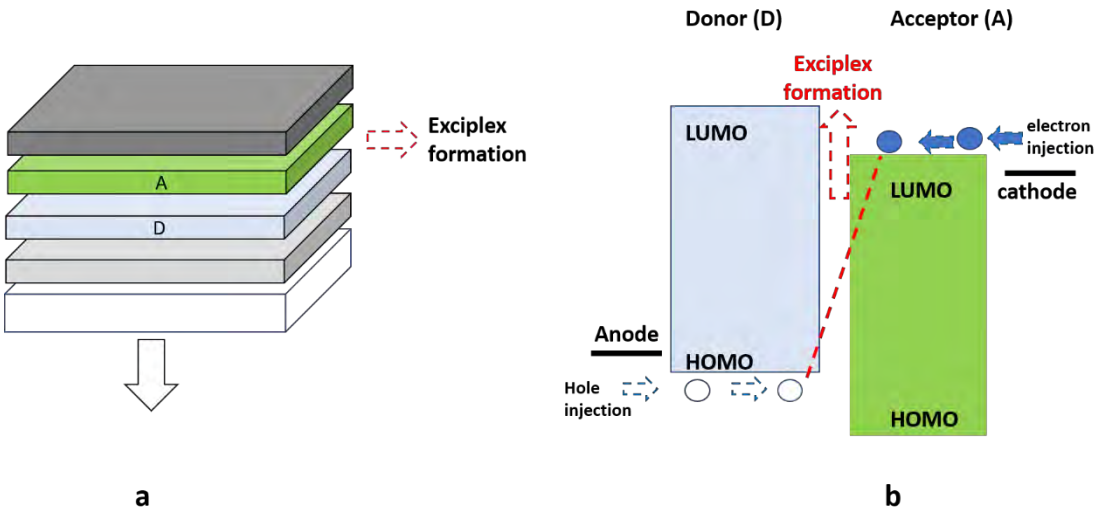

Figure 3.2. a) Basic interfacial exciplex OLED configuration, b) diagram levels of exciplex OLED configuration.

Experimental results from Luo and co-workers[102] are shown in Figure 3.3 which clarifies the white emission through exciplexes. In this work, they studied and fabricated WOLEDs based on the structure ITO/HAT-CN/TAPC/TmPyPB-II/ TmPyPB-I/LiF/Al, where 1,4,5,8,9,11-hexaazatriphenylene hexacarbonitrile (HAT-CN) and 1,3,5-tri(m-pyrid-3-yl-phenyl)benzene (TmPyPb-I) were used as HTL and ETL, respectively; while 1-bis[4-[N,N-di(4-tolyl)amino]phenyl]-cyclohexane (TAPC) (HOMO level of 5.3 eV) as the hole injection layer HIL and TmPyPB-II (LUMO=2.4 eV) was yellow emissive layer. Here due to the optoelectronic properties of TAPC and TmPyPB-II, they act as the D and A molecules, respectively.

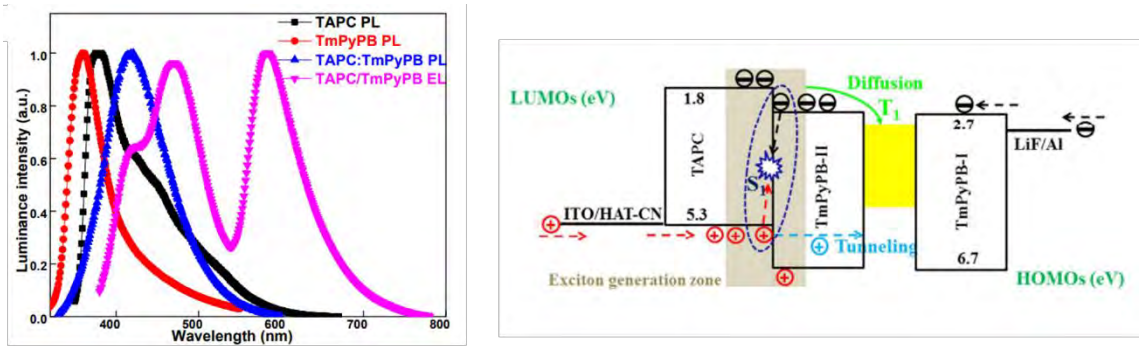

a b

Figure 3.3. Example of exciplex mechanism to white OLEDs, a) PL and EL spectra, b) energy diagram scheme of the WOLED device. The figures were taken from Luo's work. [102]

Figure 3.3a shows the PL emission of the compounds TAPC (black line), and TmPyPB (red line) with main emissions centered at 370 and 390 nm, respectively. When comparing these PL spectra, the TAPC:/TmPyPB spectrum (blue line) exhibit a red-shifted emission with the peak of 421 nm. The energy gap between the HOMO of TAPC and LUMO of TmPyPB is close to the energy of this new emission (2.9 eV), suggesting that exciplex states have been generated. Besides, in EL a wide spectrum (pink line) that corresponds to white light was observed with three main transitions (425, 468 and 585 nm); as none of the peaks of this spectrum correspond to the intrinsic emission of TmPyPB (the emissive layer) it can be concluded that the white emission emerged from exciplex states. Figure 3.3b illustrates the working mechanism of the WOLED using the diagram energy. Luo's work[102] also serves to illustrate that depending on the excitation source, light or electrical, those states can be observed. The exciplex emission at 425 nm was observed in PL only, meanwhile in El the other two (468 and 585 nm) emerged.

For the generation of exciplex states, compounds with strong blue photoluminescence (PL) are promising materials because exciplex states lead to a widening of PL spectra.[61,93,103–105] Considering this, materials such as carbazole derivatives have been studied extensively.[106–108] For example, Zassowski et al.,[109] studied the exciplex properties in an interface between new compounds synthesized of carbazole-triazine derivatives and the acceptor materials such as BPhen or TPBi. They used the structure ITO/HTL/carbazole-triazine derivatives/BPhen or TPBi/Ca/Al and reported CIE coordinates of (0.24, 0.35) and (0.27, 0.48) for devices with BPhen and TPBi, respectively. It is expected that with the help of exciplex, WOLEDs could be exhibited high efficiencies as well as lowered the fabrication cost, beside of good color coordinates (CIE and CRI), performance and emission tuning.[110–113]

3.2. Experimental Study of WOLED based on Interface Exciplexes.

As pointed out previously, the exciplex stated can be formed either into the emissive layer or at the interfaces of emissive layer with transport layers. While the former could mean an easier technique for WOLED fabrication, the control of interactions between D and A molecules into the mixture of active layer is a challenge. On the other hand, the formation of exciplex at the interfaces of active layer allow to control of the interactions of D and A molecule by changing the thickness of the films. Therefore, all the devices here studied are based on exciplex formed at interfaces of emissive layer.

3.2.1. The Role of the Barrier Energies in the Formation of the Exciplex States.

In a first approach, a WOLED was fabricated with the architecture: Glass/ITO/PEDOT:PSS/ADS232GE/ETL/Ca-Ag based on exciplex states. Three

materials have been used in these devices as ETL, which in turn have different HOMO-LUMO values. Therefore, the formation of exciplex states at an interface was investigated by examining the role of the barrier energies formed by ADS232GE and ETL.

The absorbance (Abs) and PL normalized spectra of ADS232GE, PFN, TPBi, and BPhen are shown in Figure 3.4. The EML show the peaks of absorption and emission at 385 and 460 nm, respectively, which correspond to the electronic transition π-π*. The Abs peaks to PFN, TPBi, and BPhen are 280, 300, and 415 nm, respectively. These materials used as ETLs exhibit a very weak PL response center at 637, 380 and 395 nm to PFN, TPBi and BPhen, respectively.

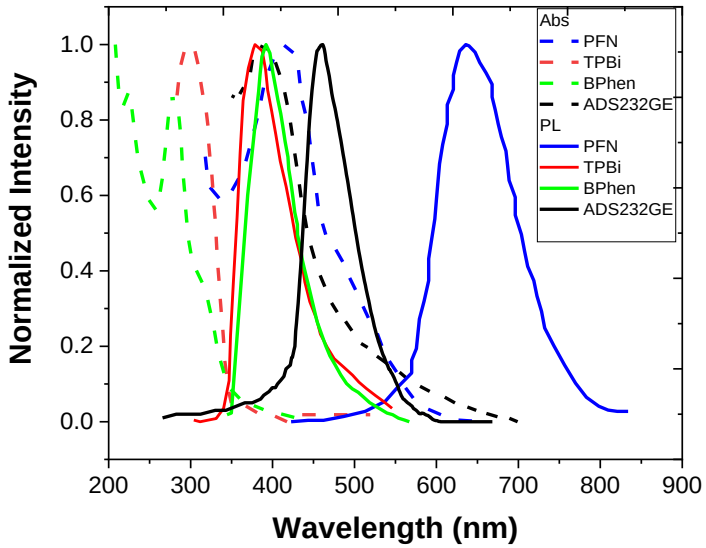

Figure 3.4. Absorbance spectra of the EML and the ETLs (PFN, TPBi and BPhen).

In Figure 3.5a shows the normalized EL spectra, at the same bias voltage (8 V), for representative fabricated devices. Spectra without be normalized are shown in Figure 3.5b. OLED-1 is the pristine device without ETL while 2, 3 and 4 correspond to devices with PFN, TPBi, and BPhen, respectively. The EL spectra for OLEDs 1 and 2 exhibited

a similar shape with a maximum emission wavelength at 490 nm. Since the EL spectra of these devices and the PL spectrum of the EML are similar, then can be established that the EL emission comes only from active layer, the CIE coordinates shown were (0.19, 0.24) corresponding to blue color. Subsequently, OLED-3 was fabricated; in this device, two main peaks can be observed, the first centered at 490 nm that corresponds to EML emission and the other peak centered at 570 nm that is assigned to exciplex states. Similar results were observed for OLED-4 but the peak assigned to exciplex states emerged at 620 nm. For device 4, the white light with CIE coordinates (0.30, 0.38) can be classified as warm white light. While for OLED-3 with CIE coordinates (0.26, 0.29) corresponds to quasi cold white light. Despite the EL spectrum of OLED-3 was broaden, the new transition (centered at 570 nm) did not allow to achieve a pure white, i.e. and emission with CIE coordinates (0.33, 0.33).

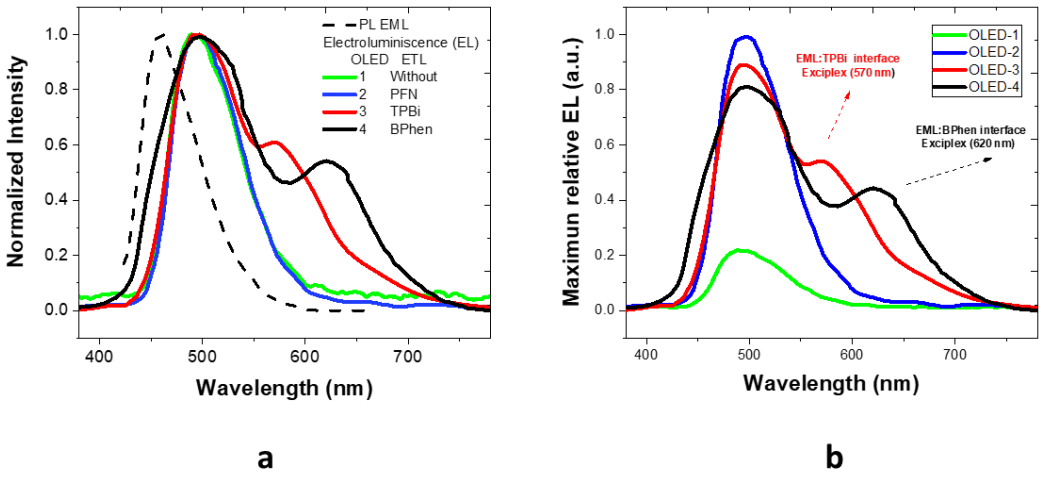

Figure 3.5. EL spectra of the OLEDs-A-D, a) Normalized EL; b) relative EL.

To analyze the differences in the EL emission of the four devices, the energy diagram of each device is shown in Figure 3.6. As can be seen in the schematic energy diagram of the OLED-1, holes are injected from ITO to the EML through the PEDOT:PSS while the electrons are injected directly from the cathode (Fig. 3.6a). Due to the absence of ETL, in

this device an imbalance in the injection of charges could be occur. This could be the reason for the weakest intensity in EL (see Fig. 3.6b). For the case of the OLED-2, a very low energy barrier of just 0.1 eV is at the ADS233GE/PFN interface; therefore, PFN help to enhance the electrons injection and a better charge balance than OLED-A could be achieved increasing EL intensity. For OLEDs 1 and 2, holes, and electrons are recombined at the emissive layer, therefore, only transition within the EML was observed in the EL spectrum. For the case of OLED-3, the energy barrier in the interface EML / ETL is of 0.3 eV whose value is enough to avoid the efficient electron injection from the LUMO of TPBi to LUMO of the EML leading to the formation of exciplex states. Due to this energy barrier, a fraction of electrons is accumulated in the LUMO of TPBi that bond with holes at the HOMO of the ADS232GE leading rise to formation of an exciplex state. Whereby, a new peak at 570 nm emerged in the EL spectra. For device 4, the energy barrier is 0.6 eV, thus, the exciplex states could also formed with a peak emission at 620 nm.

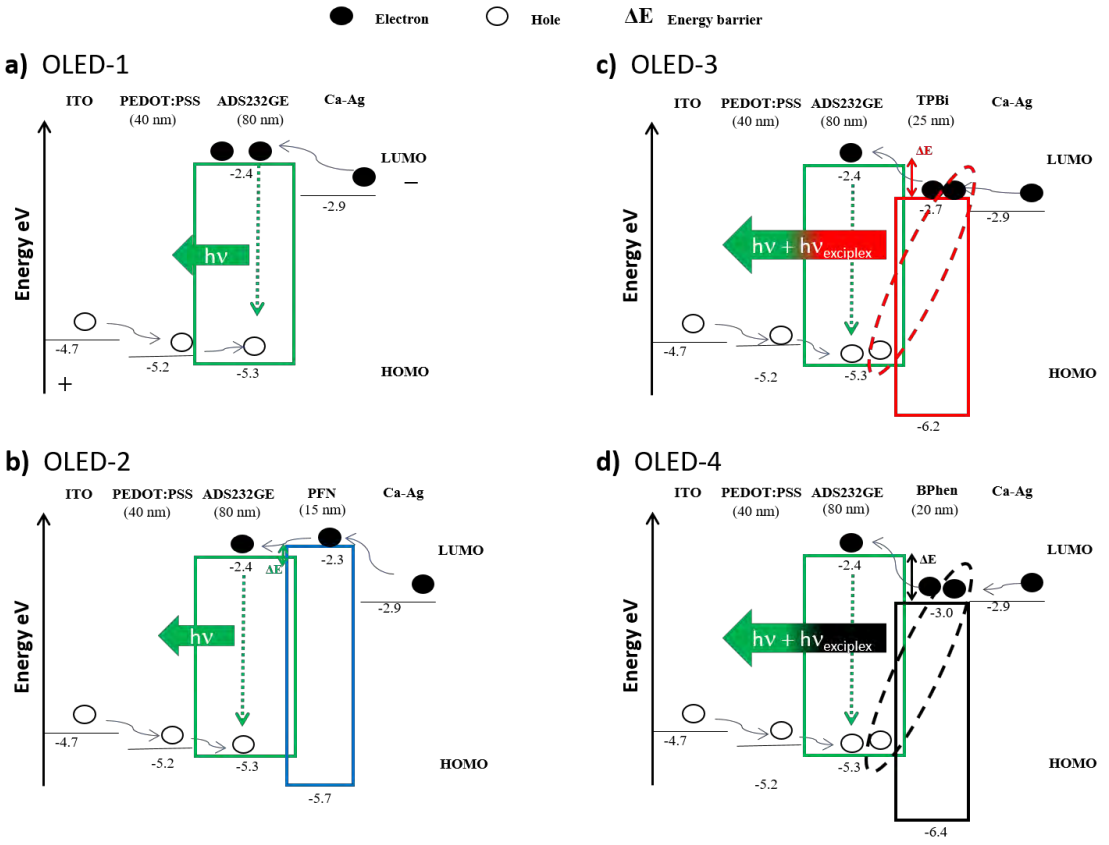

Figure 3.6. Schematics energy levels of the OLED devices, a) OLED-A; b) OLED-B; c) OLED-C; d) OLED-D.

According to Eq. (4) ($E_{exc} = hv_{exc}^{max} = IP_{EML} - AE_{ETLs} - E_C$), the exciplex energy of OLED-4 is lower than OLED-3 and for that reason the spectrum had broaden red-shift, thus, a better white emission. Theoretical exciplex energies were calculated, assuming that $IP \approx$ HOMO of the EML and $AE \approx$ LUMO of ETLs; the values were 2.6 eV (λ=476 nm) and 2.3 eV (λ540 nm) to OLED-3 and OLED-4, respectively. It is worth recalling that the emissive layer would have both properties as 4 and 1 and it is the case for ADS232GE; however, PFN, TPBi, and BPhen exhibit acceptor properties. Although the theoretical values do not have a high degree of correlation with the experimental values, it must be taken into account that the HOMO-LUMO energy values, as well as the

equation 4, are approximated values. The energy barriers and the exciplex transition for each device are summarized in Table 3.1.

Table 3.1. energy barriers and exciplex transition from $E_{exc} = hv_{exc}^{max} = IP_{EML} - AE_{ETLs} - E_C$ *for the devices fabricated.*

Device	Interface	Energy barrier (eV)	E_{exc} (eV)
OLED-1	None	*NM	None
OLED-2	ADS232GE/PFN	0.1	None
OLED-3	ADS232GE/TPBi	0.3	2.6
OLED-4	ADS232GE/BPhen	0.4	2.3

J-V-L curves characteristic of the four devices are shown in Figure 3.7. The threshold voltage, which is the minimum voltage to overcome the energies barriers and thus inject charges into the device, was 8.1 V for OLED-1 while for OLEDs 2-4 were 4.4, 5.1, and 5.8 V, respectively. The evident reduction of the threshold voltage for OLED-2, according to Koehler[54] was related with a better alignment of the energy levels of all layers that form the OLED, particularly for the PFN/Ca-Ag and EML/PFN interfaces. Thus, the improvement in the injected electrons allowed a considerably enhanced in the luminance that was of 4800 cd/m^2 while for OLED-1 was of 2090 cd/m^2. Similar results were achieved using BPhen and TPBi as ETLs; these layers formed a better energy alignment with the cathode than the EML/Ca-Ag (compared with OLED-1) but poorer than OLED-2. However, OLED-3 showed the highest luminance (5400 cd/m^2). This can be explained because the energy barrier of 0.3 eV was adequate to a better electrons injection and the balance charge was improved. This result implies that the number of holes-electrons pair increased in the recombination zones (inside EML and in the interface EML/TPBi) and thus, the number of photons generated is higher.

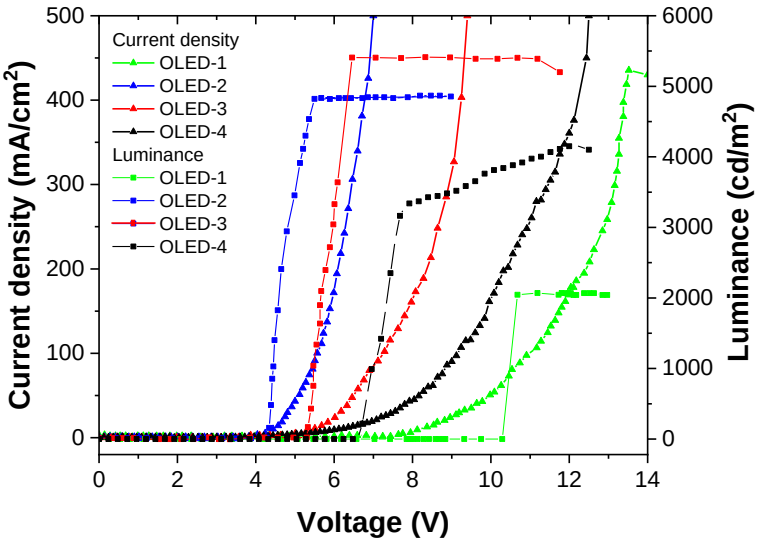

Figure 3.7. J-V-L curves of devices OLED-1-4.

Opto-electronics parameters for the four devices are summarized in Table 3.2.

Table 3.2. Opto-electronics parameters of the OLED devices.

Device	**threshold voltage (V)**	**Luminance max (cd/m²)**	**Energy barrier ETL/EML (eV)**	**CIE (x,y)**	**Color emission**
OLED-1	8.1	2090	*NM	(0.19, 0.24)	Blue
OLED-2	4.4	4800	0.1	(0.19, 0.24)	Blue
OLED-3	5.1	5400	0.3	(0.26, 0.29)	Quasi cold white
OLED-4	5.8	4160	0.4	(0.30, 0.38)	Warm white

*NM: No Measurement

Based on these results, the energy levels of the materials used play an important rule for the formation of exciplex states, as does the barrier energy formed in the ADS232GE/TPBi and ADS232GE/BPhen interfaces (0.3 and 0.6 eV respectively). For energy barrier around 0.1 eV the exciplex formation is not enable because the electrons were easily injected into EML and the recombination only occurred on it. These results

are according to Matsumoto et al.[114] who reported that values for energy barriers in the range of 0.6 - 0.8 eV allowed for a good formation of exciplex states; however, they also reported that for values lower than that range, exciplex states are not appreciable, which is contrary to our results.

3.2.2. White OLED based on Two Interface Exciplex Emissions.

The formation of exciplex states is usually observed at one of the EML interfaces, and mainly at interface with ETL. However, few reports have also reported exciplex formation at the HTL/EML interface. In our second approach of the prepared WOLED devices based on exciplex states, the compound 1,4-Bis(9H-carbazol-9-yl)phenyl)ethynyl)benzene (CZDD, Fig. 2.1) was used as EML. Micrographics of PEDOT: PSS and CZDD films are shown in the Appendix B (Fig. B.1 and B.2, respectively). The roughness of PEDOT: PSS films for the different thicknesses examined is less than 2 nm, while that of CZDD is 4 nm. The latter suggests an optimal contact between the layers, which is advantageous for the intermolecular interaction at the interface.

The compound CZDD contains two carbazole units attached to a π–bridge composed of three phenylene rings with a fully coplanar conformation. The highly π–π interaction of the π–bridge increases and enhances the electro-donating behavior of the two carbazole units. The normalized PL spectrum of compound CZDD in the solid state is showed in Figure 3.8a; the PL spectrum shows two shoulders centered at 430 and 480 nm that can be attributed to π- π^* and n-π^* transitions.

To explore the possible formation of exciplex at HTL/EML interface, the layer of HTL was varied to try to induce the accumulation of holes at this interface. Therefore, three different devices with this architecture were prepared by changing the PEDOT:PSS

thicknesses (60 nm, 45 nm and 30 nm). Others thicknesses for PEDOT:PSS were also tested, however, for thicknesses greater than 60 nm and less than 30 nm, the devices did not function properly and this was attributed to the imbalance of charge carriers inside the device. The devices prepared have the architecture ITO/PEDOT:PSS/CZDD/Ca-Ag, Figures 3.8b and 3.8c show the energy diagram of the two architectures. For OLED-5, without ETL layer (BPhen), it can be inferred that electrons are injected directly to the LUMO level of the emitting layer while the holes are injected to the HOMO level of PEDOT:PSS, and then to the HOMO level of the CZDD. In OLED-6, the electrons are injected first to the LUMO of BPhen and then to the emissive layer.

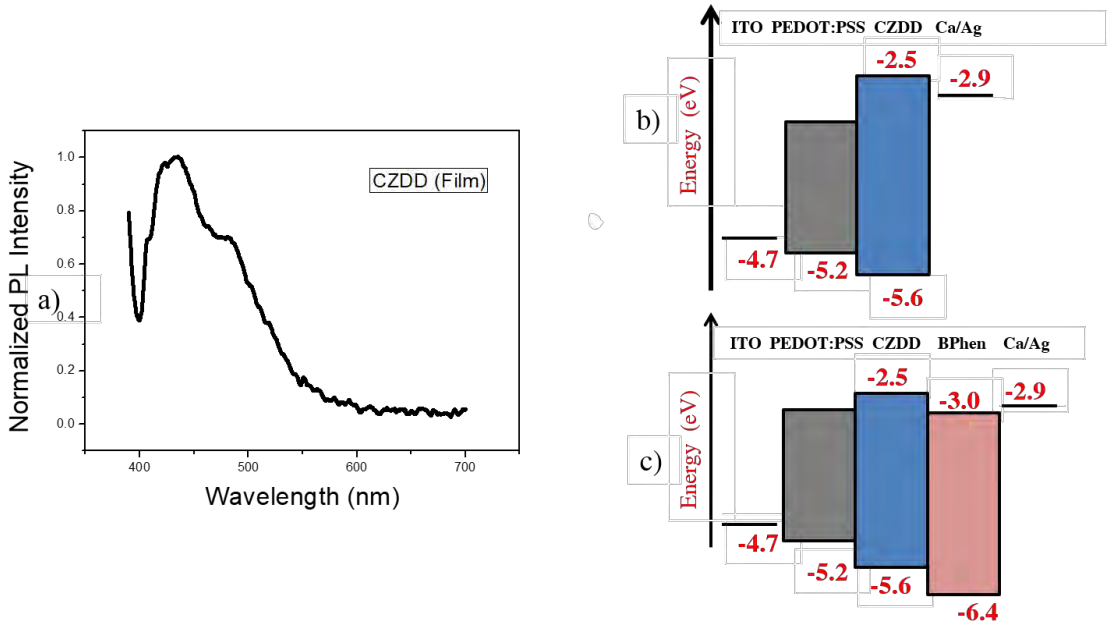

Figure 3.8. (a) Normalized PL spectrum of the CZDD material. (b)Energy level diagram of OLED-5 and (c) OLED-6; the energy band gap of CZDD is 3.1 eV with LUMO and HOMO (measured by cyclic voltammetry) levels at -2.5 and -5.6 eV, respectively.

The turn-on voltages of these devices were between 7 and 8 V. Figure 3.9 shows the PL of CZDD and EL spectra for OLED-5. The EL spectra are shown at the same driving bias of 14 V. The EL spectrum of OLED-5 with a HTL of 60 nm is similar to the PL of CZDD,

indicating that the emission is mainly due to transitions from excitons formed in EML. Nevertheless, a small shift and broadness of the spectra is observed due to the emission of exciplex states. As the thickness of the PEDOT:PSS decreases, the emission at 443 nm does, and concomitantly the peak intensity increases for emissions with wavelengths longer than 482 nm.

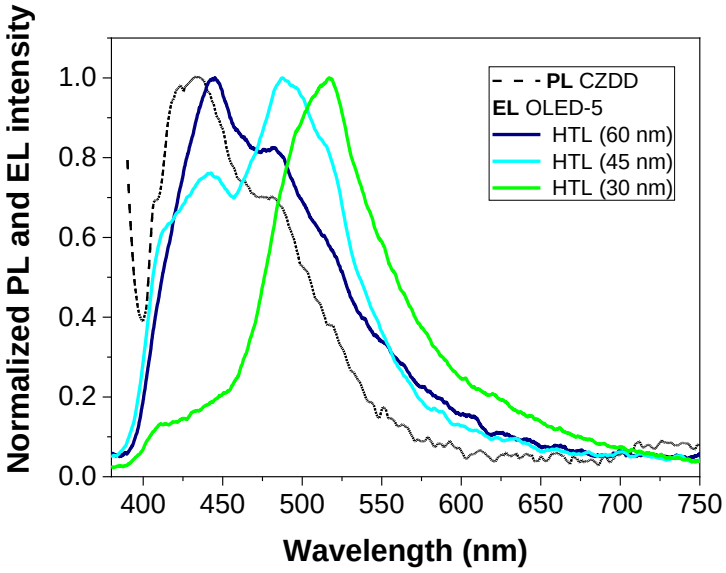

Figure 3.9.PL spectrum of the CZDD and EL spectra (bias 14 V) of the devices manufactured with the OLED-5 structure; the PEDOT:PSS thickness were 60 nm, 45 nm and 30 nm.

A similar behavior has been observed previously for white OLEDs due to the variation of the thickness of the organic layers. For example, Yang et al.,[82] reported the generation of white light with the structure ITO/TAPC/BCP/Al and found that increasing the thickness of the 2,9-dimethyl-4,7-di(phenyl)-1,10-phenanthroline (BCP) from 10 to 30 nm, the emission centered at 450 nm decreased, while the emission peak centered at 580 nm increased. This fact was attributed to exciplex transitions and they concluded that the film thickness of the acceptor layer is an important factor that influences the generation

of intermolecular states. Chapran et al.,[111] also reported that varying the thickness of BODIPY derivative from 70 to 4 nm allowed the emergence of exciplex emission. They concluded that thicknesses of materials for WOLEDs are associated with different roles. Therefore, depending on the thickness, the material can provide only the transport and injection of carriers or it can take part in the formation of exciplex states.

Table 3.3 shows the measured CIE coordinates and the wavelength of maximum emission for OLED-5. From this Table and the information in Figure. 3.9, it is evident that the color of the emission changed from blue to greenish for thicknesses of 60 nm and 30 nm of HTL, respectively (this is a color tuning shown in Fig. 3.16 below). A similar result has been reported by Kulkarni and Jenekhe,[115] who observed that according to the thicknesses of the acceptor layer, the exciplex emission from interfaces can compete with exciton emission from the emissive layer. Due to the generation of exciplex states, the blue EL emission from a bilayer system used by Kulkarni changed gradually to yellow. By changing film thickness from 43 to 7 nm in that device, transitions with yellow emission increased while the blue EL band blue-shifts from 469 to 435 nm.

Considering this, it is possible to modify the emission spectrum of the device by generating exciplex states. As reported above, the energy barrier plays a very important role to injection of charge or to the exciplex formation. In this case, to generate exciplex states at the interface of the HTL and the emissive material the barrier energy between the HOMO levels are required. If this energy difference is small, most of the resulting emission will come from excitons; in contrast, if it is large enough to generate a high-energy barrier, holes might not be injected to the emissive layer.

For the OLEDs reported here, positive carriers moving into the HTL faces an energetic barrier of 0.5 eV at the interface with CZDD (see level diagram in Fig. 3.8b), that does not allow them to be injected efficiently into its HOMO energy level. When the thickness

of the HTL layer is reduced, a positive charge accumulation takes place at the HTL/CZDD interface, which allows intermolecular interactions with electrons in the LUMO level of CZDD. Therefore, exciplex states are generated and emission at longer wavelengths than the emission of exciton states is observed. Thus, the color of the emission will change as the thickness of the HTL diminishes.

Table 3.3. CIE coordinates and maximum wavelength of emission for devices with architecture glass/ITO/PEDOT:PSS/CZDD/Ca/Ag for three different thicknesses of PEDOT:PSS layer (60 nm, 45 nm and 30 nm). Driving voltage = 14 V.

PEDOT:PSS	**60 nm**	**45 nm**	**30 nm**
CIE (x, y)	(0.20, 0.22)	(0.22, 0.28)	(0.26, 0.45)
$\boldsymbol{\lambda_{Max}}$ **(nm)**	440	490	525

For the CZDD compound the formation of exciplex at the EML/ETL interface was also studied, for which, a thin layer of BPhen (15 nm) was added in between emissive layer and cathode (OLED-6, see Fig. 3.8c). The thickness of HTL was fixed at 60 nm based on the results of OLED-5. Figure. 3.10 shows the PL spectrum of CZDD compound as well as the EL spectra for OLED-5 and OLED-6, both at a driving voltage of 12 V. Gratifyingly, the EL spectrum of OLED-6 broadened with the addition of BPhen, and excellent CIE coordinates (0.31, 0.33) were achieved. This broadening can be explained by assuming that intermolecular interactions take place between CZDD and BPhen and therefore new exciplex states were generated. These exciplex states might be generated due to charge accumulation at the CZDD/BPhen interface due to difference in energy values of the LUMO levels (see Fig. 3.8c), leading to emit at longer wavelengths than those observed in OLED-5 as shown in Figure 3.10.

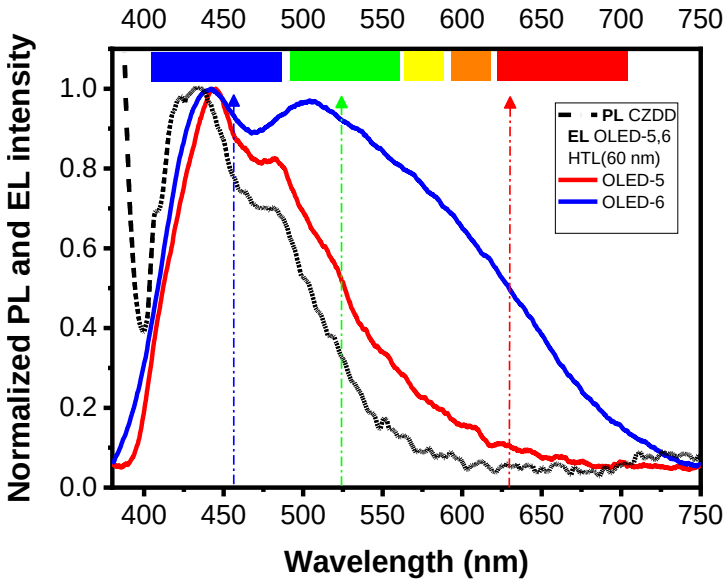

Figure 3.10. Normalized EL spectra for OLED-5 and OLED-6 (bias 12 V) with PL spectrum of the CZDD; both OLEDs have the same HTL thickness (60 nm).

The CIE coordinates for OLED-5 and OLED-6 were measured at several driving voltages (Table 3.4). It is important to note that for OLED-5 white light coordinates were not observed, but for OLED-2, for all reported voltages, the measured coordinates correspond to those identified as white light. Even more, the coordinates are closer to the ideal for white emission (0.33, 0.33) at voltages 12 and 13 V. Figure. 3.11 shows two pictures, one for the blue-greenish emission, OLED-5 (Fig. 3.11a), and other for the best operating device with white light emission, OLED-6 (Fig. 3.11b).

Table 3.4. CIE coordinates of OLEDs-5 and OLEDs-6 devices for different applied voltages and with HTL thickness of 60 nm.

Device	**CIE COORDINATES**				
	11 V	12 V	13 V	14 V	15 V
OLED-5	(0.20, 0.24)	(0.21, 0.23)	(0.20, 0.23)	(0.20, 0.22)	(0.21, 0.22)

OLED-6	(0.30, 0.33)	(0.31, 0.33)	(0.31, 0.33)	(0.29, 0.34)	(0.29, 0.32)

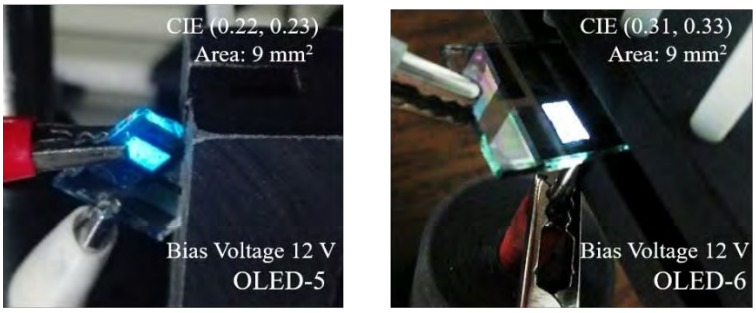

a) b)

Figure 3.11. (a) Bluish emission for OLED-5. (b) White light emission of OLED-6.

The luminance curves for the fabricated devices OLED-5 and OLED-6 are shown in Figure 3.12a. The maximum values of luminance were 2100 and 2900 cd/m^2 for OLED-5 and OLED-6 respectively, at about 14 V. Even though this can be considered as a moderate value, is relevant to emphasize that our devices have a greatly simplified structure. The graphs of current efficiency (η_{CE}) and luminous efficacy ((η_{PE}) (power efficiency) are shown in Figure 3.12b. The maximum values of current efficiency and power efficiency for OLED-5 were 4.3 cd/A and 5.2 lm/W respectively while those for OLED-6 were 4.5 cd/A and 6.3 lm/W, these reached values can be compared with other recent white OLEDs reports.[90,96,109,116] Table 3.5 compares some of the main parameters of the fabricated OLEDs; each value is the average of 16 samples. Notice that when BPhen was added, the parameters improved due to the better balance in injection of charge carriers. Likewise, in this same Table the OLEDs parameters of WOLEDs based on exciplex emissions reported in other works were added to compare.

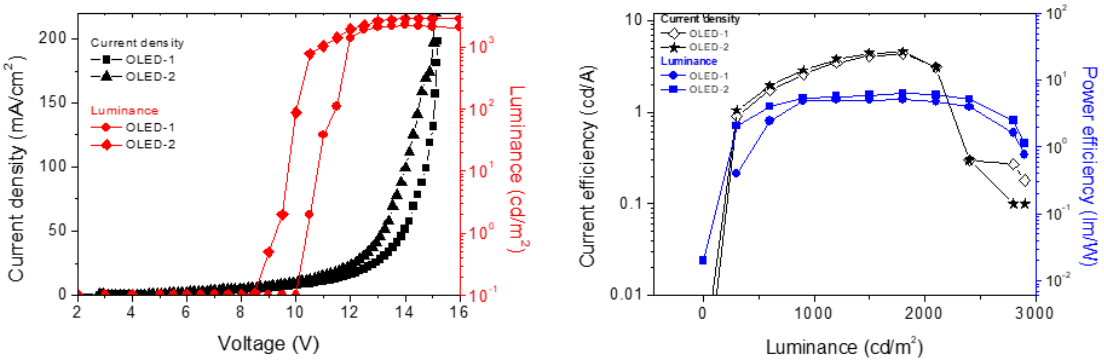

a) ***b)***

Figure 3.12. (a) J-V-L curves for the OLED-1 and OLED-2. (b) Current efficiency and luminous efficacy as function of the luminance for both OLEDs.

Table 3.5. Optoelectronics parameters of OLED-5 and OLED-6. Other WOLEDs that were reported by other groups are shown to compare.

Device	**Turn-on voltage (V)**	**Luminance (cd/m^2)**	**$\eta_{CE, Max.}$ (cd/A)**	**$\eta_{PE, Max.}$ (lm/W)**	**CIE (x,y)**
OLED-5	7.0 ±1.0	2100	4.3	5.2	(0.21, 0.23)
OLED-6	6.5 ±1.0	2900	4.5	6.3	(0.31, 0.33)
Ref[90]	3.0	15600	2.2	1.8	(0.28, 0.33)
Ref[96]	5.8	5219	6.5	2.6	(0.38, 0.45)
Ref[109]	6.7	749	0.25	0.1	(0.33, 0.37)
Ref[116]	8.5	10180	6.54	Not reported	(0.31, 0.38)

It is important to note that both OLED-5 and OLED-6, showed exciplex emissions but from different interfaces, particularly, those formed at the CZDD/BPhen interface produced white light emission. It could be due to the energy barriers of energetic levels between transport and emissive layers. The barrier for HOMO energy levels between PEDOT:PSS and CZDD is 0.4 eV, meanwhile the energy difference between the LUMO

energy levels at the interfaces CZDD/BPhen is 0.5 eV. The energy barrier leading to a higher charge accumulation and then exciplex states formation is illustrated in Figure 3.13.

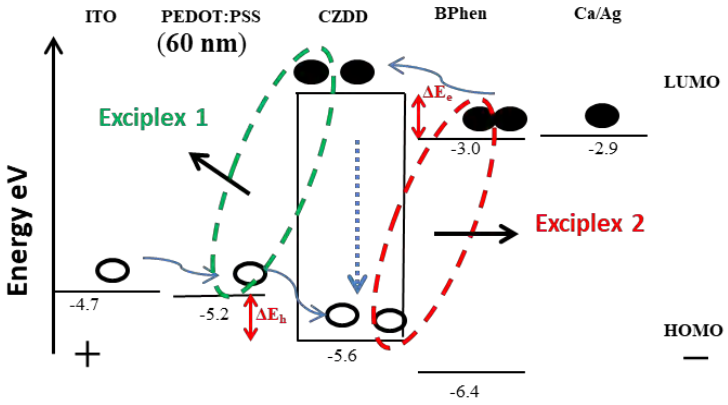

Figure 3.13. Scheme for the exciton and exciplex transitions in OLED devices. The emission of excitons is due to transitions within CZDD, meanwhile the exciplex emission 1 and 2 comes from transitions, that occur at the PEDOT:PSS/CZDD and CZDD/BPhen interfaces due to intermolecular interactions.

From the EL spectra, the energy ($E_{exc} = h\nu$) values of exciplex 1 and exciplex 2 were estimated. For the former is about 2.4 eV corresponding to λ=520 nm and contributed the greenish emission. The second one is 2.0 eV corresponding to λ=600 nm, reddish emission.

Subsequently, for OLED-6, the thickness of PEDOT:PSS was also varied to 60 nm, 45 nm and 30 nm; Figure 3.14 shows the EL spectra for such devices. These emissions show similar behavior than those observed for the configuration OLED-5 in Figure 3.9, i. e., the EL spectra were broadened as the thickness of the PEDOT:PSS was diminished. These changes in the spectra suggest that a white tuning could be reached for our devices because of the generation of exciplex states in both interfaces. Therefore, when the

thickness of the HTL was changed to 45 and 30 nm in this structure, the emission changed from cold to warm white emission.

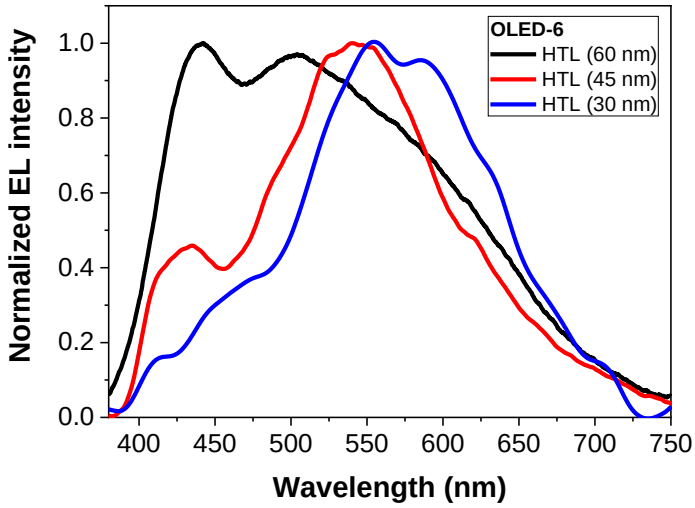

Figure 3.14. EL spectra to OLED-6 varying the thickness of the PEDOT:PSS (60 nm, 45 nm and 30 nm).

According to Equation 1, exciplex states could also occur due to the excitation of light. Therefore, films of the PEDOT:PSS-CZDD and CZDD-BPhen blends were made and their PL was measured. The CZDD-BPhen films exhibited a new emission peak centered on 600 nm as shown in Figure 3.15 so that the generation of exciplexes between these two materials was verified, while for the PEDOT:PSS-CZDD film the output of CZDD only.

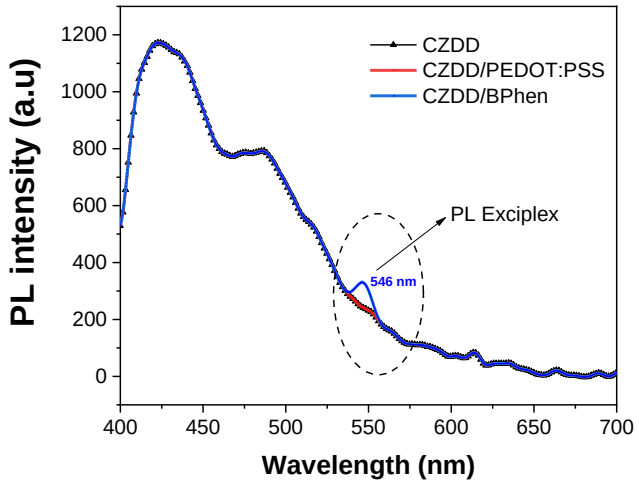

Figure 3.15. PL spectra of the blends PEDOT:PSS-CZDD and CZDD-BPhen.

The CIE chromaticity diagram for OLED-5 and OLED-6 when the thickness of the HTL was changed is shown in Figure 3.16. OLED-5 shows that by changing such thickness, from 60 nm to 30 nm, one can reach a tuning in color from bluish to greenish meanwhile OLED-6 shows a tuning from cold to warm white light. For thickness of 45 and 30 nm of the HTL the CIE coordinates for OLED-6 were (0.32, 0.42) and (0.38, 0.44) respectively. The work by Fröbel et al.,[117] demonstrated color tuning from cold to warm white light in a tandem structure based on a combination of a blue-emitting unit and a yellow-emitting unit. Similar tuning was reached with our OLED-6 configuration only by changing the thickness of the HTL. Figure 3.16 also shows the tuning in correlation color temperature (CCT); from above 10000 (cold white) K to approximately 2500 K (warm white). This modulation of white light also has been considered by Kroskus et al.[118]

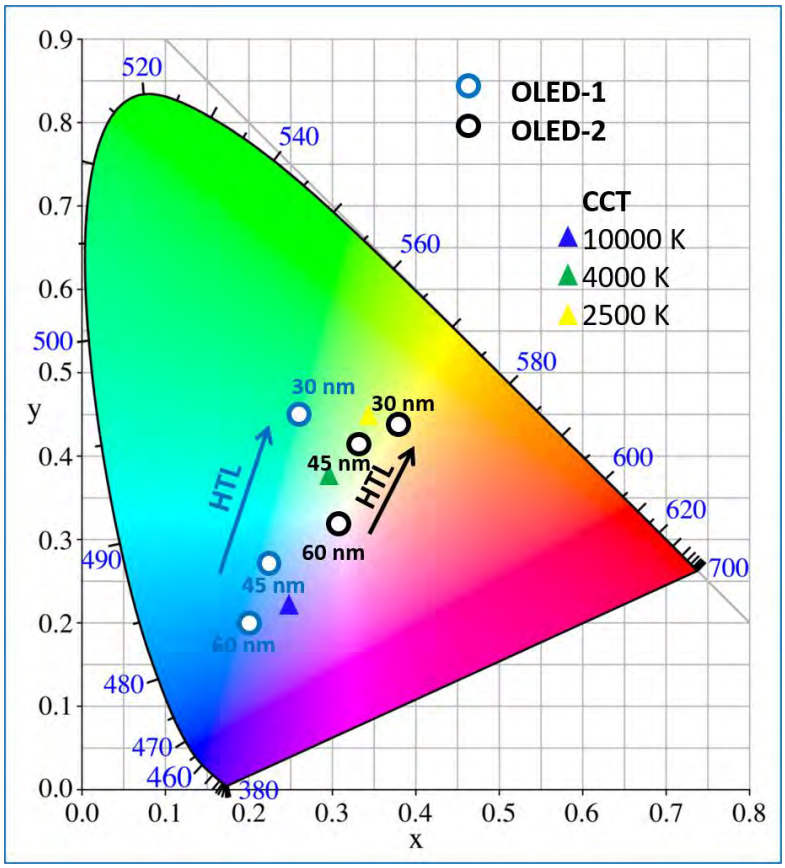

Figure 3.16. CIE coordinates of the OLEDs represented in the CIE map 1931.

To improve the electrical and luminance parameters of OLED-6 a buffer layer was added. The buffer layer was between the ITO and the EML to facilitate the effective hole migration from the anode to the emissive zone; a thin film of Poly(9-vinylcarbazole) (PVK) was employed. With this additional organic layer, the architecture was ITO/PEDOT:PSS/PVK/CDZZ/BPhen/Ca-Ag (OLED-7) and better alignment between the energy levels of the organic layers was exhibited; the HOMO energy level (5.6 eV) of PVK acted as bridge energy between the HOMOs of PEDOT:PSS and CDZZ, respectively. Therefore, the charge injection exhibited by the device was enhanced; further, the turn-on voltage was reduced from 6.5 to 5.0 V while the luminance was improved almost 4 times (maximum luminance 9600 cdm^{-2}) while the maximun power efficiency of 7.5 lm/W. The EL spectrum of OLED-7 and a photo of the device working at 8 V is shown in Figure 3.17.

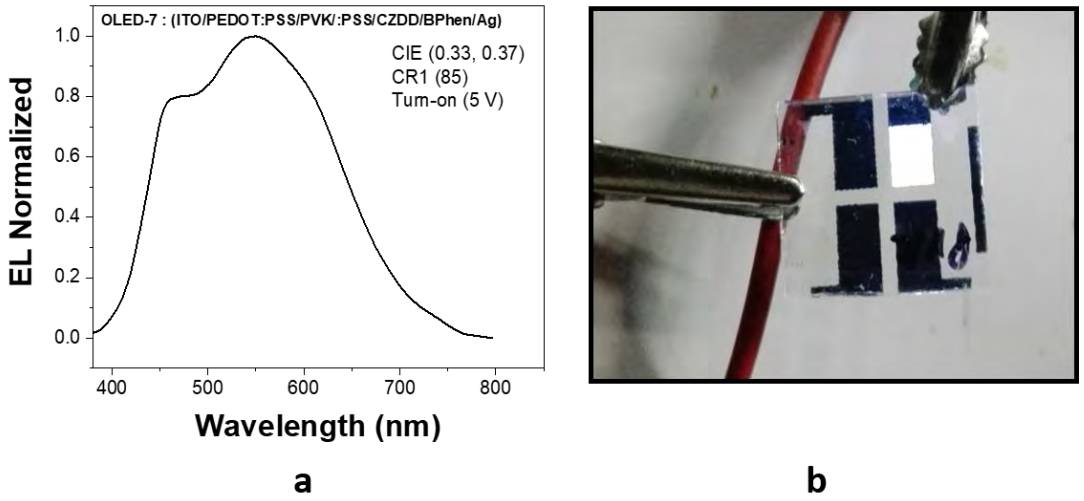

Figure 3.17. a) El spectrum of OLED-7 (ITO/PEDOT:PSS/PVK/CZDD/BPhen/Ca-Ag); b) picture of the device OLED-7 working at 8 V.

4. ORGANIC LUCO DEVICES; INORGANIC/ORGANIC WHITE LED BASED ON DOWN CONVERSION MECHANISM

As discussed in chapter 1, currently commercial white LEDs offer the highest energy efficiency, however, one problem with these devices is the use of phosphors containing REEs. It was also pointed out that organic materials are promising materials for replacing phosphors and offer advantages such as wide color range, high external quantum efficiency, low-cost manufacturing, flexible substrate compatibility. The combination of inorganic and organic materials is known as hybrid technology. In particular, LUCO devices based on down-conversion mechanism have attracted special interest; this technology uses inorganic LEDs as sources of excitation to photoluminescent organic compounds of the type "light converters".[119,120] Some works have been reported using this mechanism [121,122] and have already shown enough merits to replace rare earth doped phosphors. In a recent work, Junjie and her research group [123] reported a hybrid LUCO lamp with CRI <90 and 82 lm/W. They used perylene diimides as organic converters and were inserted into a polymeric matrix to form better films and protect them from degradation.

The narrow bandwidth emission of the LED can be complemented by a broad emission of the organic layer, which can be either a single emitting compound or a mixture of several compounds. One of the strategies for obtaining white light emission is to use a blue LED and a yellow organic material, other less common, is the use of a UV-LED and mixture of organic materials (whose emissions cover most of the visible spectrum); these strategies are known as partial and full conversion, respectively. An example of partial conversion is the case of Taylor's group.[124] they reported LUCO devices with a luminous efficiency of 368 lm/W using a blue LED of InGaN/GaN and a yellow organic converter based on BODYPI derivatives, however, the CRI was as low as 62.

A high quantum yield is one of the main optical properties that organic materials should exhibit to be used as LUCO; the closer value to the unit, the more efficient the device is. However, in solid-state, different physics and chemical processes can emerge in the molecules like excimer formation, quenching, among others, reducing the quantum yield of the materials. The quantum yield of organic converters for LUCO devices reported is in the range of 30 to 90% which corresponds to fluorescence and phosphorescence emissions; nevertheless, above 30% values, the devices would exhibit a good performance since it is comparable to inorganic white LED.[121,125,126] LUCO devices exhibit excellent properties that make them an alternative for SSL, however in the literature few details of the experimental conditions are reported, such as thicknesses and concentrations of the converter material.

4.1. Description of Down-Conversion Mechanism.

The mechanism for LUCO devices is the down-conversion, which is shown in Figure 4.1. The excitation source is a blue LED, which incises on the organic sample and two processes can take place, fluorescence and phosphorescence. For the former, electrons jump from ground state S_0 to excited state S_1, or higher energy levels. After this, a relaxation of electrons occurs and go back to S_1 and then recombine to S_0. However, electrons can also move from S_1 to the triplet state T_1 throughout internal crossing as shown in the figure. When this process takes place, the recombination of electrons and holes could happen, this is the phosphorescence phenomena. In this case the emitted light is delayed in comparison to fluorescence. The time decay of the phosphorescence is in the range 10^{-5}-10^{1}s and fluorescence 10^{-10}-10^{-7}s.[127]

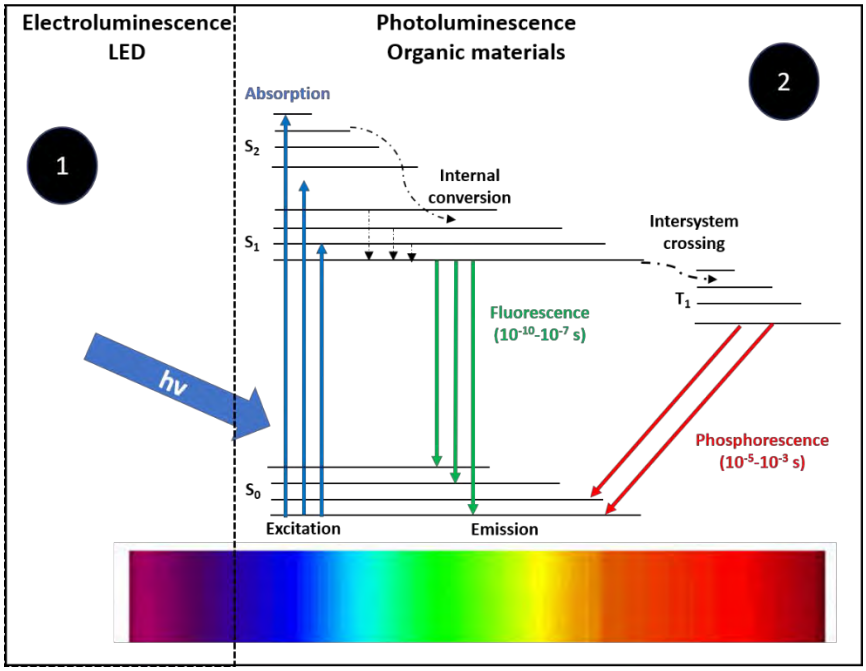

Figure 4.1. Emission Mechanism of organic LUCO devices, which imply the electroluminescence of LED (1) plus photoluminescence of the organic materials (2).

From quantum mechanics, the internal quantum efficiency for triplet states could be about 75% while for singlets 25 %. In some organic LUCO's reports, the devices are fabricated taking advantage of triplet states, which involved organic molecules with metal-free framework (MOF). These molecules require mechanisms as triplet-triplet annihilation (TTA) and upper triplet crossing to allow the intersystem crossing. Angioni et al.,[121] reported the synthesis of a MOF to LUCO application with a photoluminescence efficiency of 42% and luminous efficiency close to 35%. Details of these mechanism are described by Dos Santos and her research group.[113]

Singlet-state emission materials offer the possibility of achieving luminescence parameters comparable to other technologies despite their limited efficiency. Usually, the development of these materials is focused on polymers with a high quantum efficiency

although oligofluorenes and fluorescent dyes also are considered under study.[125,128, 129] For example, Kim and his group[126] reported a very bright white light from the LUCO LED using a commercial InGaN LED (460 nm) and a 1,8-naphthalimide derivative (DBN) dispersed in an epoxy matrix; the conversion efficiency achieved was of 82%, which is comparable to the phosphors LED and other technologies.

4.1.1. Energy Transfer Processes in the Down-Conversion Mechanism.

When the down-conversion mechanism is due to more than one organic compound, intermolecular interactions generate other excited species that could change the emission. One of those processes is the charge transfer. Independent of the weak van der Waals interaction between molecules in organic films, the energy can transport to distances substantially exceeding the size of the molecules. Such energy transfer processes are particularly important for doped organic films. The process of any transfer of energy from an excited molecule, donor (D*), to another molecule, acceptor (A), can be described by eq. (6):

$$D^* + A \rightarrow D + A^* \qquad (6)$$

Because of this energy transfer, the acceptor is promoted to a higher electronic state. There are different energy transfer processes to be distinguished; first, radiative energy transfer in which the acceptor reabsorbs the donor emission:

$$D^* \rightarrow D + h\nu, \;\; h\nu + A \rightarrow A^* \qquad (7)$$

No direct interaction of the donor with the acceptor is involved. The process requires that the emission spectrum of (D) and the absorption spectrum of (A) overlap. Thus, the efficiency of the transfer is governed by the photoluminescence yield of the donor molecules and the absorption ability of the acceptor, i.e. the extinction coefficient ε_A.

Non-radiative energy transfer is the second process which requires the presence of a specific interaction between D and A. Two types of interaction are identified: The Coulombic interaction, known as Förster energy transfer, and electron-exchange, referred as Dexter energy transfer.

The Coulomb or Förster energy transfer involves a dipole-dipole coupling of the transition dipole moments for excited donor (exciton) and the acceptor dye in its ground state. As the excited donor relaxes, its energy is transferred via the Coulomb interaction with the acceptor dye molecule as is shown in Figure 4.2. A characteristic of this energy transfer process is that the dipole-dipole interaction covers large distances, thus efficient transfer is possible over distances up to 100 Å. A measure for the efficiency of the process is the value of the rate of energy transfer relative to the radiative relaxation of the donor molecule. A high rate of the energy transfer relative to radiative relaxation will lead to emission exclusively from the acceptor.[130]

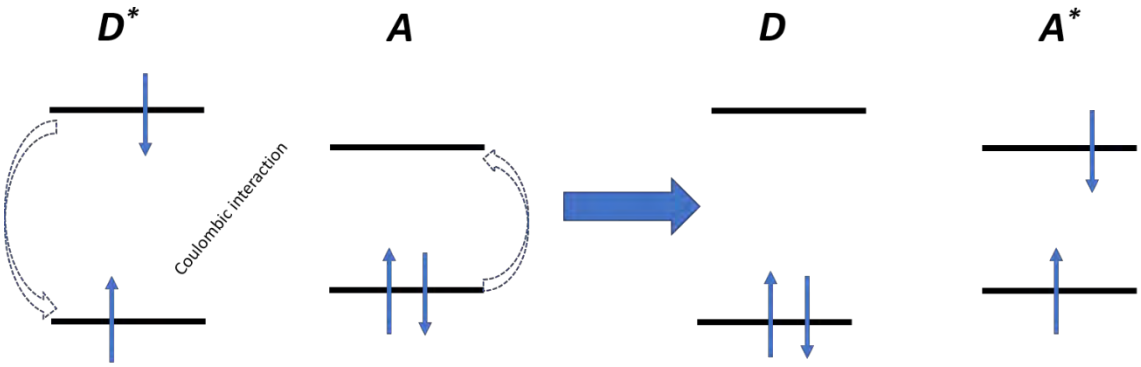

Figure 4.2. Förster energy transfer mechanism.

The electron-exchange or Dexter transfer involves an electron transfer mechanism in which the excited electron on D* transfers into the LUMO of A with a simultaneous transfer of an electron from the HOMO of A into the corresponding orbital on D (Fig.

4.3). Thus, in contrast to the Förster transfer, the Dexter transfer requires that molecules be much closer each to the others allowing for overlapping of the involved electron orbitals; typically, ~10 Å, and is effectively restricted to neighboring molecules.[131] Dexter energy transfer does not have a singlet requirement and can effectively act to transfer energy between triplet states or between singlet and triplet states.

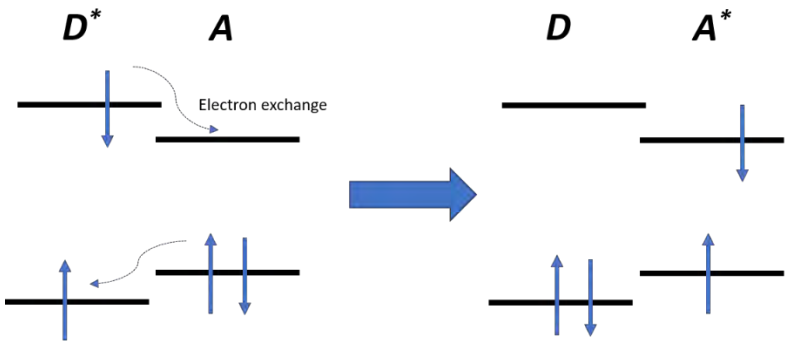

Figure 4.3. Schematic Dexter transfer mechanism.

4.2. Fabrication and Characterization of White Hybrid LUCOs.

In a LUCO configuration, the organic material is deposited on the inorganic diode; but few details of important parameters as concentrations and thicknesses of the converter materials are provided in most reports, then, several questions arise when manufacture of devices with new materials is developed. In response, the concentration, mixtures, and thicknesses study of converter material was developed in this thesis. For partial LUCO devices three commercials InGaN blue-LEDs (with wavelength emissions of 460, 465, and 475 nm) and the commercial copolymer derivative of benzothiadiazole (ADS233YE) was used as converter. For full LUCO a commercial InGa UV-LED (390 nm) and the mixture of organic converter were used; a commercial copolymer and two small molecules synthesized by our group were also employed for this case.

4.2.1. Partial Converter.

To achieve white light through partial down-conversion mechanism is necessary that EL of the Blue LED and the complementary PL from the organic converter must have a similar emission intensity (see Fig 4.4; Schematic mechanism proposed to partial converter LED). The adequate EL and PL emissions were explored by the study of the thicknesses of the organic films. The luminous parameters were compared with the commercial white LED to estimate possible advantages and challenges in this proposal.

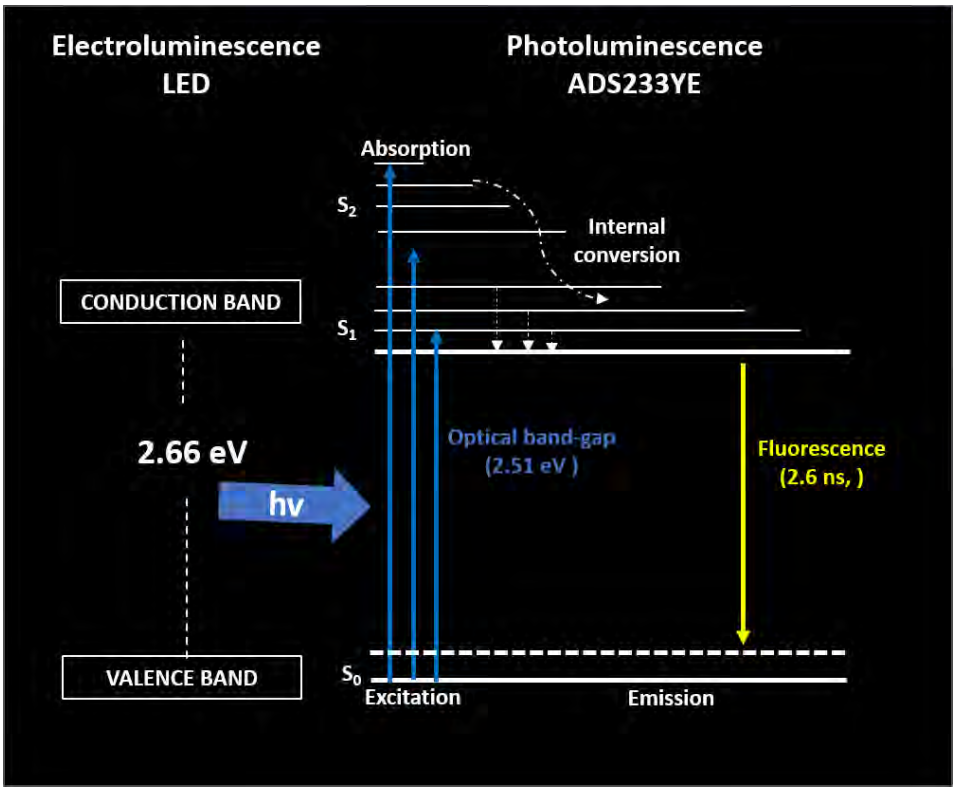

Figure 4.4. Schematic mechanism proposed to partial converter LED.

The PL, EL and Abs spectra of the used material are shown in Figure 4.5; the EL peak of the blue LED is centered at 465 nm. According to the Abs spectrum, ADS233YE exhibit two peaks; one centered at 400 nm, and another at 450 nm which corresponds to π-π* and

n-π transitions. As can be seen in the PL spectrum, this material exhibited a peak of emission centered at 540 nm. Quantum yield of ADS233YE film was of 84%, and the time decay of 2.6 ns.

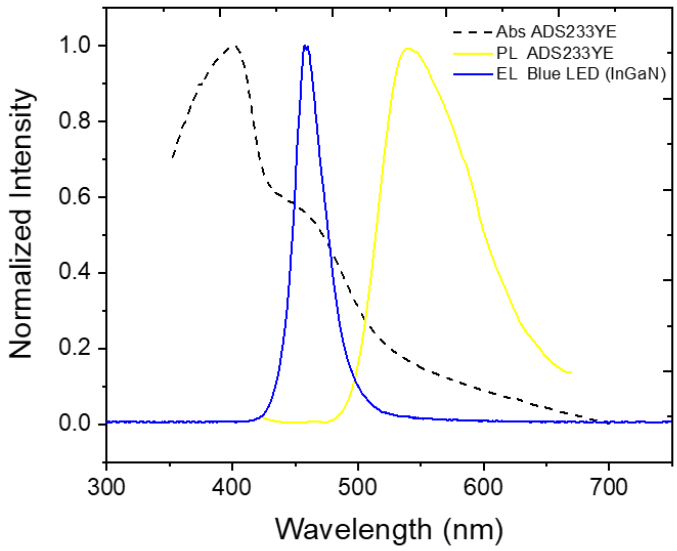

Figure 4.5. Absorption and emission spectra of the materials used in the partial LUCO.

The EL of the blue LED centered at 465 nm matches partially the absorption of the organic converter (Fig. 4.5). The emission of the blue LED (465 nm) is absorbed by the ADS233YE films and then re-emitted on a longer wavelength (540 nm). Blue InGaN LED has a band gap of 2.66 eV while 2.55 eV is the optical band-gap of the ADS233YE, calculated from absorption data (Fig. 4.5).

Then, to achieve a good complementary EL and PL emission, the thickness of ADS233YE should be evaluated. Assuming that the organic films are homogeneous, is possible to use the Lambert-Beer Law:

$$\boldsymbol{A = \varepsilon c l = -log_{10}\left(\frac{I_1}{I_0}\right)} \qquad (8)$$

that relate the absorbance $\boldsymbol{A}$ with the thickness $\boldsymbol{l}$ and the concentration $\boldsymbol{c}$ of the film. Based on this law, is clear that varying $\boldsymbol{l}$ of the converter material films, the ratio between the final $\boldsymbol{I_1}$ and initial $\boldsymbol{I_0}$ intensities $\left(\frac{\boldsymbol{I_1}}{\boldsymbol{I_0}}\right)$ is modified, where is assumed that $\boldsymbol{I_0}$ and $\boldsymbol{I_1}$ represent the EL intensities from LED before and after crossing the converter film.

In a first approximation, ADS232YE was dissolved in different concentrations from 5 to 80 mg/ml. For each ratio, films were fabricated at the same rate of 3000 rpm using spin coating technique and deposited on top of the blue LED. The bias voltage was set to 5.5V. Figure 3.8 shows the spectra for concentrations of 10, 20, 40 and 80 mg / ml, which leads to thicknesses of 40, 70, 120 and 190 nm, respectively. As expected, with increasing concentration and thickness of ADS233YE, PL also increases, while EL intensity decreases (Fig. 4.6a). Despite that PL increases, its intensity was not enough to achieve a good intensities balance (EL-PL), then white light was not achieved (see the normalized spectra of the Fig. 4.6b). By further increasing the concentration of ADS233YE, a good balance between EL and PL was achieved. However, at concentrations higher than 40 mg/ml it is difficult for the material to form films using the spin coating technique showing poor optical quality as, for example, low homogeneity.

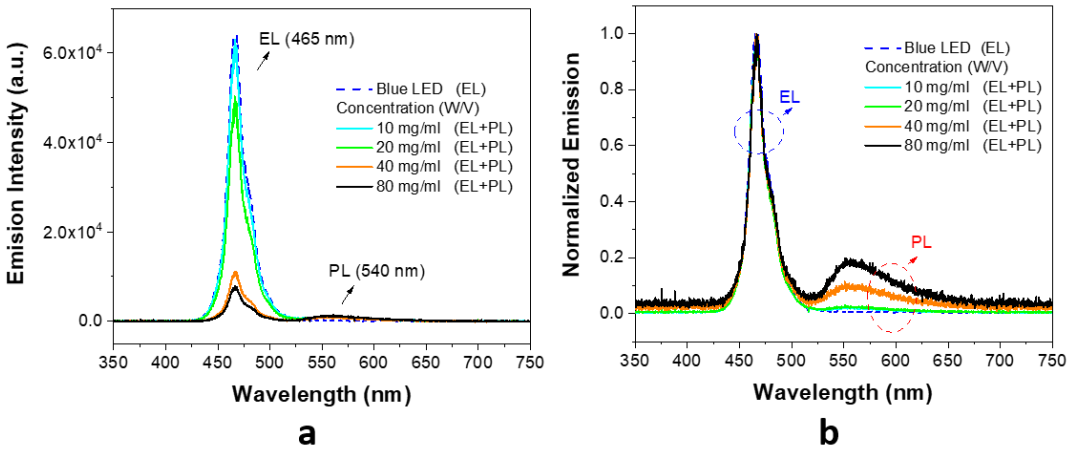

Figure 4.6. Emission spectra of the devices at different concentration, a) relative

intensity; b) normalized.

A second experiment was carried out by changing the thickness of the organic converter to larger steps (in order of microns). The concentration of ADS233YE was fixed at 30 mg/ml and the bias voltage at 5.5 V. Therefore, thicknesses were increased from 0.1 to 1.0 μm in 0.1 μm steps by varying the spinner rate. Figure 4.7 shows the emission spectra of 4 thicknesses and the relationship between thickness and color balance is evident. For thicknesses lower than 0.3 μm the EL emission is far superior to the PL; thus, the blue color is dominant. However, the formation of quasi-white emission was measured with CIE (0.23, 0.29).

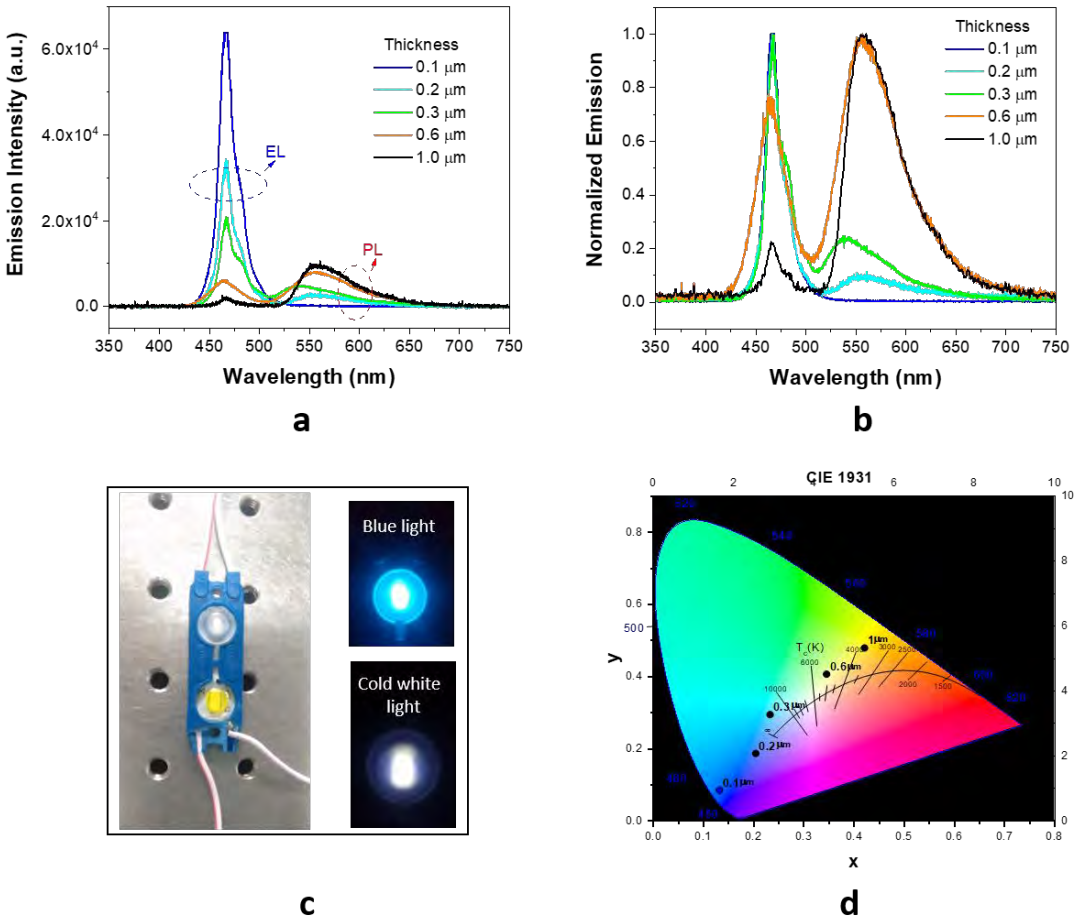

Figure 4.7. LUCO experiment in function of the thicknesses of the converter material, a) relative emission spectra; b) normalized spectra; c) photography of the devices; d) CIE map coordinates.

For thicknesses higher than 0.3 µm and lower than 1.0 µm, white emissions were obtained thanks to good complementary emissions between EL and PL. For 0.6 µm, neutral white emission was reached; for this configuration, the blue and yellow emission have an approximately equal intensity. The CCT and CIE were (5240 º K) and (0.34, 0.40), respectively. Close to 1.0 µm the CCT and CIE achieved were (<4000 º K) and (0.42, 0.47), respectively. For this thickness, the yellow emission is dominant allowing the

formation of warm white light. For values above 1.0 μm, the EL disappeared and only yellow emission was observed.

Figure 4.7c shows the LUCO devices corresponding to 0.3 μm thickness. Figure 4.7 d shows the CIE map with all the coordinates of the fabricated devices and Table 4.1 summarizes the optical and color parameters.

Table 4.1. Color and temperature coordinates of the devices in function of the converter material thicknesses.

Thicknesses	CCT (º K)	CIE	Color
0.1 μm	>20000	(0.13, 0.08)	Blue
0.2 μm	>16000	(0.20, 0.18)	Cian
0.3 μm	>10.000	(0.23, 0.29)	Quasi-cold white
0.6 μm	5240	(0.34, 0.40)	Neutral white
1.0 μm	<4000	(0.42, 0.47)	Warm white

The color emission in function of the thickness ***l*** is shown in the graphic of Figure 4.8. The values were obtained from the experimental results when the bias voltage was 6.0 V. In other words, to maintain the color emission in the voltage range (5.0 to 6.0 V), the corresponding values of ***l*** for each case must be taken. Cold white could be achieved between ~0.38 to 0.53 μm, neutral white between ~0.55 to 0.71 μm and between ~0.72 to 0.95 μm for warm white.

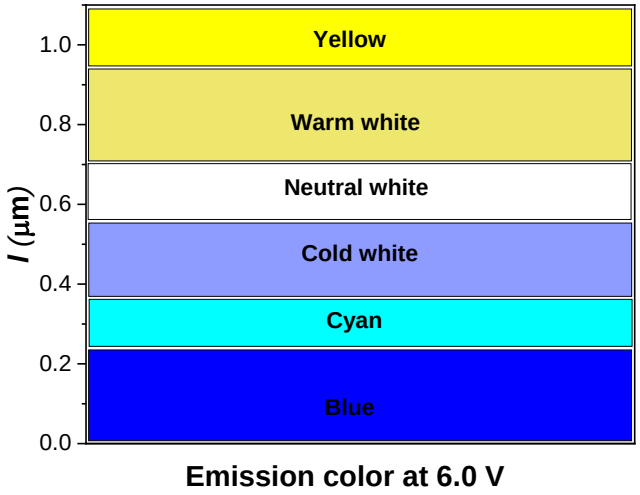

Figure 4.8. Emission color in function of the thickness ***l****.*

The above relation between color emission and thickness of converter was here proved by the fabrication of three devices: a neutral white emission (LUCO A), cold white emission (LUCO B) and warm white (LUCO C). Spectra emissions are shown with relative and with normalized intensities to observe changes more clearly (see Fig. 4.9a-f).

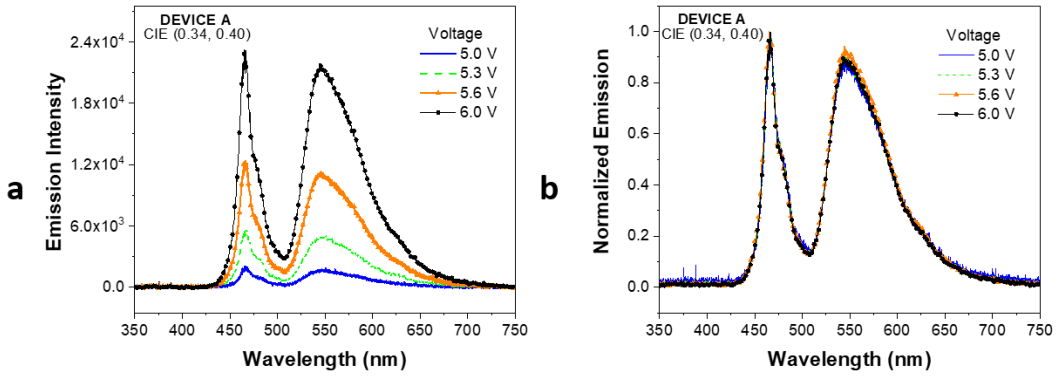

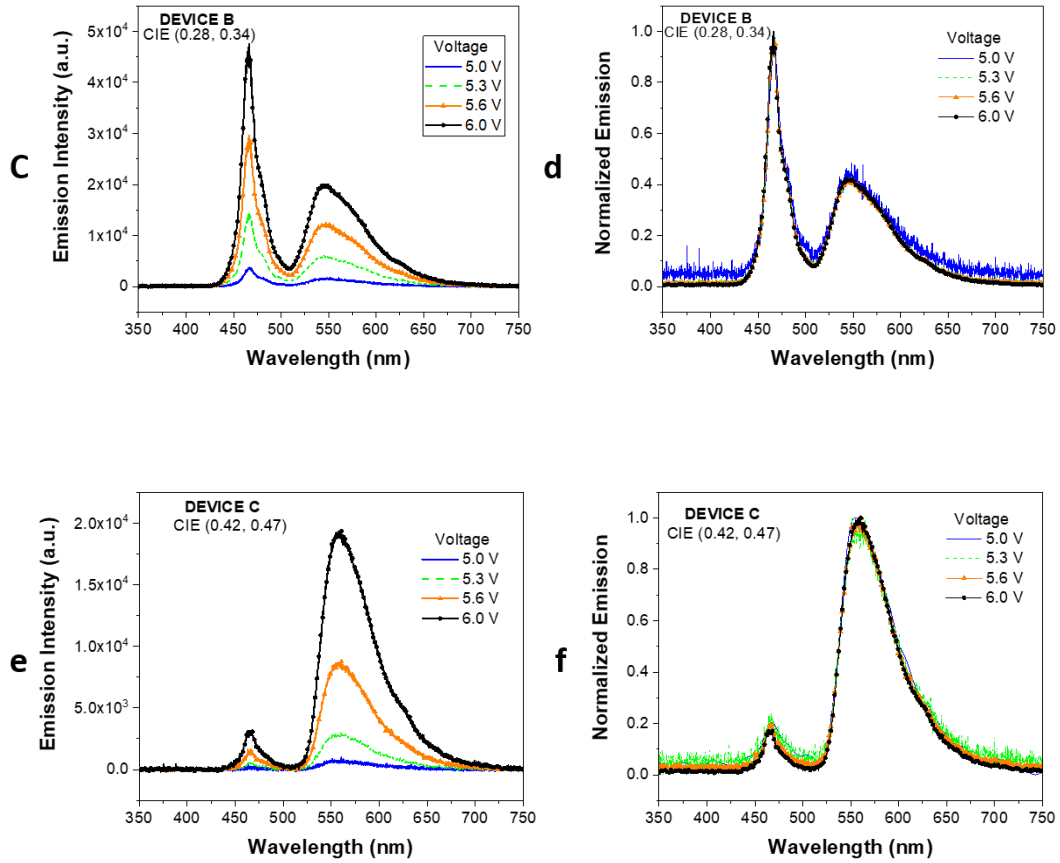

Figure 4.9. Emission spectra of different white LUCO devices as a function of the bias voltage, a) neutral white (LUCO A); b) normalized spectra (LUCO A); c) cold white (LUCO B); d) normalized spectra (LUCO B); e) warm white (LUCO C); f) normalized spectra (LUCO C).

As can be seen for each device, spectra emission was maintained from 5.0 to 6.0 V, it means that the color emission was not modified as a function of bias voltage as is illustrated in Figures 4.9b, 4.9d y 4.9f. The concentration of the converter material in devices A, B and C were 35, 45, and 30 mg/ml while the thicknesses were 0.59, 0.31 and 0.94 µm, respectively. Table 4.2 summarizes color and luminous parameters measured for the three different devices; from the parameters reported, neutral white achieved the

best CIE color (0.33, 0.42) and the highest CRI (75). The maximum luminous efficacy was reached with the cold white devices, having an acceptable value of 55 lm/W.

Table 4.2. Color quality of the LUCO devices and maximum luminous efficacy (η_{PE}).

Device	**Max η_{PE} (lm/W)**	**CCT (º K)**	**CIE (x, y)**	**CRI**	**Color**
LUCO A	51	5500	(0.33, 0.42)	75	Neutral white
LUCO B	55	8000	(0.28, 0.34)	70	Cold white
LUCO C	48	<4000	(0.42, 0.47)	<60	Warm white

Partial white LUCO and commercial white LED comparation

Three different LUCO devices were fabricated and compared with two commercial white LEDs (see Fig. 4.10a). For the three LUCO devices, ADS233YE was employed as organic converter but with different blue LEDs: LUCO D (blue InGaN LED (460 nm), LUCO E based in an InGaN/GaN (480 nm) and LUCO F, based on InGaN (SMD-5730) LED. As can be observed in the spectra of Figure 4.10a by changing the blue LED in the LUCO configurations, different white spectra could be achieved with acceptable luminous parameters that were reported in Table 4.3. The two commercial white LEDs were LED 1 and LED 2; LED 1 is based on InGaN (SMD-5730) plus the phosphor YAG:ce while commercial WLED 2 is an InGaN LED (440 nm) plus the phosphor YAG as the converter.

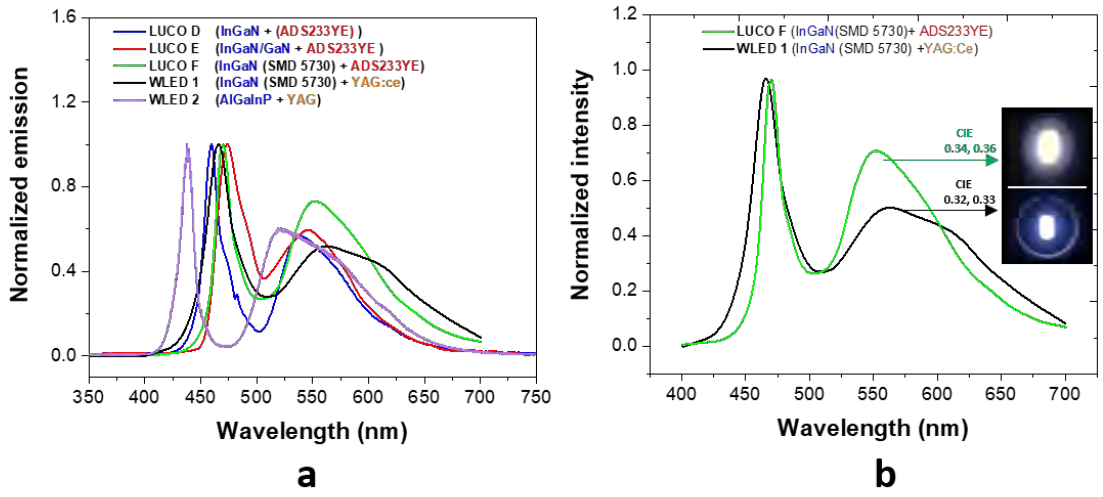

Figure 4.10. Emission spectra of different LUCO and commercial white LED, a) three different LUCO devices based on different blue LEDs and two commercial white LEDs; b) comparation of white LUCO F and commercial WLED 1, which have identical blue LED, in the same figure is shown a photography of the device's operation.

In Figure 4.9b emission spectra of LUCO F and commercial WLED 1, which uses the identical blue LED as the excitation source, are shown for a best comparation, moreover, the picture of the two devices can be observed. Both devices exhibited cold white light but the conventional YAG:Ce phosphor offer a broader emission (500-700 nm) than ADS233YE (500-675 nm), thus, WLED 1 exhibited the excellent CIE of (0.32, 0.33) and CRI (77) higher than LUCO F. Regardless the achieved CIE (0.34, 0.36) and CRI (72) with the organic material such values are acceptable within the SSL field. An advantage of this mechanism is that through the modulation of thickness, a slight improvement of the CRI can be obtained, as was evidenced with the CRI value of 74 for neutral white LUCO device reported in Table 4.3. Also, by varying the thickness of the converter, the CIE and CCT can be easily tuned. However, organic devices with a broader emission would be the best option to enhance the color performance.

The main LUCO parameter is the conversion efficiency, defined as the ratio of the number of photons emitted by the LUCO to that of the photons emitted from the blue LED. For white LUCO F, conversion efficiency has a value of 74 % while to phosphor is of 93%. That means that the phosphor YAG:Ce is a better converter than organic material ADS233YE, however, luminous parameters that exhibited the white LUCO F are highly acceptable for this technology. Nevertheless, it is superior to some conventional sources such as incandescent, halogen and fluorescent lamps and, these devices are very close in performance than the commercial WLED 2. Figure 4.11 shows the power conversion (PE) and luminous efficiency (η_{PE}) as a function of the current for the two devices, the maximum PE and η_{PE} for LUCO F were 21 and 19% lower than WLED 1.

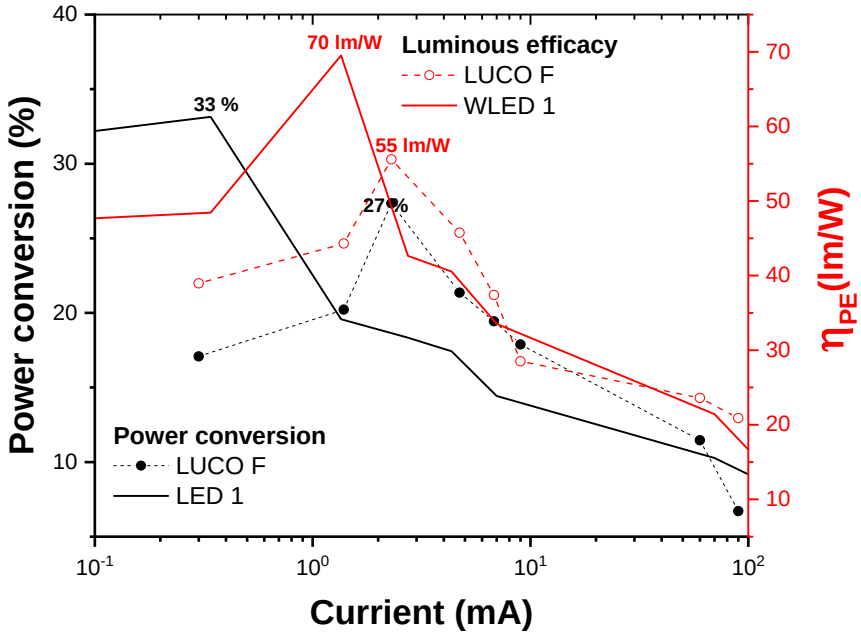

Figure 4.11. Power conversion and luminous efficacy of white LUCO F and commercial WLED 1.

Table 4.3. Luminous and color quality of the LUCO devices fabricated in this thesis and commercial white LED used as reference.

Device	Conversion efficiency (%)	η_{PE} (lm/W)	CCT (º K)	CRI (%)	CIE
LUCO D	*NM	49 ± 0.5% At 5.2 V	7800 ± 0.2%	<50	(0.28, 0.36)
LUCO E	*NM	41 ± 0.5% At 5.4 V	7200 ± 0.2%	<50	(0.28, 0.42)
LUCO F	**75**	**55 ± 0.5% At 5.4 V**	**5200 ± 0.2%**	**73**	**(0.34, 0.36)**
WLED 1	**93**	**70 ± 0.5% At 5.4 V**	**6100 ± 0.2%**	**77**	**(0.32, 0.33)**
WLED 2	*NM	52 ± 0.5% At 3.6 V	5600 ± 0.2%	74	(0.33, 0.31)

*NM: not measured

Therefore, based on these results of partial down-converter LUCOs, to find the best PL and EL combination a study of concentrations and thicknesses is necessary. Once these parameters are optimized, good and tunable white emission can be achieved. With ADS232YE in LUCO configuration it was possible to find color quality and luminous parameters as good as in commercial phosphorous. However, to improve the CIE and CRI, an organic material with a higher contribution at red wavelengths would be desirable.

4.2.2. Full Converter.

White organic LUCO device based on full down-converter are those whose white emission provides completely from the photoluminescence of organic materials with an

inorganic UV LED used as excitation source. A single organic material is unlikely to emit in the entire visible spectrum, for this reason, in this configuration is more effective to have the mixture of different materials whose emission range is from blue to red. Thus, the main focus of this study was finding the appropriate mixture of organic converters to achieve devices with acceptable luminous parameters. As converter materials two commercial copolymers (ADS232GE and ADS233Y3) and two organic dyes synthesized by our group (ACN1 and JP5) were employed.

Absorbance and photoluminescence spectra of the organic materials are shown in Figures 4.12a and 4.12b. ADS232GE has its main absorption peak centered at 395 nm while ACN1 has the peak absorption at 400 nm. ADS233YE exhibits the main peak of absorption at 400 nm and a shoulder around 450 nm. The dye JP5 shows two peaks of absorption, the main centered at 380 nm while the other, weaker, at 575 nm. These materials were chosen due to the maximum absorption in the near UV region of the four compounds that match the EL emission of the UV LED (385 nm). The PL spectra of ADS232GE and ACN1 showed peaks centered at 461 nm and 500 nm, respectively. Contrary to the absorption spectrum, ADS233YE only exhibited the main PL peak at 540 nm, while JP5 exhibits two transitions, the first at 678 nm and other with less intensity above 750 nm.

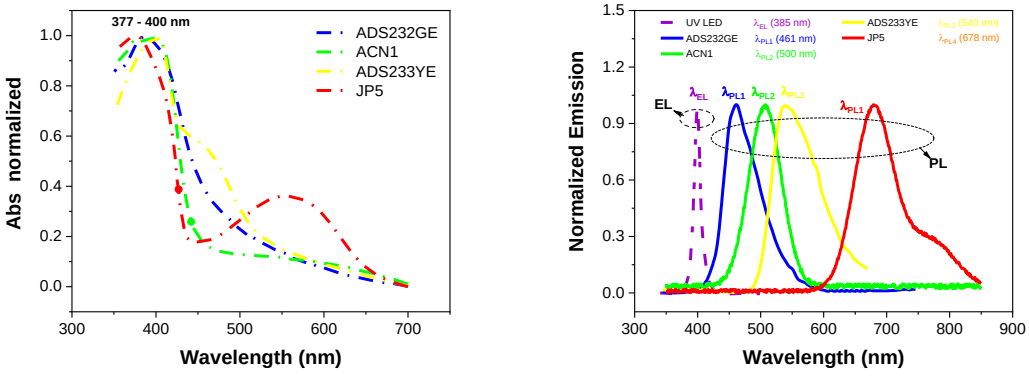

a **b**

Figure 4.12. Normalized absorption and emission spectra of the organic material employed to full LUCO devices, a) absorbance (Abs); b) emission.

For the first full LUCO device, the dyes ADS232GE and JP5 (blue and orange-red dyes) were mixed, this device was named "FULL LUCO 1". The concentration of ADS232GE was fixed as weight 1 and the weight ratios of JP5 with respect to the copolymer were 0.2, 0.4, 0.6, and 0.8. A solution with a concentration of 35 mg/ml was prepared to deposit films by spin coating, thickness was between 0.5 to 0.6 μm. Figure 4.13a shows the emission spectra of the FULL LUCO 1. Since the concentration of JP5 increases, changes in the CIE coordinates were observed as well as good emission balance between blue and orange-red wavelengths, achieved at (1:0.6) and (1:0.8) weight ratios. However, the absence of green and yellow colors in this copolymer-dye mixture did not allow the generation of white light, even though it served to estimate material weight ratios and film thickness. The quantum yield of ADS232GE film was 0.78 while for JP5 0.4. With (1:0.2) ratio, the highest conversion efficiency was achieved (68%) against the lowest value (47%) with the JP5 weight ratio (0.8). From this result, it is evident that the conversion efficiency is related to the quantum yield of each material and will be closer to the dominant material in the mixture. It should be noted that, in the LED operating range, from 2.8 to 4.0 V there was a complete conversion of the incident light.

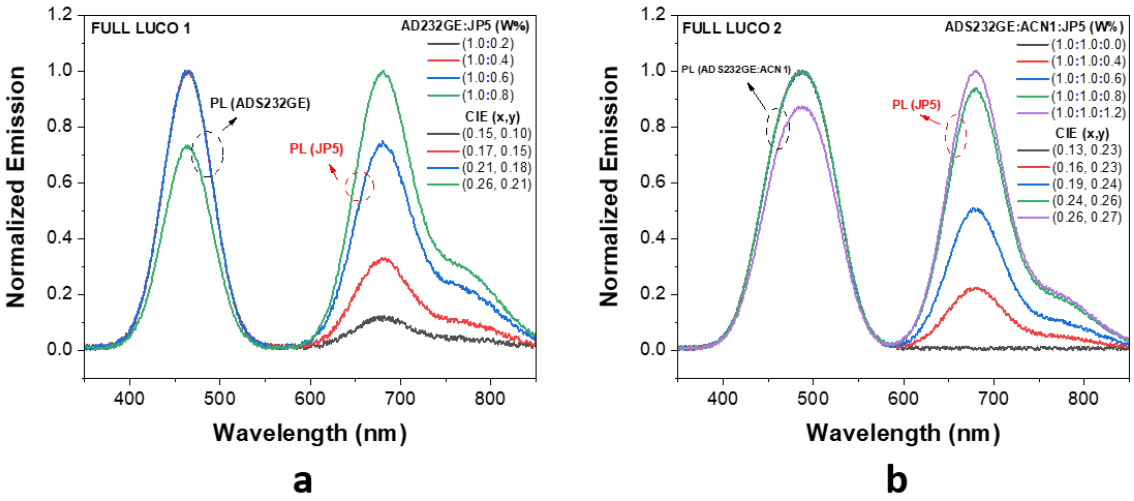

Figure 4.13. Normalized emission of the full LUCO devices, a) FULL LUCO 1 (mixture of ADS232GE and JP5); b) FULL LUCO 2 (mixture of ADS232GE, ACN1, and JP5)

In a second mixture of organic materials, three converters were employed; the copolymer ADS232GE and the dyes ACN1 and JP5. This device was named FULL LUCO 2. The thickness and ratio of the converter/solvent was the same of above. The main difficulty of this mixture was to find a common solvent for the three materials to fabricate films with acceptable optical quality. From all these tests, a mixture of toluene and chlorobenzene (1:0.1 v/v) was found to reach a good dissolution. The ratio for ADS232GE and ACN1 was fixed at (1:1) and the weight ratio of the JP5 dye was gradually increased from 0.0 to 1.2, results are shown in Figure 4.13b. As observed, emissions from ADS232GE and ACN1 are overlapped emerging in a single peak centered at 490 nm with a bandwidth from 430 to 560 nm. Although a very wide emission spectrum was obtained (450-850 nm) in all cases, the emissions achieved did not correspond to white color. The lack of yellow contribution does not allow to obtain better color coordinates, but it was closer to white color than the FULL LUCO 1 configuration. The closest to cold white was achieved when the concentration of the materials was

(1.0:1.0:1.2) with CIE (0.27, 0.26). With the same ratios, the conversion efficiency was 52%, value close to the average quantum yield of the three materials.

A third set of devices, FULL LUCO 3, was fabricated combining two materials; the ACN1 dye, which was fixed as weight 1, and the ADS23YE copolymer whose weight ratio was varied from 0.5 to 3.0. With this configuration, emission spectra between 400 to 700 nm were observed with acceptable CIE coordinates corresponding to neutral and quasi-warm white (see Fig. 4.14). For this configuration, one of the two peaks were observed at 565 nm, corresponding to the copolymer ADS233YE. However, this peak exhibited a red-shift of 25 nm with respect to the individual emission of the material (540 nm, see figure 4-12b). For the ratios (1.0:0.5), (1.0:1.0) and (1.0:1.6), a peak centered at 491 nm was observed, corresponding to the ACN1 compound but it exhibited a blue-shift of 9 nm with respect to the PL spectrum of Figure 4.13b. For the ratio (1.0:2.0), this peak is further shifted towards blue changing from 491 nm to 461 nm. These red and blue shifts influenced a greater widening of the emission spectrum and therefore the generation of acceptable white colors.

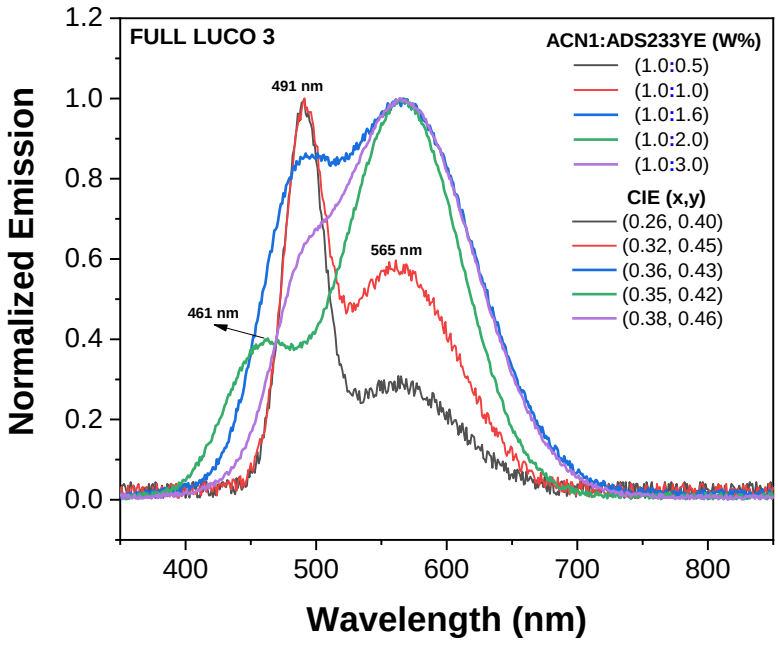

Figure 4.14. Normalized emission of the FULL LUCO 3 devices to different weigh ratios of the mixture ACN1:ADS233YE.

The shifts could be associated with the intermolecular interaction of the two materials as is shown in the scheme of Figure 4.15. The mechanism that could generate the red-shift is the exciplex process. For the ratio (1.0: 3.0) the peak centered at 461 nm becomes a shoulder around 500 nm; which means that the type of interaction is reduced for this relation and the individual transition of ACN1 is observed again. In some reports, it has been stated that the intermolecular interaction can tune the emission, for example Perez and co-workers[135] reported that a polymer matrix is a medium that induces the aggregation of the dye leading to the change in emission wavelength.

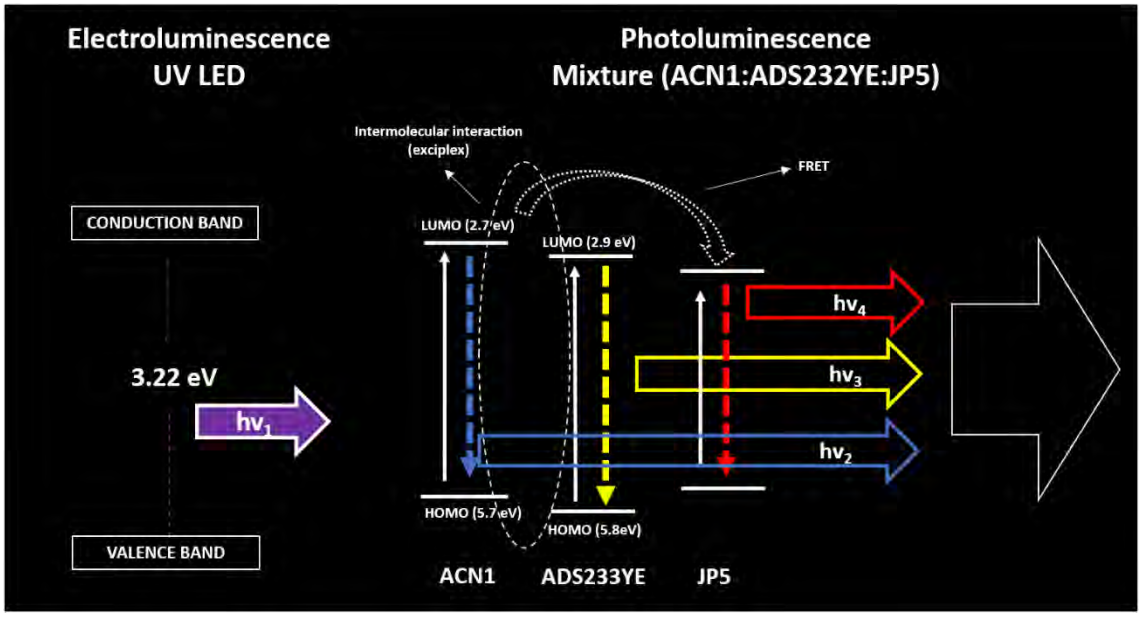

Figure 4.15. Schematic representation of the mechanisms to full LUCO devices.

Luminous and color parameters for FULL LUCO 3 are summarized in Table 4.4. The conversion efficiency of this configuration increases when the ADS233YE concentration does, this is related to the quantum yield of the materials being from 0.57 for ACN1 and 0.84 for the copolymer. This was already evidenced with the previous LUCO device. For

these devices of down-conversion mechanism, the best conversion efficiency was 78%. In addition, the luminous was also improved according to the ADS233YE ratio, being 38 lm/W the highest corresponding to the ratio (1.0:3.0). The best white light was achieved with the ratio (1.0:1.6) due to the good balance color with CIE (0.36, 0.43) that corresponds to neutral white light and CRI of 70. Despite the good values achieved, the emission of this mixture needs a better orange-red contribution to enhance the color and reach ideal white in order to have a superior performance than lighting systems.

Table 4.4. Luminous parameter of the FULL LUCO 3, where the mixture of ACN1 dye and copolymer ADS233YE was used as full converter material.

Ratio (ACN1:ADS233YE)	**Conversion efficiency**	**η_{PE} (lm/W)**	**CCT (^oK)**	**CRI**	**CIE (x,y)**
(1.0 :0.5)	57%	19	6184	51	(0.26, 0.40)
(1.0 :1.0)	60%	24	5700	56	(0.32, 0.45)
(1.0 :1.6)	66%	27	4983	70	(0.36, 0.43)
(1.0 :2.0)	71%	35	4364	65	(0.35, 0.42)
(1.0 :3.0)	78%	39	4364	61	(0.38, 0.46)

To improve quality of the white emission, the FULL LUCO 4 was fabricated which includes an orange-red dye. For this LUCO device, the mixture employed was (ACN1:ADS233YE:JP5), where the ACN1 and ADS233YE ratios weights were fixed at (1.0:1.6) taking advantage from FULL LUCO 3 performance, while the JP5 was varied to ratios of 0.1, 04, 0.8, and 1.2. The emission spectra are shown in Figure 4.16. For all ratios of JP5 (0.1 to 1.2) the emission spectrum was observed to be very broad, from 380 to 780 nm, with acceptable luminous determined values (see Table 4.5). The ratio (1.0:1.6:0.0) was plot as reference. For the ratio (1.0:1.6:0.1), three peaks were observed

at 475, 554 and 672 nm, besides, a weak shoulder at 775 nm. Unexpectedly, the highest intensity peak (475 nm) corresponding to ACN1, has a blue-shift with respect to the emission without JP5 as well as the ADS233YE peak centered at 554 nm, which exhibits a blue shift of 13 nm. For this peak (554 nm) the intensity decreases, compared with the reference, due to the small absorption of the JP5 at these wavelengths. For the ratio (1.0:1.6:0.4), the peaks observed were at 481, 554 and 659 nm, with a small red-shift for the ACN1 peak, ADS233YE emissions was kept on but the JP5 emission exhibited a blue-shift of 19 nm compared with the previous relation and its intensity increased. For (1.0:1.6:0.8), a notorious change was observed, the ADS233YE peak disappeared due to the increment of JP5; this means that JP5 absorbed the light from ADS233YE because of the matching in emission and absorption, however the spectrum conserves a considerable yellow contribution. For the last ratio tested (1.0:1.6:1.2), only two peaks were observed at 487 and 648 nm, the peak center at 487 nm was red-shift compared with the previous ratio. For all ratios, excellent CIE were measured.

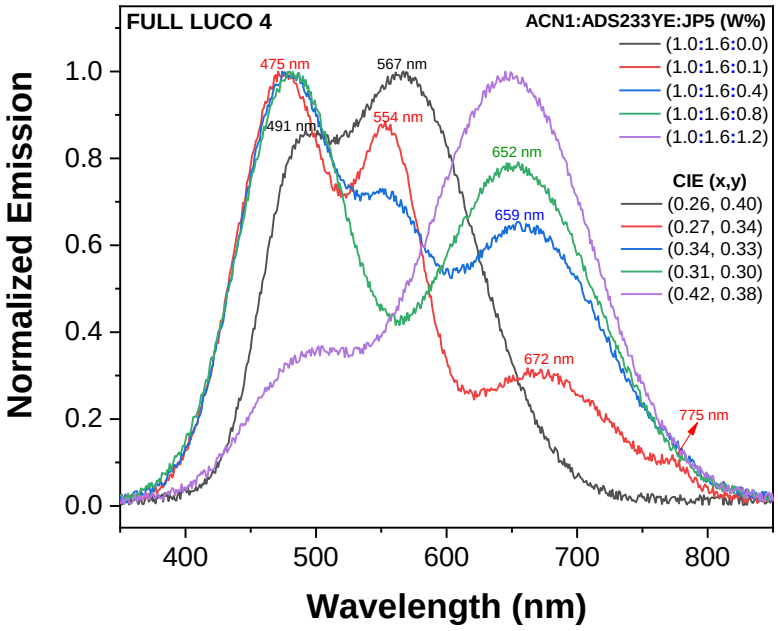

Figure 4.16. Normalized emission of the FULL LUCO 4 devices to different weigh ratios of the mixture ACN1:ADS233YE.

The blue and red shift must be explained by the intermolecular interactions emerged in this down conversion mechanism (see Fig. 4.16). Despite these possible intermolecular interactions, which were not considered in this work, the reported results and optical properties of the used materials show that the mechanisms of exciplex and FRET are related to these unexpected displacements as illustrated in Figure 4.15. Any intermolecular interaction can produce the superposition of excited sates and could be the responsible of the quenching of the shoulder centered at 775 nm that JP5 exhibited alone. Also, these processes could be the reason for the dissociation of the interactions that in the previous devices had already exhibited the compounds ACN1 and ADS233YE. Melgoza[134] reported that ACN1 interacted with other neighbor dyes, causing a modification of the expected spectrum. The morphologies of the films fabricated with the

different materials and mixtures used for the FULL LUCO 3 and FULL LUCO 4 are shown in Appendix B (Figures B.3-7). Differences in size and shape of the agglomerates of the films were observed, which could be related to the intermolecular interactions that these materials exhibited. Other authors have reported that the intermolecular interactions can modify the morphology of the organic films and at the same time the optical properties such as the emission.[136–138]

Table 4.5. Luminous and color parameter to FULL LUCO 4.

Ratio (ACN1:ADS233YE:JP5)	**Conversion efficiency**	**η_{PE} (lm/W)**	**CCT (^{o}K)**	**CRI**	**CIE (x,y)**
(1.0 :1.6:0.0)	66%	27	7780	62	(0.26, 0.40)
(1.0 :1.6:0.1)	71%	33	8800	71	(0.27, 0.34)
(1.0 :1.6:0.4)	68%	30	6832	93	(0.34, 0.33)
(1.0 :1.6:0.8)	62%	21	6627	89	(0.31, 0.30)
(1.0 :1.6:1.2)	54%	15	3299	78	(0.42, 0.38)

With this mixture of organic converters, the excellent CRI values of 89 and 93 were achieved, with CIE (0.33, 0.30) and (0.32, 0.32) respectively. In regards to luminous parameters, the conversion efficiency suppressively was improved to 71% when the JP5 weight ratio was 0.1 and at the same ratio the maximum power efficiency of 33 lm/W was exhibited. Possibly, intermolecular interactions at low JP5 concentration enhanced the down conversion mechanism, while at higher ratios as 0.8 and 1.2, it reduced the conversion.

5. A COMPARISON BETWEEN THE TWO STUDIED MECHANISMS FOR PRODUCING WHITE LIGHT FOR SSL

This chapter presents a comparative discussion of the achieved parameters (CIE, CRI, energy efficiency, luminance and bias voltage) for white light through the use of down-conversion and exciplex mechanisms. A comparison among luminescent parameters exhibited by WOLEDs and LUCOs, which are predominantly related to the technology of fabricating SSL devices, is presented.

CIE and CRI parameters: White color. Organic semiconductors were used in this thesis as emitting materials in WOLEDs and LUCOs. As discussed above, these materials can emit in all the visible spectrum. This is an advantage over inorganic semiconductors and other lighting technologies which, lacking contribution in some frequencies of the visible spectrum, exhibit low CRI and poor CIE. Moreover, as was already discussed in chapter 1, these materials could be an effective solution in the SSL free of REEs. Therefore, white OLED and full LUCO devices exhibited excellent CIE and CCT color coordinates and, the high CRI values (85 and 92, respectively) are outstanding. These values can be compared to those of commercial LEDs, CRI values oscillating around 80. Therefore, based on this comparison our devices would be good white sources, which reproduce nice colors and might be used as SSL.

In particular, it has been shown in previous chapters that broad emission from 400 to 700 nm is possible with exciplex states from a single emitting organic compound; CIE (0.31, 0.33) and CRI of 85. Therefore, the cost to produce such devices is less expensive and the manufacturing process becomes easier in comparison with other WOLEDs to obtain white light with similar characteristics. Regarding the down-conversion, white emission can be obtained very easily with the reported hybrid configuration using only one organic compound for the case of the partial conversion devices. However, the achieved white

light lacks contribution below 440 nm due to the emission properties of the used blue LED; additionally, the used organic converter lacks contribution in the reds thereby their CRI value is low (<73). Nevertheless, for comparison, the achieved emission already has the quality offered by commercial white LEDs based on phosphors. To improve the quality of white emission with partial conversion, blue LEDs with emission below 440 nm would be beneficial as well as organic converters of wider emission from green to red; for now, a single organic compound, as reported in this thesis, is unlikely to exhibit better quality. In contrast, with the full down-conversion mechanism wider emission spectra corresponding to CRI coordinates above 90 and CIE (0.32, 0.33) can be obtained. For this case, the emission from up to three organic compounds can be combined so spectra from 400 to 800 nm were observed. Thus, the full down-conversion mechanism is much better mechanism to achieved excellent white color.

WOLEDs and LUCOs devices based on the exciplex and down-conversion mechanisms are very easy to manufacture. A major limitation to induce convenient exciplex states is to find HTLs and ETLs that allow the formation of adequate energy barriers with the EMLs and be adjusted to proper values. Further, the quantum mechanics modeling for exciplex states is due to Kalinosky but there is not a high correlation between this model and experiments. For example, Kalinosky's model does not take into account the thickness of the HTLs and ETLs that, based on our study, influence the generation of those states, thereby, the proper prediction for the type of spectrum to be generated is still loose with this modeling. A deep understanding of the exciplex mechanism is necessary to improve the model.

For the case of down-conversion, the major challenge is to find materials with high quantum yield, the precise concentrations between the emitting materials, as well as to avoid re-absorption. Moreover, with this mechanism contrary to exciplex is highly

possible to design the desired color in advance, based on the individual PL spectra of each material. A model involving Lambert-Beer's law and the quantum yield of the materials could be a powerful tool to make an accurate prediction of color for the LUCO devices, although intermolecular interactions may arise causing a slight change in the expected emission spectrum.

An attractive property observed in both studied mechanisms was emission tuning. As mentioned in chapters 2 and 3, the emission from WOLED and LUCO devices can easily be tuned from cold to neutral and warm white, which would make them attractive for use in both industry and research. This tune property hardly can be exhibited by conventional emission sources including inorganic SSL.

Energy efficiency. It is necessary to emphasize two aspects concerning this concept for the adequate comparison of the achieved values reported in this work. Firstly, for SSL the efficiencies that can be calculated are external quantum efficiency (EQE), power efficiency (PE) and conversion efficiency. Any device with high EQE should exhibit high PE and high conversion efficiency; although the conversion efficiency is only applied to devices that operate under the down-conversion mechanism and is related with the quantum yield of the converter material. Secondly, for fluorescent materials such as those used in this thesis, the EQE under the EL phenomenon is limited to 5 % and LEDs to 75 % due to physical restrictions of the exciton spin-statistic and non-radiative phenomena.[139] Thus, to achieve better energy efficiency it is more convenient to use hybrid devices based on down-conversion because they combine high efficiencies of LEDs and the organic converter under EL and PL. For example, the compound ADS232GE was used as the active layer in WOLEDs, reaching a maximum PE value of ~5 lm/W while for LUCO, as converter material, its maximum PE was ~15 times higher.

The top value for the PE for WOLEDs is around <40 lm/W while for the exciplex configuration here reported was less than 10 lm/W. This low PE value is due to the limitations of the used fluorescent materials, which would reduce their use on SSL applications for high energy consumption such as indoor and outdoor lighting. However, exciplex WOLED on lower-energy consumption applications such as display screens may have a better acceptance on flexible optoelectronic devices. For this structure the energy efficiency can be enhanced through the synthesis of new materials which conserved the broad emission spectrum, of the used CZDD in our case, but with the addition of phosphorescent or thermal active delayed fluorescence (TADF) properties.

For devices under LUCO mechanism the maximum values for the conversion efficiency for partial converters is 75 % and for full converters 68 %; the YAG:Ce phosphorus is about 90 %. The PE achieved values for partial and full LUCOs in this work were 55 and 30 lm/W, respectively, which are much higher than those obtained with our best exciplex WOLED. These values are acceptable for using as white light sources and they are higher than some current light sources (incandescent and fluorescent). Taking into account the conversion efficiencies and PEs, the LUCO devices are closer than exciplex WOLED to match the inorganic LED technology. Materials with a quantum yield close to the unit would be the compound to look for better LUCO devices and they could replace LED technology based on phosphors doped with REEs.

Luminance and bias voltage. The luminance displayed by the reported devices would indicate the potential field of application. For example, the 9600 cd/m^2 achieved with exciplex WOLEDs are sufficient to be used in displays and TV screens where the brightness of the devices is within that range of 1000 cd/m^2. However, this luminance

value was achieved at 12 V, which is a bias voltage high for an industrial application. In this sense, the deep study of the use of buffer layer may reduce the bias voltages.

In the case of the LUCO's voltages, the values are the lowest of all SSL because it is an electrical intrinsic property of the efficiency LEDs used in this study at the same that their luminance; the high values of 40000 and 110000 cd/m^2 obtained with the LUCOs would be wider the range of application because with those values it could even be used in indoor or outdoor lighting.

The parameters previously compared are summarized in Table 5.1, in addition, a qualitative assessment is added as low, high, among others, to the values reported in this thesis regarding the state of the art of SSL.

Table 5.1. characteristic parameters of the organic/hybrid SSL sources manufactured in thesis work.

Technology/Mechanism	**Efficiency**	**CRI**	**Luminance (cd/m^2)**	**Turn-on**	**Tuning White/fabrication**
OLED/Exciplex					
	η_{PE}=7.5 lm/W	85	9600 (OLED-3)	5.0 V	Varying thickness and exciplex transition
	Low	**High**	**Low**	**Acceptable**	**Easy/Easy**
Hybrid/partial down-conversion	η_{PE}=55 lm/W Conversion efficiency (0.75)	73	> 110000	3.5 V 5.0 V	Varying thicknesses of organic material. The blue LED limited the broad blue contribution.
	High	**Low**	**High**	**Low**	**Limited/Easy**
Hybrid/full	η_{PE}=30 lm/W				

down-conversion	Conversion efficiency (0.68)	93	>40.000	3.5 V	Varying the ratio weight
	Acceptable	**High**	**Acceptable**	**Low**	**Easy/Easy**

To sum up, exciplex and down-conversion mechanisms employed in SSL are an alternative to fabricate easy devices with acceptable luminous parameter. For commercialization, both mechanisms present challenges to be overcome. In the case of the exciplex WOLED, an improvement in energy efficiency is necessary, as well as complete studies of lifetimes and encapsulation. In the case of LUCOs the next step is a study of thermal stability and lifetime. The advantage of LUCO over the WOLED devices studied here is that it already has the appropriate luminescent parameters for different applications within the SSL.

6. CONCLUSIONS AND FUTURE WORK.

6.1 Concluding Remarks.

Based on the mechanisms of exciplexes and down-conversion in emissive organic materials, it was shown that white light could be generated with acceptable lighting characteristics for SSL systems. It should be underlined, for the first time, the emission from both interfaces of the emissive material in exciplex devices is reported; besides, the CRI value (93) is among the highest achieved so far. The emission from both interfaces was possible through the study and use of adequate material as EML, i.e., a material with HOMO and LUMO energy levels that allow charge accumulation at both interfaces, which leads to exciplex formation. It was demonstrated the influence of the energy barrier and the thickness of the organic films for the exciplex states can be to emerge. In the first study, it showed that for the exciplex formation the energy levels of the used materials play an important rule. It was found that due to the energy barrier formed at ADS232GE/TPBi and ADS232GE/BPhen interfaces were 0.3 and 0.6 eV, respectively, allowed the formation of exciplex states, and the emission of white light was possible. While with an energy barrier around 0.1 eV the exciplex formation was not observed. In the second study, WOLED based on a new carbazole derivative showed excellent CIE coordinates (0.31, 0.33). Understanding the role of energy barriers and thickness layers was used to obtain exciplex emissions in two interfaces formed between the emissive layer with HTL and ETL. In these devices, the formation of the exciplex transitions at the HTL / EML interface is related to the change in thickness of the HTL and is responsible for the tuning emission, while the exciplex transition at the EML / ETL interface was formed due to the adequate energy barrier, being responsible for emissions at wavelengths greater than 600 nm, so the good white colors that have been obtained.

The luminous parameter reached with the simple WOLED structure ITO/PEDOT:PSS/EML/ETL/Ca-Ag were 6.5 V, 2900 cdm^{-2} and 6.3 lmW^{-1} for the turn-on, luminance and power efficiency, respectively. The importance of the buffer layer was evidenced also, all the above parameters were improved considerably by inserting a buffer layer in between the HTL and ETL, this layer enhanced holes injection, thus, the best parameters achieved were 5.0 V, 9600 cdm^{-2} and 7.5 lmW^{-1}. Furthermore, taking into account the novelty of the structures, the easy fabrication, the use of new fluorescent materials, and excellent color quality, these single white OLEDs fabricated become a valuable contribution in this field of research.

In the other hand, down-conversion mechanism was used to fabricate partial and full LUCO devices and excellent white emission was achieved. The appropriates EL and PL intensities were studied through the control of the ratios and thicknesses of the converters. White color can be reached with a wide range of thickness (0.3 to 1μm) and concentration (30 to 80 mg/ml) of the organic converter. Meanwhile, the conversion efficiency of the devices is related with the quantum yield of the organic material, thus, materials with high quantum yield are disable to guarantee a high performance of the devices. With the partial LUCO devices, the converter ADS233YE exhibit a quantum yield of 84% and the maximum conversion efficiency was of 73% while for full LUCO devices, the conversion efficiency was of 71% with the mixture (ACN1:ADS233YE:JP5) which should be related at the average quantum yield of the materials.

Regarding the emission color, it was found that with LUCO devices excellent color characteristics can be achieved where the intermolecular interaction played an additional role to broad the emissions. The overall color characteristics of the devices fabricated are acceptable compared to the other lighting sources. A close ideal CIE was exhibited of CIE (0.32, 0.33), and the CRI values (93) are among the highest reported. With this study,

it was demonstrated that organic materials as converters are an alternative in SSL field against the use of phosphors. Optical parameters and color quality are acceptable to compete with those of phosphors materials.

A deep understanding of the intermolecular interaction in the organic materials could be the indispensable way to improve the performance of these novels SSL proposed.

5.2. Future Work

Despite of the good results, challenges to improve the performance in the two mechanism are necessary to address, which are listed as follow:

- ***A better understanding of the intermolecular interactions***. A better understand of these interactions would allow us to predict the true potential of the exciplex structures as well as the exactly energies of the new transition formed. In this sense an alternative to the Kalinosky model must be developed, which enclosed other physical and chemical properties than the organic material exhibited and can be related to this interaction. In this same way, the measured time decay in electroluminescence have to be developed to determine with a larger exactitude the possible new transitions formed under electrical excitation.
- ***Better organic materials.*** News and commercial organic materials with optical properties as phosphorescence and TADF will be used in this simple OLED structure to find new white devices under exciplex mechanism with high efficiency energy. In the LUCO case, new material with high quantum yield and phosphorescent properties are desirable, where a superior conversion efficiency than phosphors materials based on REEs is expected.

- ***A theoretical model LUCO***. A general model to determine thickness, concentration, ratio, emission and conversion efficiency in LUCO devices could be developed taking into account the Beer-Lambert's law but adding parameters such as quantum yield. This would shorten the experimental work for future research.
- ***Application of these novel organic and hybrid devices***. Lifetime and stability of the devices should be studied because it is an important aspect that determine the application and commercialization of the device.

7. OTHER CONTRIBUTIONS.

6.1. Study of the intermolecular interaction due to acids and thermal treatment to tuning emission in OLED devices.

The optical properties of organic conjugated compounds are usually determined by their chemical structure and the presence of functional groups. However, some fluorescent compounds have the ability to tune their absorbance and fluorescence (PL) in response to some external stimuli such as pressure, heat, pH, mechanical grinding, solvent polarity, etc. These compounds named "smart" fluorescent materials have attracted considerable attention owing to their potential applications in optical switches, organic light-emitting diodes (OLEDs), data recording, sensors, displays or photodynamic therapy.[140–144] The external stimuli affect the molecular conformation, packing, and noncovalent interactions, leading to changes in their luminescence properties.[138,145–152] Li et al.,[137] in a recent review did an excellent description of different examples of these luminescence changes that some materials. In particular, for thermal stimuli (thermochromism) or changes in pH conditions (halochromism) have been widely reported.[153–163]

In this work, a systematic study of changes on optoelectronic-properties of (Z)-3-(4-(4,5-diphenyl-1*H*-imidazole-2-yl)phenyl)-2-phenylacrylonitrile (**DPimdPPA**) based films owing to treatments with acid or temperature, was reported. The **DPimdPPA** films treated with vapors of HNO_3, HCl or CH_3COOH exhibited a hypsochromic shift and an enhanced in the fluorescence quantum yield (Φ_F). Surprisingly, similar behavior exhibited **DPimdPPA** films when were exposed to a thermal treatment with temperatures between 100 ºC and 240 ºC. XRD study were done; the results show that **DPimdPPA** exhibited polycrystallinity and depending of the treatment, different crystal or amorphous patter is observed. Additionally, morphological studies by AFM showed that agglomerates with

different sizes and shapes were formed due to either treatments. These particular agglomerates which are correlated with the XRD habit, are responsible to the hypsochromic shift and increment of emission intensity. This fluorescence shift was used to tune the OLED emission; in particular, devices with pristine **DPimdPPA** film as well as treated with HNO_3 vapor or at temperature of 240 °C were prepared. The emission with pristine films was warm white with CIE coordinates (0.45, 0.43); with HNO_3 treatment was green with CIE coordinates (0.28, 0.40) and, when treated at 240 º C the emission was greenish-blue with CIE coordinates (0.35, 0.48). Besides, the optoelectronic parameters as threshold voltage and luminance were enhanced with the treatments; the maximum luminance of 5400 cd/m^2 while the highest luminance efficiency of 5.2 lm/W. Therefore, in this work it is shown that **DPimdPPA** can be used to fabricate OLEDs with different emission wavelength with the above easier treatments.

6.1.1. Acids treatment on DPimdPPA films.

The absorbance and photoluminescence spectra of the **DPimdPPA** films at room temperature (rt) and without any other treatment are shown in Figure 7.1a. The maximum wavelength of absorption (λ_{abs}) was at 396 nm, which corresponds to the π–π^* transition and the maximum wavelength (λ_{max}) of photoluminescence at 569 nm with the Stokes shift of 7678 cm^{-1}. Figure 7.1b shows the PL spectra of the **DPimdPPA** films exposed to HNO_3 vapors; as can be observed, λ_{max} shifted from yellow (λ_{max}=569) up to blue (λ_{max}=465 nm) as a function of the exposition time. Besides, the relative intensity was increasing. The changes occurred in a short period of time, withing one minute of exposure the blue-shift begins and after 3 minutes the blue-shifting finished. Further, after 4 minutes the intensity of emission decreased to vanish totally, this could be owing to an excess of acid that finally damage the film. As is shown in Figure 7.1c, similar blue-shift

in emission was observed when the **DPimdPPA** films were exposed to HCl and CH_3COOH. The spectra also show a blue-shift in the wavelength of maximum absorption, from 396 nm to 362, 365 and 378 nm for CH_3COOH, HCl and HNO_3, respectively. The PL emission wavelength (λ_{PL}) shows similar shifting from 569 nm to 465, 501 and 515 nm for HNO_3, CH_3COOH and HCl, respectively. The increasing of the quantum yield of the films exposed to acids was measured and is shown in Figure 6.1d.

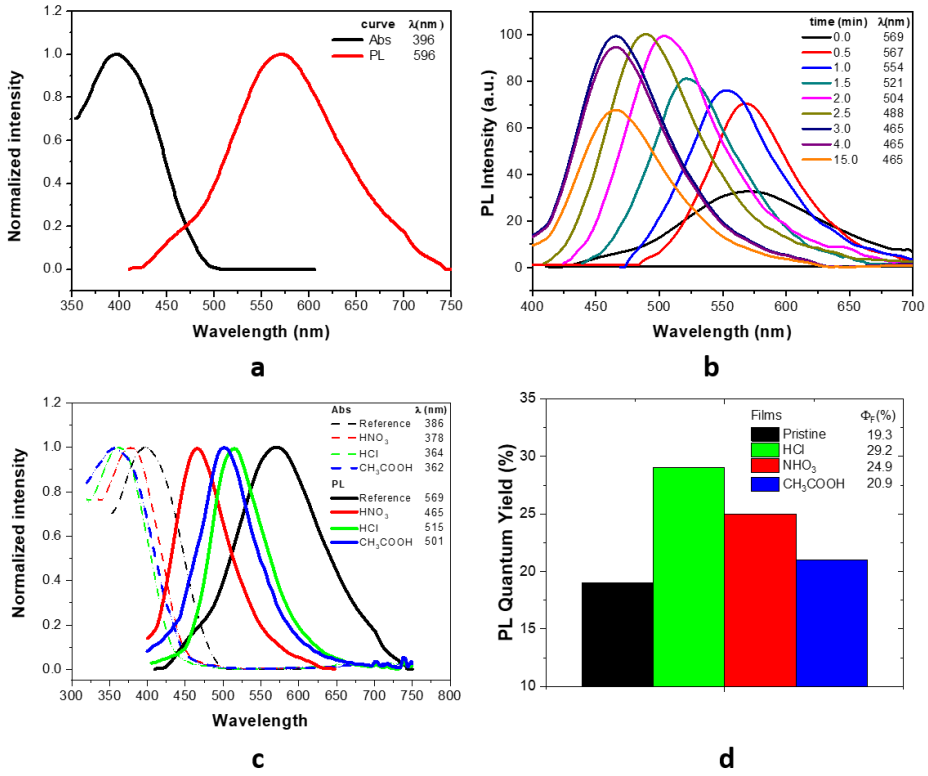

Figure 7.1. Acid treatment on ***DPimdPPA*** *film.* ***a)*** *Absorbance and photoluminescence spectra of the* ***DPimdPPA*** *film (pristine); b) Photoluminescence spectra of the* ***DPimdPPA*** *film exposed to HNO_3 vapor during time intervals; c) Absorption and photoluminescence spectra of the* ***DPimdPPA*** *films the pristine sample and those exposed to HCl, HNO_3, CH_3COOH vapors. (d) Bar diagrams showing the Φ_F due to the interaction vapors of acid.*

The changes in the Abs, PL, and Φ_F of the **DPimdPPA** films can be attributed to the proposed protonation mechanism that is shown in scheme of Figure 7.2. That is; the modification in the molecular electronic density of molecule when **DPimdPPA** interact with an acid vapor. In neutral condition, **DPimdPPA** exhibited a D-π-A structure whereas in the acidic condition it showed A'-π-A motif because of the absence of lone pair in the imidazole NH group.

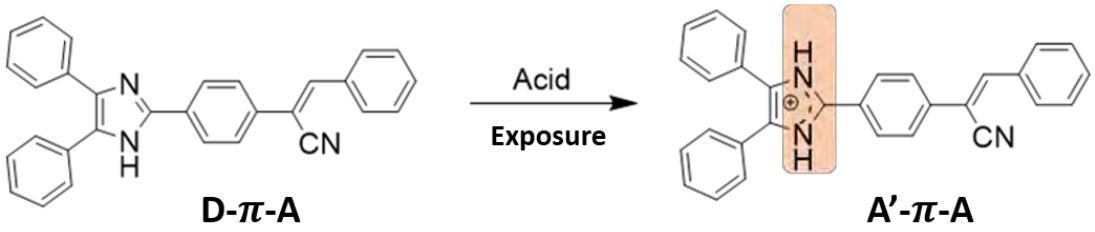

Figure 7.2. Scheme of possible protonation mechanism of DPimdPPA reacted with acid vapor.

The possible differences in the blue-shift between the three acids could be to do an auxochromic effect from the counterion, of the respective acid that affect the packing molecular that each film in turn influence the length of the hypsochromic shift, similar reports have noticed the influence of the counterions in the protonation.[164–166.] Besides, due to oxidative character of NO_3^-, there could be an increment in the band-gap value compared with other counterions. In turn it is related to the possible enhancement of the rigidity of the molecule, the treatment with NHO_3 was the only that showed a reduction in the Stokes shift compared to the pristine film.

The X-ray diffraction (XRD) measurements were done for **DPimdPPA** films exposed to acid vapor, the XRD patterns are shown in Figure 7.3. For the pristine film and the film treated with CH_3COOH no diffraction was obtained indicating an amorphous phase. The

film exposed to HCl presented only one peak at 2θ=10º. On the other hand, those films treated with NHO_3 exhibited a well-defined XRD pattern with four peaks at 8°, 9°, 15.7° and 17.7º (2θ). The two latter cases indicate that the acid treatments have induced a crystalline phase in the films. The induced crystallinity together with protonation of the molecules could be the reason for the blue-shift in fluorescence for films treated with acid vapors. Our results agree with similar studies about changes in the optical properties of organic molecules under acid environment.[155,159–163,167]

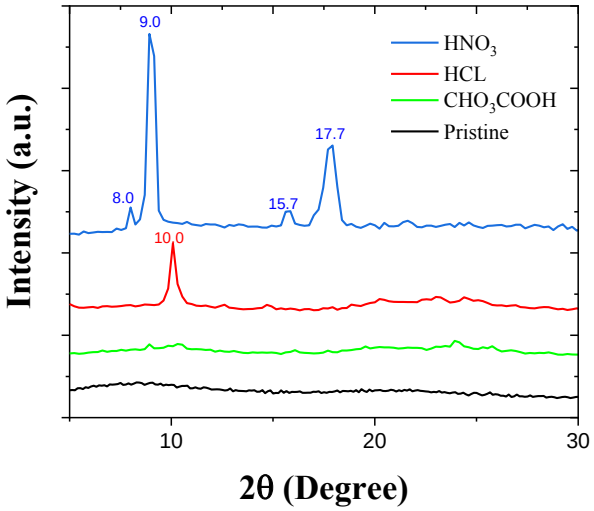

Figure 7.3. Diffractogram of ***DPimdPPA*** *films exposed to the acid's treatment.*

To correlated the induced crystallinity with the film topography, a morphological analysis by AFM was conducted to **DPimdPPA** films before and after being exposed to different acid vapors, the corresponding images are shown in Figure 7.4. As can be see, the homogeneous morphology of pristine film (see Fig. 7.4a) changes to like a needle morphology, the effect was more evident for the treatment with HNO_3 (Fig. 7.4e) while other for the CH_3COOH, the morphology remains like agglomerates and only damage on the surface is observed because the acid would dissolve the film (Fig 7.4g).

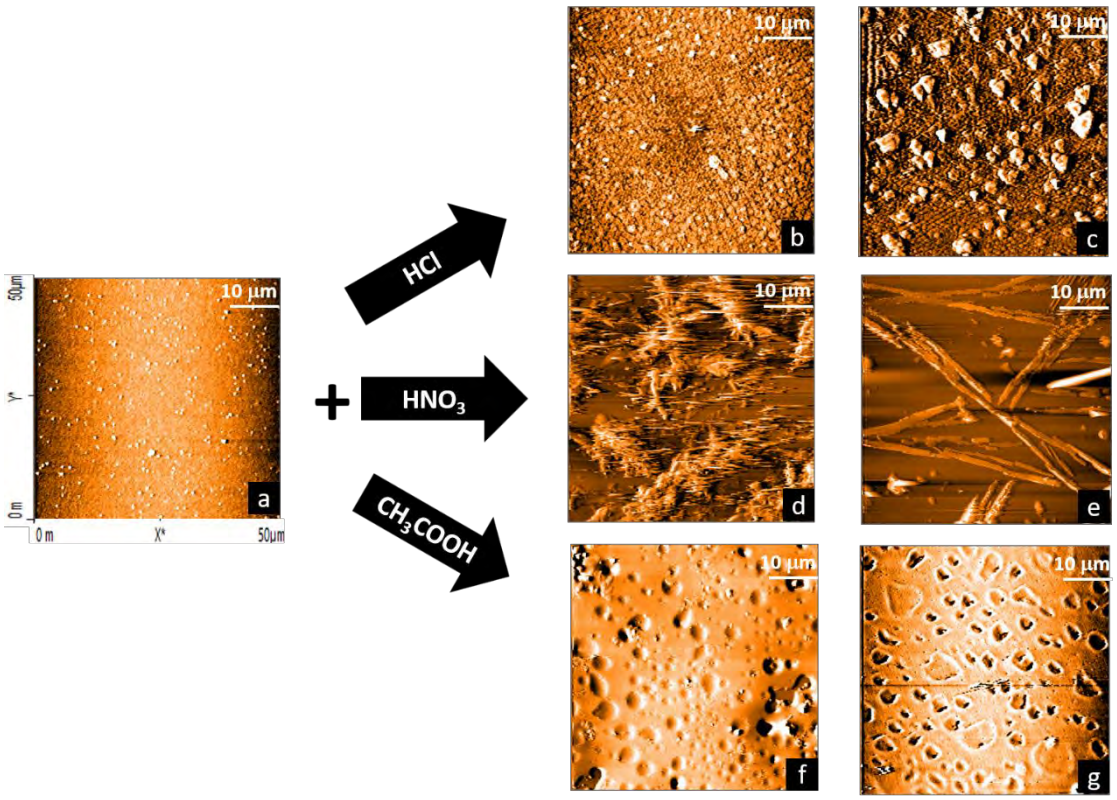

Figure 7.4. Topographies of the ***DPimdPPA*** *films. (a) before acids treatments, (b and c) treated with HCl for 1.5 min and 3 min, respectively. (d and e) treated with HNO_3 for 1.25 min and 2.5 min, respectively. (f and g) treated with CH_3COOH for 0.5 min and 1 min, respectively. In micrographs 3a, 3b and 3c, a derived filter was used to highlight the morphologies.*

7.1.2. Thermal treatment on DPimdPPA films.

Thermal treatments to organic films have been reported in order to improve their optoelectronics properties.[168–171] To analyze the effect of temperature on optical properties of **DPimdPPA** films deposited by either spin coating or vacuum evaporation methods, films were subjected to heating treatments on a hot plate. It should be worth noting that with the heat treatment the films exhibited a similar hypsochromic effect as was evident with the acids like is shown in Figure 7.5. Fig 7.5a shows the absorption

spectrum of the **DPimdPPA** film at room temperature and 240 ºC (less than the **DPimdPPA** melting point, 250 °C). Before thermal treatment, the film showed the absorption λ_{max} at 392 nm and after heating at 240 ºC, a slight hypsochromic shift at 373 nm

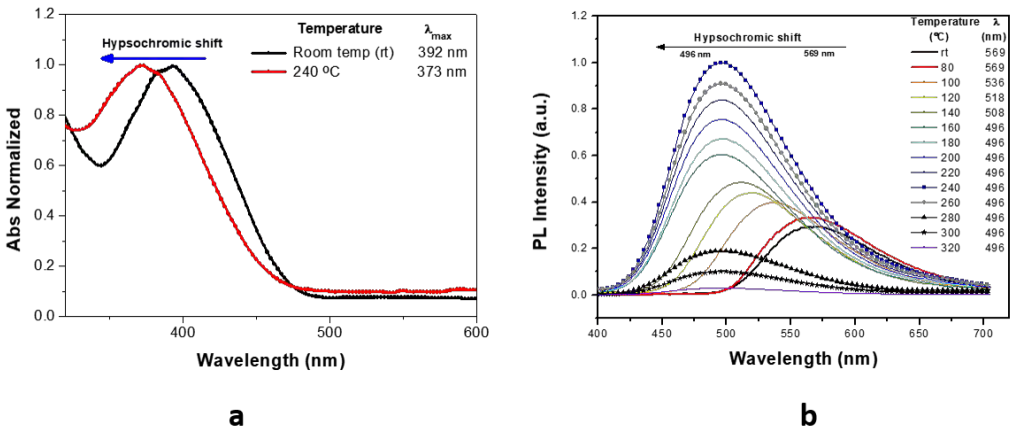

Figure 7.5. ***DPimdPPA*** *films under thermal treatment. a) Abs spectra of before and for the thermal treatment at 240 º C; b) PL at different temperatures.*

The hypsochromic shift was also observed in PL analysis (Fig. 7.5b) and it agreed with the absorption results. At temperatures lower than 100 °C, the initial λ_{PL} for **DPimdPPA** films (566 nm) was not affected. However, at 100°C, the emission wavelength changed to 536 nm (yellowish-green) and remains shifting as the temperature increase up to 496 nm at 160°C (bluish-green color). Along with the blue-displacement, an increase of emission intensity was also observed and these increments followed until 240 °C. The Φ_F at room temperature, 100, 160 and 240 °C was 17, 20.5, 22 and 23 % respectively.

The morphology of thermal treated **DPimdPPA** films, was studied through AFM. Figure 7.6a-d shows the AFM images of films deposited by spin coating method and subjected to different temperatures: rt, 100 ºC, 160 ºC and 240 °C. The deposited **DPimdPPA** films

showed a messy morphology (Fig. 7.6a), however, as the temperature increase an ordered on the morphology appear (Fig. 7.6b). For films heated at 160 ºC its morphology showed the appearance of agglomerates (Fig. 7.6c) and for temperature of 240 °C crystals with needle shaped as large as 10 μm was evidenced (Fig 7.6d).

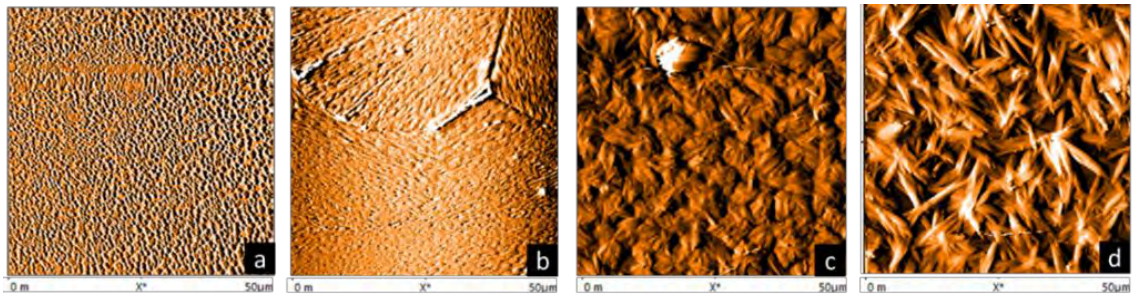

Figure 7.6. Topographies of ***DPimdPPA*** *films deposited by thermal evaporation. (a) rt condition, (b) treated at 100 ºC, c) treated at 160 ºC and d) treated at 240 ºC.*

XRD measurements were conducted for pristine **DPimdPPA** films and treated at three representative temperatures (100, 170, and 240 ºC) at which changes in fluorescence were observed. The XRD patterns for the pristine and treated films are shown in Figure 7.7. Initially, the pristine film exhibited an amorphous phase, however, as the temperature increased, the pattern showed some peaks indicating the formation of a crystalline phase. The XRD pattern for film heated at 100 ºC (temperature after which blue-shift begins), exhibited one peak at 2θ=12.1º. For treatments at 170 and 240 ºC (temperatures for the maximum blue-shift and the maximum emission increment, respectively) a well-defined pattern with peaks at 6.1°, 11.9°, 12.7°, and 19.1° (2θ), were observed. Therefore, the heat treatment induces crystallinity in the **DPimdPPA** films, changing intermolecular interactions that lead to a hypsochromic effect in optical properties as well as improvement in fluorescence quantum yield. A rearrangement in the molecular

orientation owing to heat treatment also induce a change in films morphology as revealed by AFM analyzes in Figure 7.6b-d.

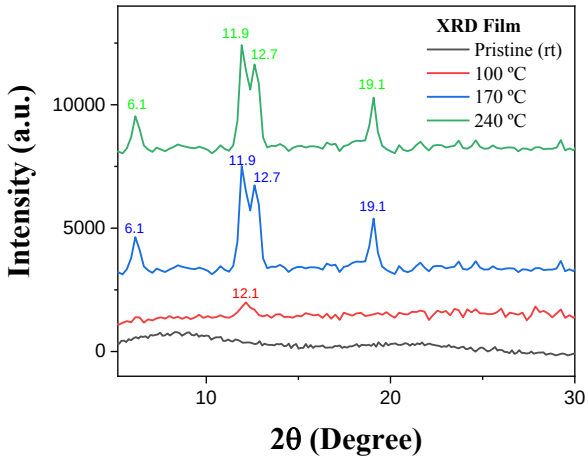

Figure 7.7. XRD of ***DPimdPPA*** *films to different temperatures. (a) rt condition, (b) treated at 100 ºC, c) treated at 170 ºC and d) treated at 240 ºC.*

Interestingly, the treatment at 240 ºC produced similar effect to that of treatment with HNO_3 vapors, both induced crystallinity on the films. For these treatments, the blue-shift in emission was the larger and for the case of temperature the higher quantum yield was also achieved. Further, the treatments were able to change the films morphology and lead to the formation of crystals with needle like shape

7.1.3. Electroluminescence properties.

The **DPimdPPA** films were used as active layer for OLED devices. Three different types of OLEDs were prepared, one where active layer was used without any treatment (OLED-1), one treated with HNO_3 vapor (OLED-2) and another one with thermal treatment at 240 °C (OLED-3). The treatments features were those where the higher hypsochromic effect was observed. The electroluminescence spectra of OLEDs 1-3 are shown in Figure

6-8 as well as the picture of working devices. OLED-1 with pristine active layer shows a broad emission spectrum with two emission peaks at 550 and 655 nm with CIE coordinates (0.45, 0.43), this can be considered warm white light. The emission centered at 550 nm corresponds to π- π transitions, while the emission at 655 nm, which was not evident in PL, could be due to intermolecular interactions possibly of exciplex nature.

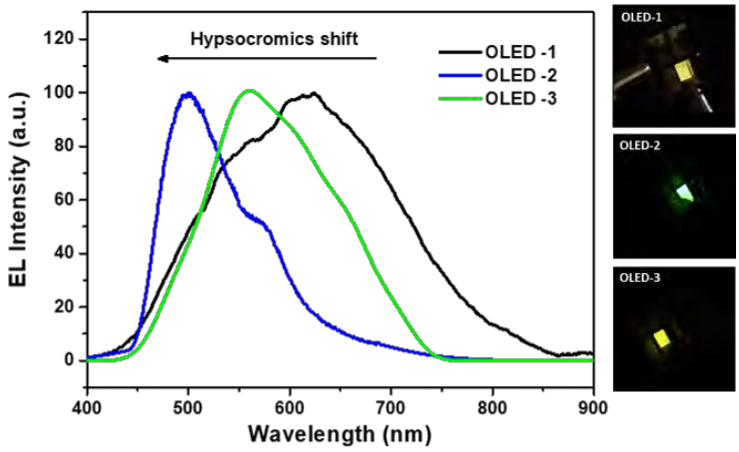

Figure 7.8. Electroluminescence spectra for OLED devices with ***DPimdPPA*** *as active layer. OLED-1 (without treatments), OLED-2 (NHO_3 vapor exposure), and OLED-3 (thermal treated at 240 °C).*

For OLED-2 a hypsochromic shift in EL like the recorded for PL owing to NHO_3 vapor was observed. The EL spectrum showed a hypsochromic shift with respect to OLED-1 and a bluish-green emission was observed, with CIE coordinates (0.28, 0.40). The EL spectra shows two peaks, the π-π transition at 500 nm and that corresponding to exciplex formation at 575 nm. Compared with the EL spectra for pristine device, the peak assigned to π-π transitions increase while the peak assigned to exciplex decrease. In the case of OLED-3, the blue-shift observed for PL was not evident, for EL the wavelength of maximum emission centered about 530 nm shifted 125 nm compared with thus for pristine device (655 nm). However, the broad EL spectrum has CIE coordinates (0.35,

0.48) quite similar to the recorded for OLED-1. According with these results, the tuning emission is evident due to the acid and thermal treatment compare with the reference OLED-1 whose EML was not exposed to neither treatment; the blue-shifts were 55 and 26 nm, to OLED-2 and OLED-3, respectively.

Conclusion

A tunable hypsochromic effect in absorption and fluorescence, as well as an increment in the intensity of emission, of **DPimdPPA** films are reported owing to treatment with acid vapors of HCl, HNO_3, and CH_3COOH or by heating at temperatures above 100 ºC. Both treatments induced crystallinity in the films and the XRD pattern showed a preferential molecular orientation. The induced crystallinity modifies the molecular arrangement and intermolecular interactions since a change in the film morphology was observed. Therefore, the induced crystallinity and molecular rearrangement effects are responsible for the changes in optical properties. The changes in emission owing to acid and thermal treatments were used to prepare OLEDs with different electroluminescence properties. This is an easy way for tuning the device's emission that also improves its electrical parameters.

7.2. Encapsulation OLED.

Encapsulation OLED study was a contribution developed in this work, in the follow section the summarized of the result more important will be described.

Once the OLEDs are fabricated, encapsulation is the last process they must undergo to ensure that they work by longer time. Without encapsulation process, these devices only worked for a few hours due to the degradation that organic materials exhibit in the presence of oxygen while with encapsulation they can last up to thousands of hours and

depending on the stability of the compounds used. The devices fabricated were monitored using the LT50 parameter, which defines the life time of the device when the initial luminescence drops by 50%.

Two types of encapsulation were made in this work; one, using the E131 resin and another using a hybrid composed, formed by the NOA 76 resin and silicon nanoparticles. Both resins were acquired from OSSILA company. In the Figure 7.9 is shown a process diagram for the encapsulation of both structures; firstly, 25 µL of the E131 resin or 50 µL for the hybrid resin was deposited on the surface of the OLED. Then the resins were dried with a UV lamp with wavelength of 365 nm. The curing time for the E131 resin was 3 seconds, while for the hybrid it was 2 minutes. It is important to mention that the coating was developed under ambient conditions.

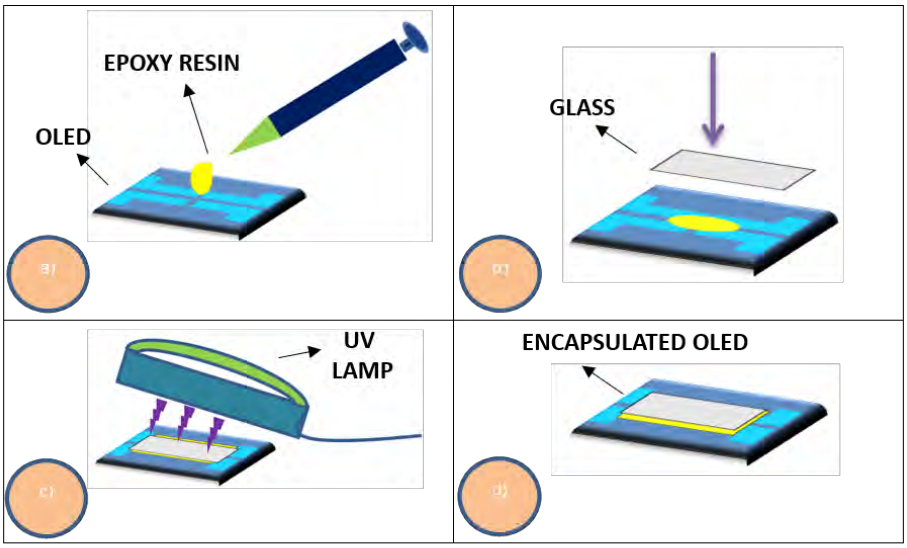

Figure 7.9. Encapsulation process to OLED devices, a) deposit of epoxy resin; b) put the coating glass; c) curing with the UV lamp; d) encapsulated OLED.

The OLED structure was ITO/PEDOT:PSS/ADS232GE/BPhen/Ca-Ag. In Figure 7.10 is shown the luminance measured in different times, to the device encapsulated with the epoxy resin E131, according with the results the LT50 to these devices was of 360 h. The devices were encapsulated immediately after to be fabricated, these were left out of the glove box in laboratory environment and monitored for luminescence every 6 hours.

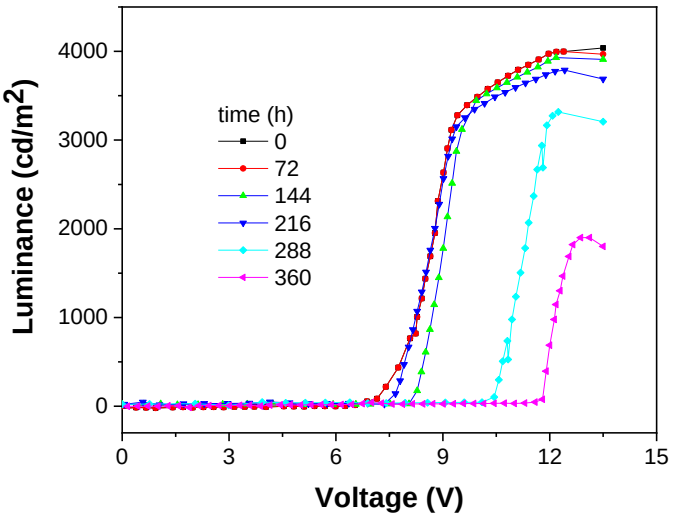

Figure 7.10. Luminance curve in function of bias voltage to different times (hours).

To compare this result with the LT50 that was achieved with the devices without encapsulation and using the hybrid epoxy resin (NOA 76: silicon nanoparticles), the Figure 7.11 is shown. As can be seen in the luminance curve, the LT50 to the devices are 24, 78, and 360 to without encapsulation, NOA 76, and E131, respectively. According to the results, E131 offer the highest LT50, possibly because of the short time to cure (3s) not allow the penetration as occur with the NOA (2 min). As was to expect, the devices without encapsulation reducing his lifetime very fast, and pass 70 h, let to work.

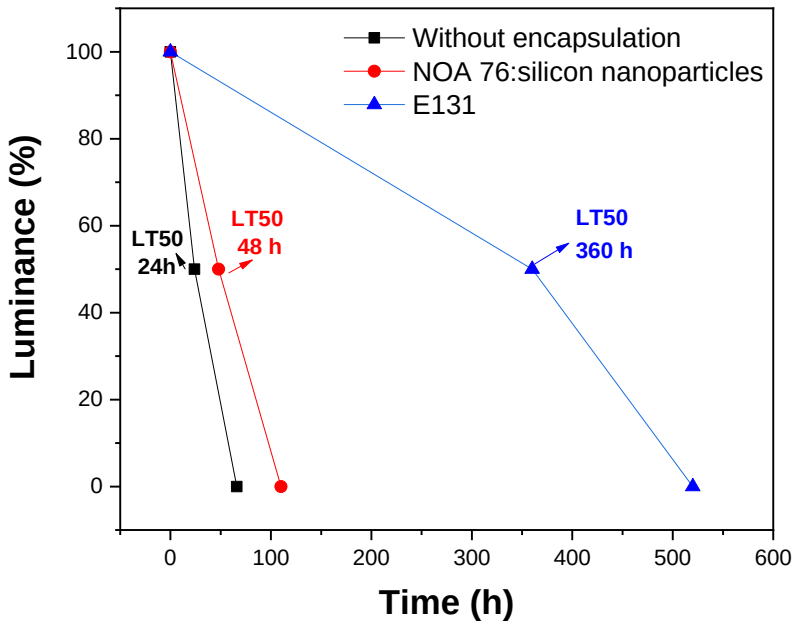

Figure 7.11. Luminance in function of the time.

The encapsulated devices, in comparison with the non-encapsulated ones, managed to delay the degradation process, with lifetimes of up to 360 hours for the first resin, however, the lifetimes of the devices in both cases are below the values reported by other authors. whereby is required further and deep study to extend the time of the OLED devices above 10000 hours.

From this study, the material engineering thesis was done titled " Encapsulado de Dispositivos Leds Orgánicos (OLEDs) Mediante el uso de Resinas Epóxicas[172] by the student Alejandra Daniela Mercado Ramírez from Tecnológico de Estudios Superiores de Jocotitlán.

7.3 Ablation laser to OLED patrons.

Laser ablation method was implemented for the engraving of patterns OLED on ITO-coated glass substrates (Indium and tin oxide), besides the method was employed to fabricate matrix OLEDs.

As it is a surface emission, the exact delimitation of the OLED area is very important. There are several methods to carry out this process, among the most used is the wet etching method, which consists in removing layers of material by means of a chemical attack. This method is widely used because of its simplicity and because no special equipment is needed, but, poor delimitation in areas of microns has been evidenced as will be shown later.

Laser ablation for ITO occurs when a laser beam uniformly strikes the ITO which in turn absorbs the energy from the laser. This energy must be intense enough to produce a significant increase in temperature of the material producing a thermoplastic force, which allows the separation of ITO from the glass substrate where usually it is deposited. The representative schematic and a photography of the optical array used for ablation are shown in Figures 7.12a and 7.12b, respectively.

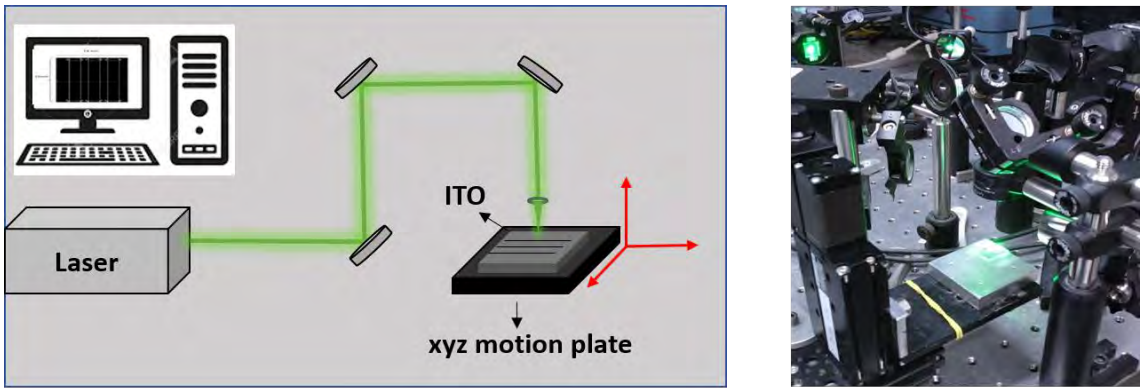

Figure 7.12. schematic of the optical array used for ablation laser.

For the implementation of the laser ablation technique an Nd:YAG laser (yttrium aluminum garnet doped with neodymium impurities) was used, with a wavelength of 532 nm, repetition frequency of 1000 Hz, pulse width of 300 ps, energy of 35 μJ and in pulsed operation mode. For the engraving system, a New Focus platform was used, controlled by three motors that move the y, x, z axes. The motors were controlled by drivers and serial communication, using the Matlab software. The patterns were designed by creating a program in the ATOM code editor, using the C programming language.

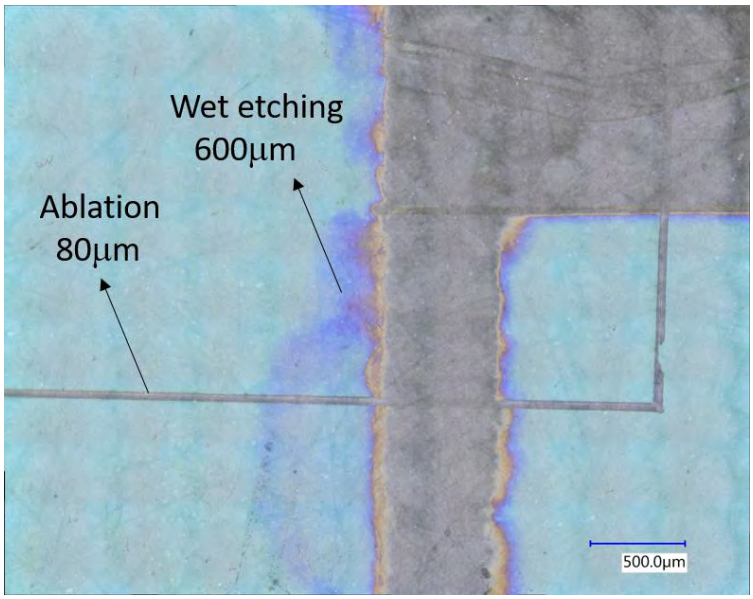

Figure 7.13. ITO substrate through the 5000X optical microscope.

Figure 7.13 shows an image of the ITO substrate through the 5000X optical microscope. In the image can observed the line with which the ablation removed the ITO (80 microns thick) while in the same image you can see that at the scale shown the ITO removal with wet etching is not uniform, which generates that the area of the OLED devices is not exact, which in turn brings problems for the reproducibility of them.

Once the technique was optimized, were design and manufacture OLED patterns, such as the one shown in Figure 7.14. In Figure 7.14a, an image of the patterns made with ablation is shown through the optical microscope. as can be observe the delimitation is very uniform. Figure 7.14b shows 3 different patterns that were manufactured in addition to one of the OLED matrixes where a blue emission is seen from 9 small mini OLEDs.

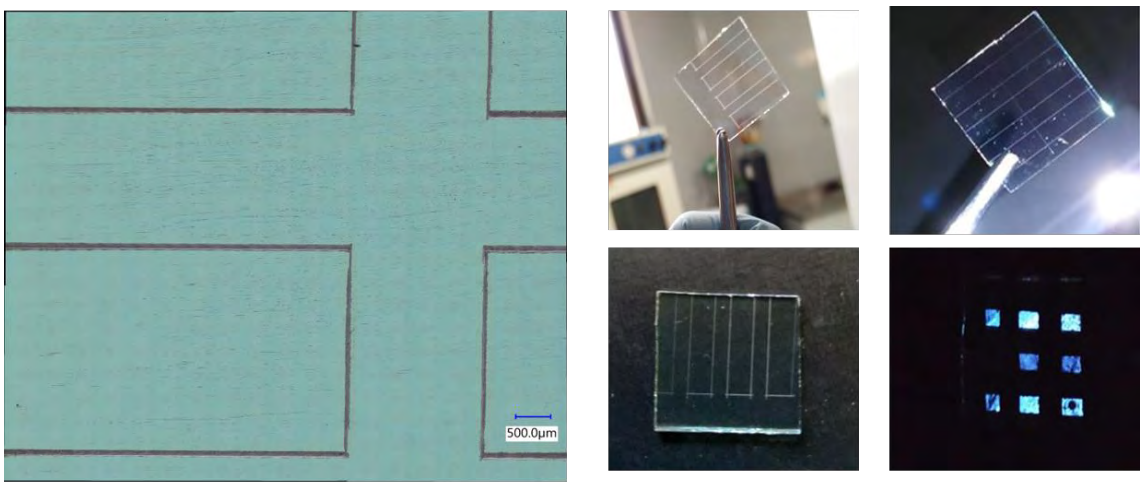

Figure 7.14. a) image of a patron OLED on ITO substrate through the 5000X optical microscope; b) images of ITO substrates with the patron's OLED and a matrix OLED working.

In conclusion, it was possible to implement the laser ablation method for the manufacture of patterns in OLED devices, thus achieving an improvement in the performance of the devices compared to those manufactured with wet etching. Among the parameters that were improved are: defined and repeatable emission area in all devices, reduction of time for pattern making and select from a wide range of patterns.

From this study, the electronic engineering thesis was done titled "*Diseño y Fabricación de una Luminaria OLED para Una Lampara de Escritorio*" by the student Jazzia Michelle Sánchez Avalos from Universidad de Guanajuato.

7.4. Publications relate to this thesis.

First author:

- Bernal W, Barbosa-Garcia O, Aguilar-Granda André, Pérez-Gutiérrez E, Maldonado J-L, Percino MJ, Rodríguez-Molina B, White Organic Light emitting diodes based On exciplex states by using a new carbazole derivative as single emitter Layer. *Dyes and Pigments.* 163 (2019) 754–760.

- Wilson Bernal*, Karnambaram Anandhan, M. Judith Percino, Oracio Barbosa-García, Enrique Pérez-Gutiérrez, Margarita Cerón, Jose-Luis Maldonado, Martha Sosa Rivadeneyra and Subbiah Thamotharan. Optoelectronic properties of (Z)-3-(4-(4,5-diphenyl-1H-imidazole-2-yl)phenyl)-2-phenylacrylonitrile films under acid and thermal environments for tuning OLED emission. *Dyes and Pigments*. (2021).

Co-author

- Enrique Pérez–Gutiérrez*, M. Judith Percino1*, Wilson Bernal, Margarita Cerón, Paulina Ceballos, Martha Sosa Rivadeneyra, Maxime A. Siegler and Subbiah Thamotharan. Fluorescence Tuning with a Single Dye Embedded in a Polymer Matrix and its Application on Multicolor OLEDs. *Dyes and Pigments.* (2021).

- M. Judith Percino, * Margarita Cerón, Perumal Venkatesan, Enrique Pérez-Gutiérrez, a Pilar Santos, Paulina Ceballos, Armando E. Castillo, Paola Gordillo-Guerra, Karnambaram Anandhan, Oracio Barbosa-García, Wilson Bernal and Subbiah Thamotharan. A low molecular weight OLED material: 2-(4-((2-hydroxyethyl)(methyl)amino)benzylidene)malononitrile. Synthesis, crystal structure, thin film morphology, spectroscopic characterization and DFT calculations. *RSC Adv*., 2019, 9, 28704–28717.

- Enrique Pérez-Gutiérrez, Margarita Cerón, Pilar Santos, Paulina Ceballos, VenkatesanPerumal, Subbiah Thamotharan, Wilson Bernal-Pinilla, Oracio Barbosa-García and M. Judith Percino*. Films Morphology of Acrylonitrile Materials Deposited by Solution Process and Vacuum Evaporation. Supramolecular Interactions, Optoelectronic Properties and an Approximation by Computational Calculations. *New J. Chem*., (2019) 43, 15513-15524.

- Diana Marcela Montoya, Enrique Pérez-Gutiérrez, Oracio Barbosa-Garcia, Wilson Bernal, José-Luis Maldonado, M. Judith Percino, Marco-Antonio Meneses, Margarita Cerón. Defects at the interface electron transport layer and alternative counter electrode, their impact on perovskite solar cells performance., *Solar Energy*, 195 (2020) 610–617.

7. REFERENCES.

(1) Liu, W.; Lustig, W. P.; Li, J. Luminescent Inorganic-Organic Hybrid Semiconductor Materials for Energy-Saving Lighting Applications. *EnergyChem* **2019**, 100008.

(2) De Almeida, A.; Santos, B.; Paolo, B.; Quicheron, M. Solid State Lighting Review – Potential and Challenges in Europe. *Renew. Sustain. Energy Rev.* **2014**, *34*, 30–48.

(3) Montoya, F. G.; Peña-García, A.; Juaidi, A.; Manzano-Agugliaro, F. Indoor Lighting Techniques: An Overview of Evolution and New Trends for Energy Saving. *Energy Build.* **2017**, *140*, 50–60.

(4) Nakamura, S.; Krames, M. R. History of Gallium–Nitride-Based Light-Emitting Diodes for Illumination. *Proc. IEEE* **2013**, *101* (10), 2211–2220.

(5) Zissis, G. Energy Consumption and Environmental and Economic Impact of Lighting: The Current Situation. In *Handbook of Advanced Lighting Technology*; Springer International Publishing: Cham, 2016; pp 1–13.

(6) Nardelli, A.; Deuschle, E.; de Azevedo, L. D.; Pessoa, J. L. N.; Ghisi, E. Assessment of Light Emitting Diodes Technology for General Lighting: A Critical Review. *Renew. Sustain. Energy Rev.* **2017**, *75*, 368–379.

(7) Branas, C.; Azcondo, F. J.; Alonso, J. M. Solid-State Lighting: A System Review. *IEEE Ind. Electron. Mag.* **2013**, *7* (4), 6–14.

(8) Held, G. *Introduction to Light Emitting Diode Technology and Applications*, 1st ed.; Auerbach Publications, 2009.

(9) Tsujimura, T. *OLED Display Fundamentals and Applications*, 2nd ed.; WILEY, Ed.; 2017.

(10) Giovanella, U.; Pasini, M.; Botta, C. Organic Light-Emitting Diodes (OLEDs): Working Principles and Device Technology; 2016; pp 145–196.

(11) National Academies of Sciences. *Assessment of Solid-State Lighting, Phase Two*; The National Academies Press: Washington, DC, 2017.

(12) U.S. Department of Energy. *Light at Night: The Latest Science. s.l.: Solid-State Lighting Program*; 2010.

(13) Envirolink Northwest. *Introductory Guide to LED Lighting*; Warrington, UK, 2011.

(14) Halonen, L. Energy Efficient Electric Lighting for Buildings. In *In: proceedings of IEA technical conference*; Copenhagen, 2010.

(15) Zou, S.-J.; Shen, Y.; Xie, F.-M.; Chen, J.-D.; Li, Y.-Q.; Tang, J.-X. Recent Advances in Organic Light-Emitting Diodes: Toward Smart Lighting and Displays. *Mater. Chem. Front.* **2020**, *4* (3), 788–820.

(16) Chen, B.; Liu, B.; Zeng, J.; Nie, H.; Xiong, Y.; Zou, J.; Ning, H.; Wang, Z.; Zhao, Z.; Tang, B. Z. Efficient Bipolar Blue AIEgens for High-Performance Nondoped Blue OLEDs and Hybrid White OLEDs. *Adv. Funct. Mater.* **2018**, *28*

(40), 1803369.
(17) Wang, Q.; Tian, Q.-S.; Zhang, Y.-L.; Tang, X.; Liao, L.-S. High-Efficiency Organic Light-Emitting Diodes with Exciplex Hosts. *J. Mater. Chem. C* **2019**, *7* (37), 11329–11360.
(18) Popovic, Z. D.; Aziz, H. Reliability and Degradation of Small Molecule-Based Organic Light-Emitting Devices (OLEDs). *IEEE J. Sel. Top. Quantum Electron.* **2002**, *8* (2), 362–371.
(19) Chitnis, D.; Thejo kalyani, N.; Swart, H. C.; Dhoble, S. J. Escalating Opportunities in the Field of Lighting. *Renew. Sustain. Energy Rev.* **2016**, *64*, 727–748.
(20) LG. https://www.lg.com/cac/televisores/lg-55EA9700 https://www.lg.com/cac/televisores/lg-55EA9700.
(21) OLED INFO. ETRI https://www.oled-info.com/etri-shows-new-70lmw-white-light-oleds.
(22) Huami. Huami's Amazfit X smartwatch with a wraparound OLED display https://www.xda-developers.com/amazfit-x-smartwatch-wraparound-oled-display/.
(23) OSRAM. OLED Development @ OSRAM Past, Present and Future Topics. 2017.
(24) ROUND, H. J. A Note on Carborundum. In *Semiconductor Devices: Pioneering Papers*; WORLD SCIENTIFIC, 1991; pp 879–879.
(25) Zheludev, N. The Life and Times of the LED — a 100-Year History. *Nat. Photonics* **2007**, *1* (4), 189–192.
(26) Morton Jr, D. L.; Gabriel, J. *Electronics: The Life Story of a Technology*; Greenwood Press: Baltimore, 2004.
(27) Harris, P.; den Engelsen, D.; Fern, G.; Silver, J. AC Electroluminescent Lamps: Shedding Some Light on Their Mysteries. *J. Mater. Sci. Mater. Electron.* **2017**, *28* (10), 7006–7012.
(28) Schubert, E. F. *Light-Emitting Diodes*, 3rd ed.; New York, USA, 2018.
(29) Tsao, J. Y. Solid-State Lighting. *IEEE Circuits Devices Mag.* **2004**, *20* (3), 28–37.
(30) Huang, W.; Li, J.-M.; Yang, L.-M.; Jin, Z.-L.; Zhong, Z.-G.; Liu, Y.; Chou, Q.-Y.; Li, F. Local Dimming Algorithm and Color Gamut Calibration for RGB LED Backlight LCD Display. *Opt. Laser Technol.* **2011**, *43* (1), 214–217.
(31) Ng, S. K.; Loo, K. H.; Lai, Y. M.; Tse, C. K. Color Control System for RGB LED With Application to Light Sources Suffering From Prolonged Aging. *IEEE Trans. Ind. Electron.* **2014**, *61* (4), 1788–1798.
(32) Cho, J.; Park, J. H.; Kim, J. K.; Schubert, E. F. White Light-Emitting Diodes: History, Progress, and Future. *Laser Photon. Rev.* **2017**, *11* (2), 1600147.
(33) DENG, S.; QIU, Z.; ZHANG, M.; ZHOU, W.; ZHANG, J.; LI, C.; RONG, C.; YU, L.; LIAN, S. Tricolor Emitting and Energy Transfer in the Phosphor Ba2ZnSi2O7:Ce3+,Eu3+,Eu2+ for White-LED Based near-UV Chips. *J. Rare Earths* **2015**, *33* (5), 463–468.
(34) Zhang, Z.; Sun, L.; Devakumar, B.; Liang, J.; Wang, S.; Sun, Q.; Dhoble, S. J.; Huang, X. Novel Highly Luminescent Double-Perovskite Ca2GdSbO6:Eu3+ Red Phosphors with High Color Purity for White LEDs: Synthesis, Crystal Structure, and Photoluminescence Properties. *J. Lumin.* **2020**, 117105.
(35) Yao, D.; Yang, J.; Xie, Y.; Wang, Y.; Wang, Y.; Li, H. Warm White-Light Phosphor Based on a Single-Phase of Ag+/Eu3+/Zn2+ Loading SOD Zeolites with Application to White LEDs. *J. Alloys Compd.* **2020**, *823*, 153778.

(36) Shi, Q.; Ling, K.; Duan, S.; Wang, X.; Xu, S.; Zhang, D.; Wang, Q.; Li, S.; Zhao, L.; Wang, W. Single-Phased Emission-Tunable Mg and Ce Co-Doped ZnO Quantum Dots for White LEDs. *Spectrochim. Acta Part A Mol. Biomol. Spectrosc.* **2020**, *231*, 118096.
(37) Y. Shimizu. Japanese Patent Application Publication H08– 7614, 1996.
(38) Y. Shimizu, K. Sakano, Y. Noguchi, and T. Moriguchi. Japanese Priority Patent Applications to U. S. Patent 5, 998, 925, 1996.
(39) BANDO, K.; SAKANO, K.; NOGUCHI, Y.; SHIMIZU, Y. Development of High-Bright and Pure-White LED Lamps. *J. Light Vis. Environ.* **1998**, *22* (1), 2–5.
(40) Nakamura, S.; Fasol, G. *The Blue Laser Diode*; Springer Berlin Heidelberg: Berlin, Heidelberg, 1997.
(41) B. Baretz and M. A. Tischler. U. S. Patent 6, 600, 175, 2003.
(42) Peralta, S.; Ruda, H. Applications for Advanced Solid-State Lamps. *IEEE Ind. Appl. Mag.* **1998**, *4* (4), 31–42.
(43) Nyalosaso, J. L.; Boonsin, R.; Vialat, P.; Boyer, D.; Chadeyron, G.; Mahiou, R.; Leroux, F. Towards Rare-Earth-Free White Light-Emitting Diode Devices Based on the Combination of Dicyanomethylene and Pyranine as Organic Dyes Supported on Zinc Single-Layered Hydroxide. *Beilstein J. Nanotechnol.* **2019**, *10*, 760–770.
(44) Chen, D.; Xiang, W.; Liang, X.; Zhong, J.; Yu, H.; Ding, M.; Lu, H.; Ji, Z. Advances in Transparent Glass–Ceramic Phosphors for White Light-Emitting Diodes—A Review. *J. Eur. Ceram. Soc.* **2015**, *35* (3), 859–869.
(45) Wang, M.-S.; Guo, G.-C. Inorganic–Organic Hybrid White Light Phosphors. *Chem. Commun.* **2016**, *52* (90), 13194–13204.
(46) Mondal, T.; Mondal, S.; Bose, S.; Sengupta, D.; Ghorai, U. K.; Saha, S. K. Pure White Light Emission from a Rare Earth-Free Intrinsic Metal–Organic Framework and Its Application in a WLED. *J. Mater. Chem. C* **2018**, *6* (3), 614–621.
(47) MOSS Raymond; Evangelos, T.; Hudai, K.; Peter, W.; Jaakko, K. *Critical Metals in Strategic Energy Technologies - Assessing Rare Metals as Supply-Chain Bottlenecks in Low-Carbon Energy Technologies*; 2011.
(48) Alonso, E.; Sherman, A. M.; Wallington, T. J.; Everson, M. P.; Field, F. R.; Roth, R.; Kirchain, R. E. Evaluating Rare Earth Element Availability: A Case with Revolutionary Demand from Clean Technologies. *Environ. Sci. Technol.* **2012**, *46* (6), 3406–3414.
(49) Hatch, G. P. Dynamics in the Global Market for Rare Earths. *Elements* **2012**, *8* (5), 341–346.
(50) Balachandran, G. Extraction of Rare Earths for Advanced Applications. In *Treatise on Process Metallurgy*; Elsevier, 2014; pp 1291–1340.
(51) Nair, G. B.; Swart, H. C.; Dhoble, S. J. A Review on the Advancements in Phosphor-Converted Light Emitting Diodes (Pc-LEDs): Phosphor Synthesis, Device Fabrication and Characterization. *Prog. Mater. Sci.* **2020**, *109*, 100622.
(52) Guo, C.; Huang, Y.; Pan, Q.; Tao, T.; Li, F.; Zhang, Q.; Jin, X.; Li, Q. The Role of Deep-Red Emission CuInS 2 /ZnS QDs in White Light Emitting Diodes. *Semicond. Sci. Technol.* **2019**, *34* (3), 035025.
(53) Chen, H.-S.; Yang, P.; Khan, Z. H.; Wu, J. M.; Li, G.; Kamali, A. R. Quantum Dots and Nanoparticles in Light Emitting Diodes, Displays, and Optoelectronic Devices. *J. Nanomater.* **2015**, *2015*, 1–2.
(54) Köhler, A.; Heinz, B. *Electronic Processes in Organic Semiconductors*, 1st ed.;

Wiley-VCH: Weinheim, Germany, 2015.
(55) Bernanose, A. Electroluminescence of Organic Compounds. *Br. J. Appl. Phys.* **1955**, *6* (S4), S54–S55.
(56) Tang, C. W.; VanSlyke, S. A. Organic Electroluminescent Diodes. *Appl. Phys. Lett.* **1987**, *51* (12), 913–915.
(57) Burroughes, J. H.; Bradley, D. D. C.; Brown, A. R.; Marks, R. N.; Mackay, K.; Friend, R. H.; Burns, P. L.; Holmes, A. B. Light-Emitting Diodes Based on Conjugated Polymers. *Nature* **1990**, *347* (6293), 539–541.
(58) Klauk, H. *Organic Electronics: Materials, Manufacturing, and Applications*, 1st ed.; Wiley, Ed.; 2006.
(59) Wong, C. . *Polymers for Electronic and Photonic Applications*; Academic Press, Ed.; San Diego, 1993.
(60) Schwab, T.; Lüssem, B.; Furno, M.; Gather, M. C.; Leo, K. Organic Light-Emitting Diodes (OLEDs). In *Handbook of Organic Materials for Optical and (Opto)electronic Devices*; Elsevier, 2013; pp 508–534.
(61) Kalinowski, J.; Cocchi, M.; Virgili, D.; Fattori, V.; Williams, J. A. G. Mixing of Excimer and Exciplex Emission: A New Way to Improve White Light Emitting Organic Electrophosphorescent Diodes. *Adv. Mater.* **2007**, *19* (22), 4000–4005.
(62) Wu, Z.; Ma, D. Recent Advances in White Organic Light-Emitting Diodes. *Mater. Sci. Eng. R Reports* **2016**, *107*, 1–42.
(63) Chen, Y.; Tian, H.; Chen, J.; Geng, Y.; Yan, D.; Wang, L.; Ma, D. Highly Efficient Tandem White Organic Light-Emitting Diodes Based upon C60/NaT4 Organic Heterojunction as Charge Generation Layer. *J. Mater. Chem.* **2012**, *22* (17), 8492.
(64) Kanno, H.; Holmes, R. J.; Sun, Y.; Kena-Cohen, S.; Forrest, S. R. White Stacked Electrophosphorescent Organic Light-Emitting Devices Employing MoO3 as a Charge-Generation Layer. *Adv. Mater.* **2006**, *18* (3), 339–342.
(65) Lee, S.; Shin, H.; Kim, J.-J. High-Efficiency Orange and Tandem White Organic Light-Emitting Diodes Using Phosphorescent Dyes with Horizontally Oriented Emitting Dipoles. *Adv. Mater.* **2014**, *26* (33), 5864–5868.
(66) Zhao, D.; Qin, Z.; Huang, J.; Yu, J. Progress on Material, Structure and Function for Tandem Organic Light-Emitting Diodes. *Org. Electron.* **2017**, *51*, 220–242.
(67) Reineke, S.; Thomschke, M.; Lüssem, B.; Leo, K. White Organic Light-Emitting Diodes: Status and Perspective. *Rev. Mod. Phys.* **2013**, *85* (3), 1245–1293.
(68) Tsuboi, T. Recent Advances in White Organic Light Emitting Diodes with a Single Emissive Dopant. *J. Non. Cryst. Solids* **2010**, *356* (37–40), 1919–1927.
(69) Kim, Y. M.; Park, Y. W.; Choi, J. H.; Ju, B. K.; Jung, J. H.; Kim, J. K. Spectral Broadening in Electroluminescence of White Organic Light-Emitting Diodes Based on Complementary Colors. *Appl. Phys. Lett.* **2007**, *90* (3), 033506.
(70) Song, W.; Lee, I.; Lee, J. Y. Host Engineering for High Quantum Efficiency Blue and White Fluorescent Organic Light-Emitting Diodes. *Adv. Mater.* **2015**, *27* (29), 4358–4363.
(71) Zheng, C.-J.; Wang, J.; Ye, J.; Lo, M.-F.; Liu, X.-K.; Fung, M.-K.; Zhang, X.-H.; Lee, C.-S. Novel Efficient Blue Fluorophors with Small Singlet-Triplet Splitting: Hosts for Highly Efficient Fluorescence and Phosphorescence Hybrid WOLEDs with Simplified Structure. *Adv. Mater.* **2013**, *25* (15), 2205–2211.
(72) Mazzeo, M.; Pisignano, D.; Favaretto, L.; Sotgiu, G.; Barbarella, G.; Cingolani, R.; Gigli, G. White Emission from Organic Light Emitting Diodes Based on Energy Down-Convertion Mechanisms. *Synth. Met.* **2003**, *139* (3), 675–677.
(73) Gohri, V.; Hofmann, S.; Reineke, S.; Rosenow, T.; Thomschke, M.; Levichkova,

M.; Lüssem, B.; Leo, K. White Top-Emitting Organic Light-Emitting Diodes Employing a Heterostructure of down-Conversion Layers. *Org. Electron.* **2011**, *12* (12), 2126–2130.

(74) D'Andrade, B. W.; Adamovich, V.; Hewitt, R.; Hack, M.; Brown, J. J. 2005 , 593. In *Proc. SPIE-Int. Soc. Opt. Eng.*; 2005; p 5937.

(75) Yang, X.; Zhao, Y.; Zhang, X.; Li, R.; Dang, J.; Li, Y.; Zhou, G.; Wu, Z.; Ma, D.; Wong, W.-Y.; et al. Thiazole-Based Metallophosphors of Iridium with Balanced Carrier Injection/Transporting Features and Their Two-Colour WOLEDs Fabricated by Both Vacuum Deposition and Solution Processing-Vacuum Deposition Hybrid Strategy. *J. Mater. Chem.* **2012**, *22* (15), 7136.

(76) Chen, Z.; Ho, C.; Wang, L.; Wong, W. Single-Molecular White-Light Emitters and Their Potential WOLED Applications. *Adv. Mater.* **2020**, 1903269.

(77) Williams, E. L.; Haavisto, K.; Li, J.; Jabbour, G. E. Excimer-Based White Phosphorescent Organic Light-Emitting Diodes with Nearly 100 % Internal Quantum Efficiency. *Adv. Mater.* **2007**, *19* (2), 197–202.

(78) Liu, J.; Chou, S.-Y.; Tong, K.; Luan, X.; Zhao, F.; Pei, Q.; Li, H. Study of White Electroluminescence from a Single-Component Polymer Using an Electrolyte-Gated Diode. *J. Phys. Chem. C* **2017**, *121* (18), 10112–10118.

(79) Wang, J.; Chen, J.; Qiao, X.; Alshehri, S. M.; Ahamad, T.; Ma, D. Simple-Structured Phosphorescent Warm White Organic Light-Emitting Diodes with High Power Efficiency and Low Efficiency Roll-Off. *ACS Appl. Mater. Interfaces* **2016**, *8* (16), 10093–10097.

(80) Thejokalyani, N.; Dhoble, S. J. Novel Approaches for Energy Efficient Solid State Lighting by RGB Organic Light Emitting Diodes – A Review. *Renew. Sustain. Energy Rev.* **2014**, *32*, 448–467.

(81) Wu, S.-F.; Li, S.-H.; Wang, Y.-K.; Huang, C.-C.; Sun, Q.; Liang, J.-J.; Liao, L.-S.; Fung, M.-K. White Organic LED with a Luminous Efficacy Exceeding 100 Lm W −1 without Light Out-Coupling Enhancement Techniques. *Adv. Funct. Mater.* **2017**, *27* (31), 1701314.

(82) Yang, S.; Jiang, M. White Light Generation Combining Emissions from Exciplex, Excimer and Electromer in TAPC-Based Organic Light-Emitting Diodes. *Chem. Phys. Lett.* **2009**, *484* (1–3), 54–58.

(83) Aguilar-Granda, A.; Pérez-Estrada, S.; Roa, A. E.; Rodríguez-Hernández, J.; Hernández-Ortega, S.; Rodriguez, M.; Rodríguez-Molina, B. Synthesis of a Carbazole-[Pi]-Carbazole Molecular Rotor with Fast Solid State Intramolecular Dynamics and Crystallization-Induced Emission. *Cryst. Growth Des.* **2016**, *16* (6), 3435–3442.

(84) Ewing, J. J. Excimer Laser Technology Development. *IEEE J. Sel. Top. Quantum Electron.* **2000**, *6* (6), 1061–1071.

(85) Lakoba, I. S.; Yakovlenko, S. I. Active Media of Exciplex Lasers (Review). *Sov. J. Quantum Electron.* **1980**, *10* (4), 389–410.

(86) Anger, I.; Rykova, E.; Bagaturyants, A. MD/QC Simulation of the Structure and Spectroscopic Properties of α-NPD-BAlq Exciplexes at an α-NPD/BAlq Interface in OLEDs. *ChemistrySelect* **2017**, *2* (29), 9495–9500.

(87) Jeon, S. K.; Lee, J. Y. Highly Efficient Exciplex Organic Light-Emitting Diodes by Exciplex Dispersion in the Thermally Activated Delayed Fluorescence Host. *Org. Electron.* **2020**, *76*, 105477.

(88) Wang, S.; Zhang, H.; Zhang, B.; Xie, Z.; Wong, W.-Y. Towards High-Power-Efficiency Solution-Processed OLEDs: Material and Device Perspectives. *Mater. Sci. Eng. R Reports* **2020**, *140*, 100547.

(89) Zhao, Y.; Duan, L.; Zhang, X.; Zhang, D.; Qiao, J.; Dong, G.; Wang, L.; Qiu, Y. White Light Emission from an Exciplex Based on a Phosphine Oxide Type Electron Transport Compound in a Bilayer Device Structure. *RSC Adv.* **2013**, *3* (44), 21453.
(90) Jhulki, S.; Seth, S.; Rafiq, S.; Ghosh, A.; Chow, T. J.; Moorthy, J. N. Nitrogen-Free Bifunctional Bianthryl Leads to Stable White-Light Emission in Bilayer and Multilayer OLED Devices. *ACS Omega* **2018**, *3* (2), 1416–1424.
(91) Hung, W.-Y.; Wang, T.-C.; Chiang, P.-Y.; Peng, B.-J.; Wong, K.-T. Remote Steric Effect as a Facile Strategy for Improving the Efficiency of Exciplex-Based OLEDs. *ACS Appl. Mater. Interfaces* **2017**, *9* (8), 7355–7361.
(92) Janghouri, M. Going from Green to White Color Electroluminescence through a Nanoscale Complex of Zinc (II). *Mater. Sci. Semicond. Process.* **2017**, *66*, 117–122.
(93) Deksnys, T.; Simokaitiene, J.; Keruckas, J.; Volyniuk, D.; Bezvikonnyi, O.; Cherpak, V.; Stakhira, P.; Ivaniuk, K.; Helzhynskyy, I.; Baryshnikov, G.; et al. Synthesis and Characterisation of a Carbazole-Based Bipolar Exciplex-Forming Compound for Efficient and Color-Tunable OLEDs. *New J. Chem.* **2017**, *41* (2), 559–568.
(94) Pander, P.; Kudelko, A.; Brzeczek, A.; Wroblowska, M.; Walczak, K.; Przemyslaw, D. Analysis of Exciplex Emitters. *J. Disp. Imaging* **2017**, *2*, 265–277.
(95) Wang, J.-F.; Kawabe, Y.; Shaheen, S. E.; Morrell, M. M.; Jabbour, G. E.; Lee, P. A.; Anderson, J.; Armstrong, N. R.; Kippelen, B.; Mash, E. A.; et al. Exciplex Electroluminescence from Organic Bilayer Devices Composed of Triphenyldiamine and Quinoxaline Derivatives. *Adv. Mater.* **1998**, *10* (3), 230–233.
(96) Angioni, E.; Chapran, M.; Ivaniuk, K.; Kostiv, N.; Cherpak, V.; Stakhira, P.; Lazauskas, A.; Tamulevičius, S.; Volyniuk, D.; Findlay, N. J.; et al. A Single Emitting Layer White OLED Based on Exciplex Interface Emission. *J. Mater. Chem. C* **2016**, *4* (17), 3851–3856.
(97) Kalinowski, J. Excimers and Exciplexes in Organic Electroluminescence. *Mater. Sci.* **2009**, *27* (3).
(98) Cocchi, M.; Virgili, D.; Sabatini, C.; Kalinowski, J. Organic Electroluminescence from Singlet and Triplet Exciplexes: Exciplex Electrophosphorescent Diode. *Chem. Phys. Lett.* **2006**, *421* (4–6), 351–355.
(99) Jenekhe, S. A.; Osaheni, J. A. Excimers and Exciplexes of Conjugated Polymers. *Science (80-.).* **1994**, *265* (5173), 765–768.
(100) Yang, Y.; Pei, Q. Light-Emitting Electrochemical Cells from a Blend of p- and n-Type Luminescent Conjugated Polymers. *Appl. Phys. Lett.* **1997**, *70* (15), 1926–1928.
(101) Lin, T.; Song, Q.; Liu, Z.; Chu, B.; Li, W.; Luo, Y.; Lee, C. S.; Su, Z.; Li, Y. Effects of Acceptor on the Performance of Exciplex-Based OLED. *Synth. Met.* **2017**, *234*, 95–99.
(102) Luo, D.; Li, X.-L.; Zhao, Y.; Gao, Y.; Liu, B. High-Performance Blue Molecular Emitter-Free and Doping-Free Hybrid White Organic Light-Emitting Diodes: An Alternative Concept To Manipulate Charges and Excitons Based on Exciplex and Electroplex Emission. *ACS Photonics* **2017**, *4* (6), 1566–1575.
(103) Cekaviciute, M.; Simokaitiene, J.; Volyniuk, D.; Sini, G.; Grazulevicius, J. V. Arylfluorenyl-Substituted Metoxytriphenylamines as Deep Blue Exciplex Forming Bipolar Semiconductors for White and Blue Organic Light Emitting

Diodes. *Dye. Pigment.* **2017**, *140*, 187–202.
(104) Jesuraj, P. J.; Hafeez, H.; Kim, D. H.; Lee, J. C.; Lee, W. H.; Choi, D. K.; Kim, C. H.; Song, M.; Kim, C. S.; Ryu, S. Y. Recombination Zone Control without Sensing Layer and the Exciton Confinement in Green Phosphorescent OLEDs by Excluding Interface Energy Transfer. *J. Phys. Chem. C* **2018**, *122* (5), 2951–2958.
(105) Sahasithiwat, S.; Sooksimuang, T.; Kangkaew, L.; Panchan, W. 3,12-Dimethoxy-5,6,9,10-Tetrahydro-7,8-Dicyano-[5]Helicene as a New Emitter for Blue and White Organic Light-Emitting Diodes. *Dye. Pigment.* **2017**, *136*, 754–760.
(106) Sasabe, H.; Toyota, N.; Nakanishi, H.; Ishizaka, T.; Pu, Y.-J.; Kido, J. 3,3′-Bicarbazole-Based Host Materials for High-Efficiency Blue Phosphorescent OLEDs with Extremely Low Driving Voltage. *Adv. Mater.* **2012**, *24* (24), 3212–3217.
(107) Agarwal, N.; Nayak, P. K.; Ali, F.; Patankar, M. P.; Narasimhan, K. L.; Periasamy, N. Tuning of HOMO Levels of Carbazole Derivatives: New Molecules for Blue OLED. *Synth. Met.* **2011**, *161* (5–6), 466–473.
(108) Bezuglyi, M.; Ivaniuk, K.; Volyniuk, D.; Gražulevičius, J. V.; Bagdžiūnas, G. An Approach to Discovering Novel Exciplex Supramolecular Complex Based on Carbazole-Containing 1,8-Naphthalimide. *Dye. Pigment.* **2018**, *149*, 298–305.
(109) Zassowski, P.; Ledwon, P.; Kurowska, A.; Herman, A. P.; Lapkowski, M.; Cherpak, V.; Hotra, Z.; Turyk, P.; Ivaniuk, K.; Stakhira, P.; et al. 1,3,5-Triazine and Carbazole Derivatives for OLED Applications. *Dye. Pigment.* **2018**, *149*, 804–811.
(110) Hung, W.-Y.; Fang, G.-C.; Lin, S.-W.; Cheng, S.-H.; Wong, K.-T.; Kuo, T.-Y.; Chou, P.-T. The First Tandem, All-Exciplex-Based WOLED. *Sci. Rep.* **2015**, *4* (1), 5161.
(111) Chapran, M.; Angioni, E.; Findlay, N. J.; Breig, B.; Cherpak, V.; Stakhira, P.; Tuttle, T.; Volyniuk, D.; Grazulevicius, J. V.; Nastishin, Y. A.; et al. An Ambipolar BODIPY Derivative for a White Exciplex OLED and Cholesteric Liquid Crystal Laser toward Multifunctional Devices. *ACS Appl. Mater. Interfaces* **2017**, *9* (5), 4750–4757.
(112) Xiao, P.; Dong, T.; Xie, J.; Luo, D.; Yuan, J.; Liu, B. Emergence of White Organic Light-Emitting Diodes Based on Thermally Activated Delayed Fluorescence. *Appl. Sci.* **2018**, *8* (2), 299.
(113) dos Santos, P. L.; Dias, F. B.; Monkman, A. P. Investigation of the Mechanisms Giving Rise to TADF in Exciplex States. *J. Phys. Chem. C* **2016**, *120* (32), 18259–18267.
(114) Matsumoto, N.; Nishiyama, M.; Adachi, C. Exciplex Formations between Tris(8-Hydoxyquinolate)Aluminum and Hole Transport Materials and Their Photoluminescence and Electroluminescence Characteristics. *J. Phys. Chem. C* **2008**, *112* (20), 7735–7741.
(115) Kulkarni, A. P.; Jenekhe, S. A. Blue-Green, Orange, and White Organic Light-Emitting Diodes Based on Exciplex Electroluminescence of an Oligoquinoline Acceptor and Different Hole-Transport Materials. *J. Phys. Chem. C* **2008**, *112* (13), 5174–5184.
(116) Das, D.; Peddaboodi, G.; Ashish, S.; Dey, A.; Iyer, P. K. Efficient Blue and White Polymer Light Emitting Diodes Based on a Well Charge Balanced, Core Modified Polyfluorene Derivative†. *Phys. Chem. Chem. Phys.* **2016**, *18* (10, 2016), 7389–7394.
(117) Fröbel, M.; Schwab, T.; Kliem, M.; Hofmann, S.; Leo, K.; Gather, M. C. Get It

White: Color-Tunable AC/DC OLEDs. *Light Sci. Appl.* **2015**, *4* (2), e247–e247.
(118) Krotkus, S.; Kasemann, D.; Lenk, S.; Leo, K.; Reineke, S. Adjustable White-Light Emission from a Photo-Structured Micro-OLED Array. *Light Sci. Appl.* **2016**, *5* (7), e16121–e16121.
(119) Niklaus, L.; Dakhil, H.; Kostrzewa, M.; Coto, P. B.; Sonnewald, U.; Wierschem, A.; Costa, R. D. Easy and Versatile Coating Approach for Long-Living White Hybrid Light-Emitting Diodes. *Mater. Horizons* **2016**, *3* (4), 340–347.
(120) Lin, H.-Y.; Sher, C.-W.; Lin, C.-H.; Tu, H.-H.; Chen, X. Y.; Lai, Y.-C.; Lin, C.-C.; Chen, H.-M.; Yu, P.; Meng, H.-F.; et al. Fabrication of Flexible White Light-Emitting Diodes from Photoluminescent Polymer Materials with Excellent Color Quality. *ACS Appl. Mater. Interfaces* **2017**, *9* (40), 35279–35286.
(121) Angioni, E.; Marshall, R. J.; Findlay, N. J.; Bruckbauer, J.; Breig, B.; Wallis, D. J.; Martin, R. W.; Forgan, R. S.; Skabara, P. J. Implementing Fluorescent MOFs as Down-Converting Layers in Hybrid Light-Emitting Diodes. *J. Mater. Chem. C* **2019**, *7* (8), 2394–2400.
(122) Wiles, A. A.; Bruckbauer, J.; Mohammed, N.; Cariello, M.; Cameron, J.; Findlay, N. J.; Taylor-Shaw, E.; Wallis, D. J.; Martin, R. W.; Skabara, P. J.; et al. A Poly(Urethane)-Encapsulated Benzo[2,3- D :6,7- d ′]Diimidazole Organic down-Converter for Green Hybrid LEDs. *Mater. Chem. Front.* **2020**, *4* (3), 1006–1012.
(123) He, J.; Yang, S.; Zheng, K.; Zhang, Y.; Song, J.; Qu, J. One-Pot Synthesis of Dispersible Thermally Stable Organic Downconversion Materials under DBU Catalyzation for High Performance Hybrid-LED Lamps. *Green Chem.* **2018**, *20* (15), 3557–3565.
(124) Taylor-Shaw, E.; Angioni, E.; Findlay, N. J.; Breig, B.; Inigo, A. R.; Bruckbauer, J.; Wallis, D. J.; Skabara, P. J.; Martin, R. W. Cool to Warm White Light Emission from Hybrid Inorganic/Organic Light-Emitting Diodes. *J. Mater. Chem. C* **2016**, *4* (48), 11499–11507.
(125) Jin, J.-Y.; Kim, Y.-M.; Lee, S.-H.; Lee, Y.-S. Synthesis of an Acrylic Copolymer Bearing Fluorescent Dye Pendants and Characterization as a Luminescence Conversion Material in Fabrication of a Luminescence Conversion Light-Emitting Diode. *Synth. Met.* **2009**, *159* (17–18), 1804–1808.
(126) Kim, H.-J.; Jin, J.-Y.; Lee, Y.-S.; Lee, S.-H.; Hong, C.-H. An Efficient Luminescence Conversion LED for White Light Emission, Fabricated Using a Commercial InGaN LED and a 1,8-Naphthalimide Derivative. *Chem. Phys. Lett.* **2006**, *431* (4–6), 341–345.
(127) Yuan, W. Z.; Shen, X. Y.; Zhao, H.; Lam, J. W. Y.; Tang, L.; Lu, P.; Wang, C.; Liu, Y.; Wang, Z.; Zheng, Q.; et al. Crystallization-Induced Phosphorescence of Pure Organic Luminogens at Room Temperature. *J. Phys. Chem. C* **2010**, *114* (13), 6090–6099.
(128) Heliotis, G.; Itskos, G.; Murray, R.; Dawson, M. D.; Watson, I. M.; Bradley, D. D. C. Hybrid Inorganic/Organic Semiconductor Heterostructures with Efficient Non-Radiative Energy Transfer. *Adv. Mater.* **2006**, *18* (3), 334–338.
(129) Findlay, N. J.; Orofino-Peña, C.; Bruckbauer, J.; Elmasly, S. E. T.; Arumugam, S.; Inigo, A. R.; Kanibolotsky, A. L.; Martin, R. W.; Skabara, P. J. Linear Oligofluorene-BODIPY Structures for Fluorescence Applications. *J. Mater. Chem. C* **2013**, *1* (11), 2249.
(130) Bulovic, V.; Baldo, M. A.; Forrest, S. R. Organic Electronic Materials, Conjugated Polymers and Low Molecular Weight Organic Solids; Grosso, R. F. and G., Ed.; Springer-Verlag: Berlin, 2001.
(131) Klessinger, M.; Michl, J. *Excited States and Photochemistry of Organic*

Molecules; VCH: New York, 1995.
(132) Ishi-i, T.; Ikeda, K.; Kichise, Y.; Ogawa, M. Red-Light-Emitting System Based on Aggregation of Donor–Acceptor Derivatives in Polar Aqueous Media. *Chem. – An Asian J.* **2012**, *7* (7), 1553–1557.
(133) Ishi-i, T.; Ikeda, K.; Ogawa, M.; Kusakaki, Y. Light-Emitting Properties of Donor–Acceptor and Donor–Acceptor–Donor Dyes in Solution, Solid, and Aggregated States: Structure–Property Relationship of Emission Behavior. *RSC Adv.* **2015**, *5* (108), 89171–89187.
(134) Melgoza Ramírez, M. L. DEVELOPMENT AND OPTICAL CHARACTERIZATION OF WHITE LIGHT EMISSION ORGANIC NANOMATERIALS, Centro de Investigaciones en Óptica. A.C, 2015.
(135) Perez, E. Fluorescence Tuning with a Single Dye Embedded in a Polymer Matrix and Its Application on Multicolor OLEDs. *Dye. Pigment.* **2021**.
(136) Grządziel, L.; Żak, J.; Szuber, J. On the Correlation between Morphology and Electronic Properties of Copper Phthalocyanine (CuPc) Thin Films. *Thin Solid Films* **2003**, *436* (1), 70–75.
(137) Li, E.; Jie, K.; Liu, M.; Sheng, X.; Zhu, W.; Huang, F. Vapochromic Crystals: Understanding Vapochromism from the Perspective of Crystal Engineering. *Chem. Soc. Rev.* **2020**, *49* (5), 1517–1544.
(138) Percino, M. J.; Cerón, M.; Pérez-Gutiérrez, E.; Perumal, V.; Siegler, M. A.; Subbiah, T.; Ceballos, P.; Gordillo-Guerra, P.; Bonilla-Cruz, J.; Longoria, F. E.; et al. Preferential Orientation of Crystals and Its Influence on the Emission Wavelength of Acrylonitrile Derivatives Treated with Polar Solvents. *Cryst. Res. Technol.* **2019**, *54* (7), 1800156.
(139) Xu, Z.; Tang, B. Z.; Wang, Y.; Ma, D. Recent Advances in High Performance Blue Organic Light-Emitting Diodes Based on Fluorescence Emitters. *J. Mater. Chem. C* **2020**, *8* (8), 2614–2642.
(140) Xu, S.; Yuan, Y.; Cai, X.; Zhang, C.-J.; Hu, F.; Liang, J.; Zhang, G.; Zhang, D.; Liu, B. Tuning the Singlet-Triplet Energy Gap: A Unique Approach to Efficient Photosensitizers with Aggregation-Induced Emission (AIE) Characteristics. *Chem. Sci.* **2015**, *6* (10), 5824–5830.
(141) Ding, Y.; Tang, Y.; Zhu, W.; Xie, Y. Fluorescent and Colorimetric Ion Probes Based on Conjugated Oligopyrroles. *Chem. Soc. Rev.* **2015**, *44* (5), 1101–1112.
(142) Sagara, Y.; Kato, T. Mechanically Induced Luminescence Changes in Molecular Assemblies. *Nat. Chem.* **2009**, *1* (8), 605–610.
(143) Feng, H.-T.; Xiong, J.-B.; Zheng, Y.-S.; Pan, B.; Zhang, C.; Wang, L.; Xie, Y. Multicolor Emissions by the Synergism of Intra/Intermolecular Slipped π–π Stackings of Tetraphenylethylene-DiBODIPY Conjugate. *Chem. Mater.* **2015**, *27* (22), 7812–7819.
(144) Shao, A.; Xie, Y.; Zhu, S.; Guo, Z.; Zhu, S.; Guo, J.; Shi, P.; James, T. D.; Tian, H.; Zhu, W.-H. Far-Red and Near-IR AIE-Active Fluorescent Organic Nanoprobes with Enhanced Tumor-Targeting Efficacy: Shape-Specific Effects. *Angew. Chemie Int. Ed.* **2015**, *54* (25), 7275–7280.
(145) Srujana, P.; Radhakrishnan, T. P. Extensively Reversible Thermal Transformations of a Bistable, Fluorescence-Switchable Molecular Solid: Entry into Functional Molecular Phase-Change Materials. *Angew. Chemie Int. Ed.* **2015**, *54* (25), 7270–7274.
(146) Varghese, S.; Das, S. Role of Molecular Packing in Determining Solid-State Optical Properties of π-Conjugated Materials. *J. Phys. Chem. Lett.* **2011**, *2* (8), 863–873.

(147) Venkatesan, P.; Cerón, M.; Ceballos, P.; Pérez-Gutiérrez, E.; Thamotharan, S.; Percino, M. J. Experimental Study and DFT Calculation for the Strength of Intermolecular Interactions in Schiff Base with the Phenylarsonic Acid Scaffold. *J. Mol. Struct.* **2019**, *1196*, 306–322.
(148) Venkatesan, P.; Cerón, M.; Pérez-Gutiérrez, E.; Castillo, A. E.; Thamotharan, S.; Robles, F.; Siegler, M. A.; Percino, M. J. Experimental and Theoretical Insights into the Optical Properties and Intermolecular Interactions in Push-Pull Bromide Salts. *ChemistryOpen* **2019**, *8* (4), 483–496.
(149) Guo, Z.-H.; Jin, Z.-X.; Wang, J.-Y.; Pei, J. A Donor–Acceptor–Donor Conjugated Molecule: Twist Intramolecular Charge Transfer and Piezochromic Luminescent Properties. *Chem. Commun.* **2014**, *50* (46), 6088.
(150) Anthony, S. P. Organic Solid-State Fluorescence: Strategies for Generating Switchable and Tunable Fluorescent Materials. *Chempluschem* **2012**, *77* (7), 518–531.
(151) Qi, Q.; Qian, J.; Tan, X.; Zhang, J.; Wang, L.; Xu, B.; Zou, B.; Tian, W. Remarkable Turn-On and Color-Tuned Piezochromic Luminescence: Mechanically Switching Intramolecular Charge Transfer in Molecular Crystals. *Adv. Funct. Mater.* **2015**, *25* (26), 4005–4010.
(152) Anthony, S. P.; Draper, S. M. Nano/Microstructure Fabrication of Functional Organic Material: Polymorphic Structure and Tunable Luminescence. *J. Phys. Chem. C* **2010**, *114* (27), 11708–11716.
(153) Kundu, A.; Karthikeyan, S.; Moon, D.; Anthony, S. P. Self-Reversible Thermofluorochromism of D–A–D Triphenylamine Derivatives and the Effect of Molecular Conformation and Packing. *CrystEngComm* **2017**, *19* (46), 6979–6985.
(154) Luo, X.; Zhao, W.; Shi, J.; Li, C.; Liu, Z.; Bo, Z.; Dong, Y. Q.; Tang, B. Z. Reversible Switching Emissions of Tetraphenylethene Derivatives among Multiple Colors with Solvent Vapor, Mechanical, and Thermal Stimuli. *J. Phys. Chem. C* **2012**, *116* (41), 21967–21972.
(155) Zhang, J.; Chen, J.; Xu, B.; Wang, L.; Ma, S.; Dong, Y.; Li, B.; Ye, L.; Tian, W. Remarkable Fluorescence Change Based on the Protonation–Deprotonation Control in Organic Crystals. *Chem. Commun.* **2013**, *49* (37), 3878.
(156) Hariharan, P. S.; Mothi, E. M.; Moon, D.; Anthony, S. P. Halochromic Isoquinoline with Mechanochromic Triphenylamine: Smart Fluorescent Material for Rewritable and Self-Erasable Fluorescent Platform. *ACS Appl. Mater. Interfaces* **2016**, *8* (48), 33034–33042.
(157) Zhou, T.; Jia, T.; Zhao, S.; Guo, J.; Zhang, H.; Wang, Y. Acid-Stimuli-Luminescence and Carbonyl-Proton Interaction Dependent Emission Properties of 2,6-Biphenyl-4-Pyrone Crystals. *Cryst. Growth Des.* **2012**, *12* (1), 179–184.
(158) Sato, T.; Higuchi, M. A Vapoluminescent Eu-Based Metallo-Supramolecular Polymer. *Chem. Commun.* **2012**, *48* (41), 4947.
(159) Dou, C.; Han, L.; Zhao, S.; Zhang, H.; Wang, Y. Multi-Stimuli-Responsive Fluorescence Switching of a Donor−Acceptor π-Conjugated Compound. *J. Phys. Chem. Lett.* **2011**, *2* (6), 666–670.
(160) Xue, P.; Yang, Z.; Chen, P. Hiding and Revealing Information Using the Mechanochromic System of a 2,5-Dicarbazole-Substituted Terephthalate Derivative. *J. Mater. Chem. C* **2018**, *6* (18), 4994–5000.
(161) Fujii, K.; Sakon, A.; Sekine, A.; Uekusa, H. Reversible Color Switching of an Organic Crystal Induced by Organic Solvent Vapors. *Cryst. Growth Des.* **2011**, *11* (10), 4305–4308.

(162) Sakon, A.; Sekine, A.; Uekusa, H. Powder Structure Analysis of Vapochromic Quinolone Antibacterial Agent Crystals. *Cryst. Growth Des.* **2016**, *16* (8), 4635–4645.
(163) Xue, P.; Chen, P.; Jia, J.; Xu, Q.; Sun, J.; Yao, B.; Zhang, Z.; Lu, R. A Triphenylamine-Based Benzoxazole Derivative as a High-Contrast Piezofluorochromic Material Induced by Protonation. *Chem. Commun.* **2014**, *50* (20), 2569–2571.
(164) Kappaun, S.; Horner, S.; Kelterer, A.-M.; Waich, K.; Grasse, F.; Graf, M.; Romaner, L.; Niedermair, F.; Müllen, K.; Grimsdale, A. C.; et al. The Effect of Protonation on the Optical Properties of Conjugated Fluorene-Pyridine Copolymers. *Macromol. Chem. Phys.* **2008**, *209* (20), 2122–2134.
(165) Yamashita, Y.; Maeda, H.; Hoffmann, H. Counterion Specificity in the Phase Behavior of Tetradecyldimethylamine Oxides at Different Degrees of Protonation. *J. Colloid Interface Sci.* **2006**, *299* (1), 388–395.
(166) Liu, Y.; Porcar, L.; Hong, K.; Shew, C.-Y.; Li, X.; Liu, E.; Butler, P. D.; Herwig, K. W.; Smith, G. S.; Chen, W.-R. Effect of Counterion Valence on the PH Responsiveness of Polyamidoamine Dendrimer Structure. *J. Chem. Phys.* **2010**, *132* (12), 124901.
(167) Wang, K.; Huang, S.; Zhang, Y.; Zhao, S.; Zhang, H.; Wang, Y. Multicolor Fluorescence and Electroluminescence of an ICT-Type Organic Solid Tuned by Modulating the Accepting Nature of the Central Core. *Chem. Sci.* **2013**, *4* (8), 3288.
(168) Pıravadılı Mucur, S.; Kacar, R.; Meric, C.; Koyuncu, S. Thermal Annealing Effect on Light Emission Profile of Polyfluorenes Containing Double Bond Subunit. *Org. Electron.* **2017**, *50*, 55–62.
(169) de Azevedo, D.; Freitas, J. N.; Domingues, R. A.; Faleiros, M. M.; de Almeida Santos, T. E.; Atvars, T. D. Z. Tuning the Emission Color of a Single-Layer Polymer Light-Emitting Diode with a Solution-Processed External Layer. *Synth. Met.* **2016**, *222*, 205–210.
(170) Lampert, Z. E.; Lappi, S. E.; Papanikolas, J. M.; Lewis Reynolds, C.; Osama Aboelfotoh, M. Morphology and Chain Aggregation Dependence of Optical Gain in Thermally Annealed Films of the Conjugated Polymer Poly[2-Methoxy-5-(2′-Ethylhexyloxy)-p-Phenylene Vinylene]. *J. Appl. Phys.* **2013**, *113* (23), 233509.
(171) Liu, J.; Guo, T.-F.; Yang, Y. Erratum: “Effects of Thermal Annealing on the Performance of Polymer Light Emitting Diodes” [J. Appl. Phys. 91 , 1595 (2002)]. *J. Appl. Phys.* **2002**, *91* (11), 9437–9437.
(172) Mercado, A. ENCAPSULADO DE DISPOSITIVOS LEDs ORGÁNICOS (OLEDs) MEDIANTE EL USO DE RESINAS EPÓXICAS., Tecnologíco de Estudios Superiores de Jocotitlan, 2020.

APPENDIX A.

Buffer layer: In OLEDs, buffer layer is an organic thin film used to facilitate effective hole migration from the anode to the emissive zone.

CIE: The International Commission on Illumination (CIE) proposed the CIE coordinates are a standard reference which has been used as the basis for defining most other color spaces. This map human color perception based on the two CIE parameters **x** and **y**. In this work was used the CIE 1931.

Color rendering: Effect of an illuminant on the color appearance of objects by conscious or subconscious comparison with their color appearance under a reference illuminant.

CRI: A color rendering index (CRI) is a quantitative measure of the ability of a light source to reveal the colors of various objects faithfully in comparison with an ideal or natural light source.

EML: Emissive layer.

ETL: Electrons transport layer.

HTL: Hole transport layer.

Intermolecular interactions: Interactions between two or more molecules that occur between all types of molecules or ions in all states of matter.

Intramolecular interactions: Interactions between the atoms within a molecule.

Luminance: the luminous intensity of a surface in a given direction per unit of projected area.

APPENDIX B.

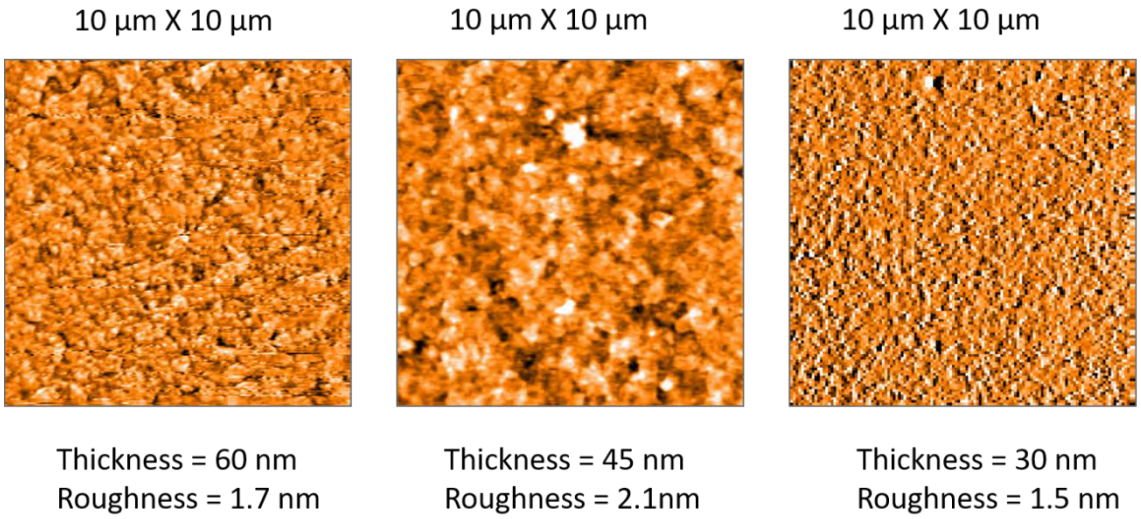

Figure B1. Micrographics of PEDOT:PSS films at thicknesses of 60, 45 and 30 nm.

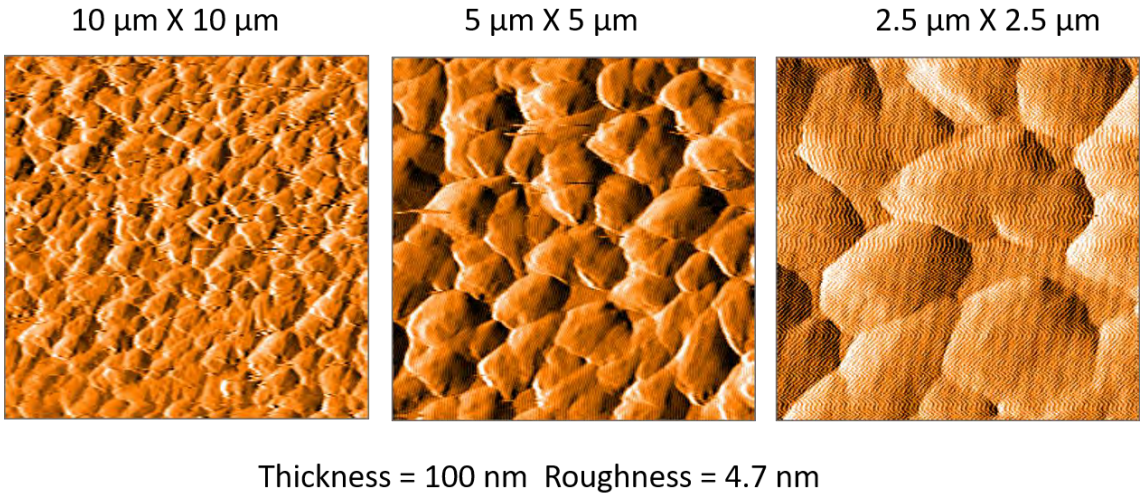

Figure B2. Micrographics of CZDD at scales of 10, 5 and 2.5 µm.

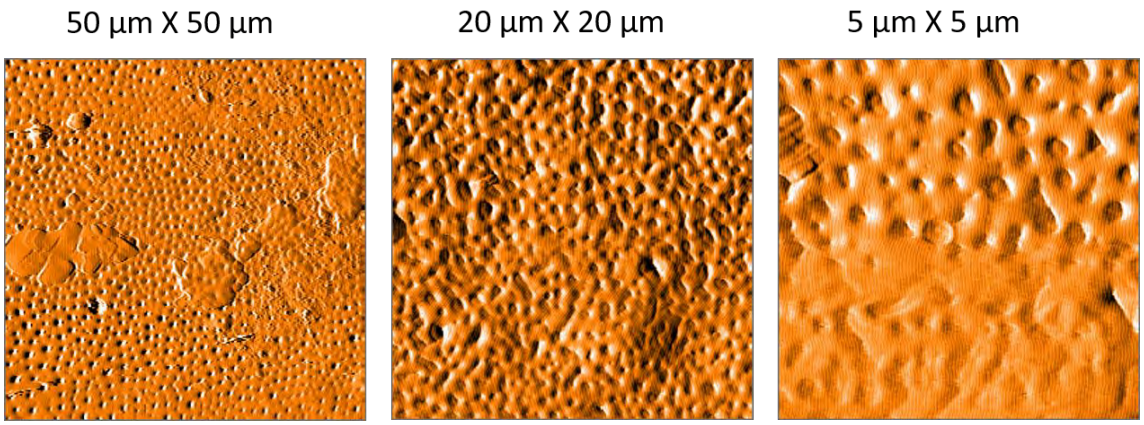

Figure B3. Micrographics of ADS233YE at scales of 50, 20 and 5 µm.

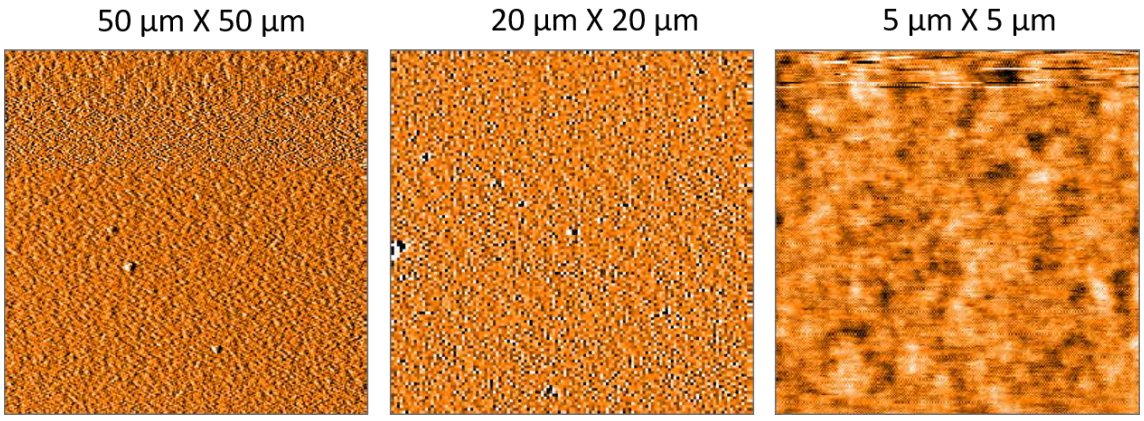

Figure B4. Micrographics of ACN1 at scales of 50, 20 and 2.5 µm.

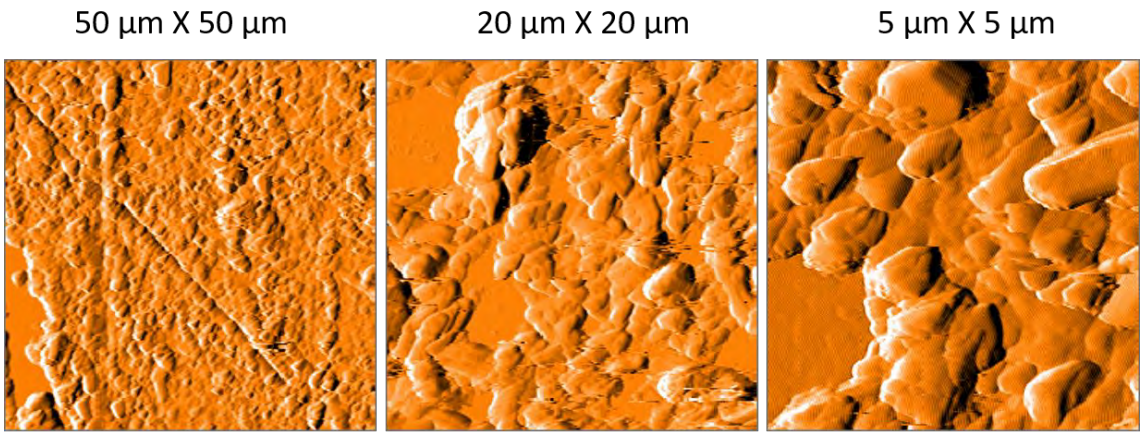

Figure B5. Micrographics of JP5 at scales of 50, 20 and 5 µm.

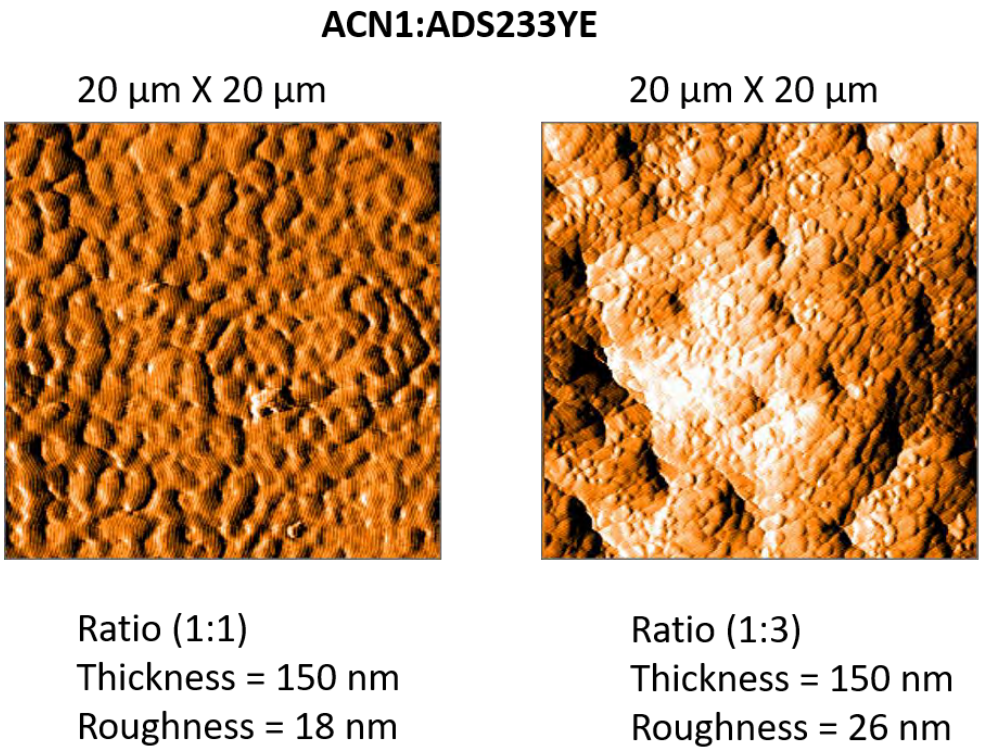

Figure B6. Micrographics of the mixture ACN1:ADS233YE at the scale of 20 µm, ratio 1:1(left) and ratio 1:3 (right).

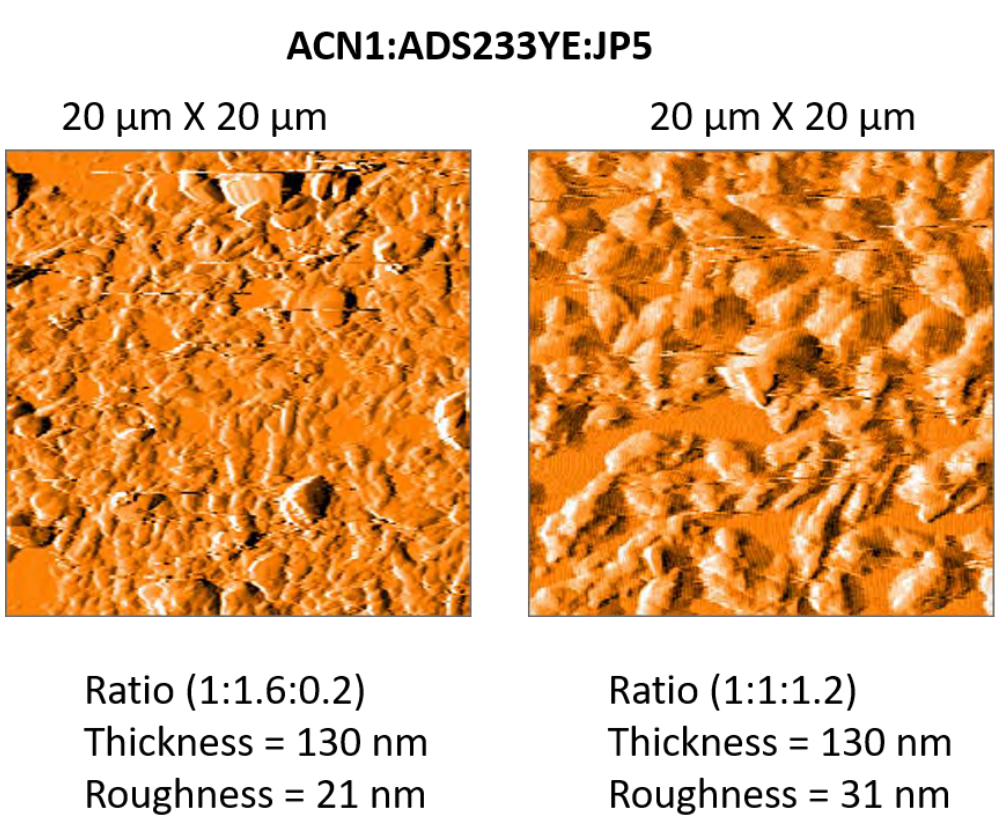

Figure B7. Micrographics of the mixture ACN1:ADS233YE:JP5 at the scale of 20 µm, ratio 1:1.6:0.4 (left) and ratio 1:1.6:0.8 (right).